Wisconsin Highway Research Program

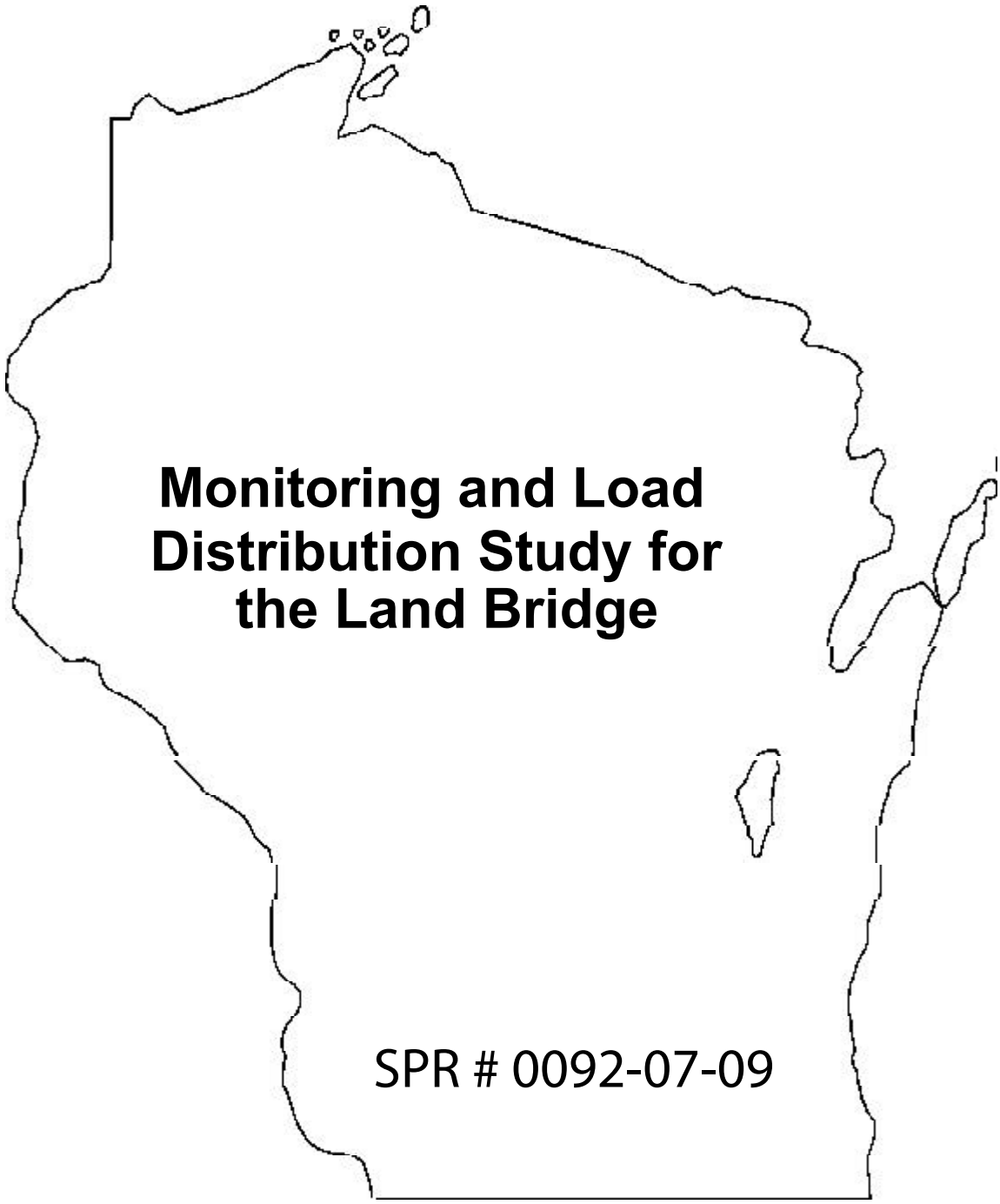

Monitoring and Load Distribution Study for the Land Bridge

SPR # 0092-07-09

Al Ghorbanpoor, Ph.D, Eric P. Feile, and Cory E. Schultz.
University of Wisconsin - Milwaukee
Department of Civil Engineering and Mechanics

September 2010

WHRP 10-12

WISCONSIN HIGHWAYY RESEARCH PROGRAM # 0092-07-09

MONITORING AND LOAD DISTRIBUTION STUDY FOR THE LAND BRIDGE

Final Report

by

Al Ghorbanpoor, Eric P. Feile, and Cory E. Schultz

Department of Civil Engineering and Mechanics

University of Wisconsin-Milwaukee

Submitted to

The Wisconsin Department of Transportation

September 2010

Disclaimer

This research was funded through the Wisconsin Highway Research Program by the Wisconsin Department of Transportation and the Federal Highway Administration under Project 0092-07-09. The contents of this report reflect the views of the authors who are responsible for the facts and the accuracy of the data presented herein. The contents do not necessarily reflect the official views of the Wisconsin Department of Transportation or the Federal Highway Administration at the time of publication.

Technical Report Documentation Page

1. Report No.: WHRP 10-12	2. Government Accession No	3. Recipient's Catalog No
4. Title and Subtitle: Monitoring and Load Distribution Study for the Land Bridge		5. Report Date: September 2010 6. Performing Organization Code
7. Authors: Ghorbanpoor, Al, Feile, Eric P., and Schultz, Cory E.		8. Performing Organization Report No.
9. Performing Organization Name and Address: University of Wisconsin-Milwaukee Department of Civil Engineering and Mechanics 3200 North Cramer St., Milwaukee, WI 53211		10. Work Unit No. (TRAIS) 11. Contract or Grant No.: 0092-07-09
12. Sponsoring Agency Name and Address: Wisconsin Department of Transportation 4802 Sheboygan Avenue Madison, WI 53707		13. Type of Report and Period Covered: Final Report 2006 to 2010 14. Sponsoring Agency Code
15. Supplementary Notes		

16. Abstract

A monitoring program and a live load distribution study were conducted for the Land Bridge, located on State Highway 131 between Ontario and LaFarge in southwest Wisconsin. The bridge is a 275-ft long curved double trapezoidal steel box girder construction. Hybrid HPS70W and A588 weathering steels were used for the construction of the bridge. The monitoring program included measurements of live load and thermal strains as well as displacements for the girders over a four-year period. The effects of the in-service live load, in terms of both the applied stresses and the number of load cycles, were found to be insignificant. The thermal stress levels were found to be more significant but with only a limited number of load cycles. It was also found that there was no significant change in the load pattern, for both the stress level and number of load cycles, over the four years of the monitoring program for the bridge. The observed stress levels in the bridge were found to be below the fatigue stress threshold prescribed by AASHTO. This indicated that an infinite life could be expected for the bridge when fatigue is a consideration for the steel box girders.

The live load distribution study for the Land Bridge included a field testing, a 3-D numerical simulation, and a comparative study of the results with those determined by the provisions of the AASHTO standard and LRFD specifications. Good agreement was achieved between the load distribution factor values that were obtained from the field testing and the numerical simulation. The comparison of the results with the values obtained from the AASHTO specifications indicated that over-conservative results yielded from the standard specifications while the results from the LRFD specifications were under-conservative. It is recommended that an additional study be performed to overcome this shortcoming of the current design specifications.

17. Key Words: Box girder bridges, high performance steel (HPS), curved bridges, structural monitoring, field testing strain measurement, thermal response, load distribution factor, bridges.	18. Distribution Statement: No restriction. This document is available to the public through the National Technical Information Service 5285 Port Royal Road Springfield VA 22161

19. Security Classif. (of this report) Unclassified	19. Security Classif. (of this page) Unclassified	20. No. of Pages 165	21. Price

ACKNOWLEDGEMENTS

This study was made possible through funding and support from the FHWA Innovative Bridge Research and Construction program, the WHRP (WisDOT), the Structural Engineering Laboratory of the University of Wisconsin-Milwaukee, WisDOT - Southwest Region, and PDM Bridge, LLC.

The research team expresses its appreciation to Mr. Scott Becker and Mr. Travis McDaniel of Wisconsin Department of Transportation as well as the Structures Technical Oversight Committee of the Wisconsin Highway Research Program for their support, guidance, and input.

Executive Summary

The primary objectives of this study included structural monitoring and live load distribution investigation for Wisconsin's first High-Performance Steel (HPS) bridge that is called the Land Bridge. Land Bridge is located in the southwest region of the state on the State Trunk Highway 131 between Ontario and LaFarge. It spans approximately 275 feet and consists of two side-by-side curved trapezoidal hybrid HPS box girders. With its' improved properties, HPS70W steel has become popular in the construction of highway bridges. Wisconsin Department of Transportation (WisDOT) completed the construction of the Land Bridge in 2002.

In order to evaluate the performance of the structure constructed with this new steel, a long-term monitoring program was established. The monitoring program was intended to assess the in-service behavior of the constructed HPS bridge members, as well as to evaluate the overall response of the structure through monitoring strain, temperature, and displacement. The two primary goals of the structural monitoring program were to 1) evaluate the in-service live load stress cycles and 2) evaluate the stress cycles and thermal response of the bridge structure due to thermal loads. It was found that there was no significant change in the traffic load pattern over the four years of monitoring. It was also found that live load stress cycles on the structure had relatively small magnitudes and occurrences. The approach employed with this research also allowed load cycles due to thermal loads to be observed independent of other in-service loads. It is noted that the thermal stresses as reported in this research are based on the total measured strain. Since it was observed that some relief of thermal strain is occurring within this structure, the thermal stresses reported here would be somewhat

conservative. It was found that thermal stress cycles proved to be more significant than other in-service loads in terms of magnitude, while producing a limited quantity of cycles. From the four-year-long structural monitoring of the Land Bridge, it was found that the observed stress levels in the box girders of the bridge were smaller than the fatigue stress threshold values prescribed by AASHTO. Accordingly, it was concluded that the bridge would have infinite life when fatigue is a consideration.

In order to better estimate live load distribution among the box girders of the Land Bridge, a program of field testing and numerical simulation was performed and the results were compared with the corresponding values from the AASHTO Standard specifications and LRFD specifications. The study yielded good agreement between the results of the field tests and the numerical simulation. It was found that live load distribution factors determined from the AASHTO Standard specifications yielded over-conservative results when compared with those from the field tests and numerical simulation. In contrast, load distribution factors determined from the AASHTO LRFD specifications were under-conservative. The finding must be taken into account with the understanding that load distribution factors for curved box girders are not specifically addressed by either of the two AASHTO specifications and the derived load distribution factor values from both specifications are at best only approximate.

TABLE OF CONTENTS

LIST OF FIGURES

LIST OF TABLES

CHAPTER 1

INTRODUCTION

1.1. Introduction and Problem Statement

In 1994, the American Iron and Steel Institute (AISI), the Federal Highway Administration (FHWA), and the U.S. Navy, began a program to develop a new kind of steel that could be used in bridge construction. Their goal was to develop an improved high strength weathering steel with greater fracture toughness and more favorable welding characteristics. A moderately priced high strength steel, such as this one, would result in lighter-weight sections. This would not only make bridges safer, because of higher fracture toughness, and more economical, it would also simplify the transportation and erection of bridge structures and would permit greater bridge loads. The newly developed high performance weathering steels have 70 ksi minimum yield strength (HPS70W) and 100 ksi minimum yield strength (HPS100W).

As of September 2007, there were 401 bridge projects in the United States that included HPS steel. Among those bridges 210 were in service, 81 were under construction, and 110 were in the planning or design stage (1). In 2002, the Wisconsin Department of Transportation (WI DOT) completed the construction of their first HPS70W bridge structure. As of September 2007, Wisconsin had 11 additional bridges under construction that included HPS steel.

During the design stage of the WisDOT's 2002 HPS bridge, minimal experimental results existed on the performance of the new HPS steel. A number of tests had been conducted at the FHWA's Turner-Fairbank Structural Laboratory and Lehigh University to evaluate fatigue and fracture characteristics of HPS plates and welded

girders. Although the extent of the testing had not been very significant in terms of the number of test specimens, all results indicated that the performance of the HPS plates and girders were by no means inferior to other bridge steels. Since HPS steel has much greater fracture toughness than other bridge steels, fatigue design issues could be affected. These issues, which need to be explored in more detail, include safe tolerance of larger fatigue cracks, easier and less frequent inspections, the possibility of raising the fatigue limit for category C details, and better load re-distribution in the hybrid system that would improve the conditions of fracture critical details. Before any of this could take place, however, it was necessary to perform additional tests to develop a sufficient database of results. With this accomplished, it would be possible to establish accurate fracture and fatigue resistance properties and characteristics for HPS bridge members with various configurations and details. These properties and characteristics can then be compared with previous results from different steels and applied in the design of hybrid HPS70W/A588W steel bridge members.

As part of the WI DOT HPS bridge construction project, a two-phase study was performed at the University of Wisconsin-Milwaukee (UWM). The first phase involved establishing much needed fatigue data for the hybrid HPS70W/A588W steel details that were used in the bridge. The second phase of the study was to implement an in-service structural monitoring program to evaluate Wisconsin's first HPS bridge. Later, the Phase II study was extended to include load distribution factor investigation for the bridge girders. These studies were partially funded by the Innovative Bridge Research and Construction (IBRC) program, the Transportation Equity Act for the 21st Century (TEA-

21). Funding was also provided by the WisDOT's Wisconsin Highway Research Program (WHRP), and the University of Wisconsin-Milwaukee.

1.2 Fatigue Resistance Evaluation

The primary objective of this study was to obtain fatigue resistance data that would define the fatigue strength under constant-amplitude fatigue loading of certain hybrid details using HPS70W and A588W steel. This would allow the comparison of the data with that from previous tests performed on similar details, but made of different kinds of steel, to verify the accuracy of the AASHTO fatigue design data for use with HPS70W/A588W hybrid details. The testing in this project was limited to constant-amplitude cyclic loading since previous experimental work has been with this type of loading and specification provisions have relied heavily on this basic loading condition (2).

1.2.1 Welded Beams

1.2.1.1 Test Specimens

The design used for the construction of the bridge, located in Vernon County, Wisconsin, included two simply supported, side-by-side, trapezoidal shaped box girders. To maximize economy, HPS steel plates were used for the bottom flanges in the high positive moment region of the span, while A588 weathering steel was used for the other parts of the girders.

I-shaped welded beams were used in this study to simulate several of the welded details that were used in the box girder bridge structure. Fillet welds, connecting the flanges to the web, and butt-welds, used to splice together the flanges, were both included in the test beams. Both of these details are classified as a category B detail, as defined by

the AASHTO Specifications (3). The test specimens consisted of a 14 inch deep, I-shaped, welded beam with flanges that were 1 ¼ inches thick and 6 inches wide. The web plate thickness was 3/8 inch and the longitudinal fillet welds connecting the flanges to the web were 5/16 inch. All dimensions for each welded beam were carefully measured before testing. The actual depth of the beams ranged from 13.94 to 14.17 inches. The flange dimensions ranged from 1.22 to 1.27 inches thick and 6.04 to 6.27 inches wide. The thickness of the web ranged from .37 to .38 inches. The test beams, each 18 feet long, were separated into two groups and classified as 1G1 and 1G2 based on the grade of the steel used to make the hybrid beams. All of the beams had webs made of one continuous piece of A588W Grade 50 steel. Half of the beams were classified as type 1G1 beams because their hybrid flanges were fabricated using A588W Grade 50 steel, spliced in the center with a one foot section of A709 Grade HPS70W steel. The other half of the beams were classified as type 1G2 beams because their flanges were made entirely of A709 Grade HPS70W steel, with a one foot section of the flange in the center of the beam spliced together using butt welds. The butt welds were finished smooth and flush with the base metal on all surfaces by grinding in the direction of the applied stress.

1.2.1.2 Material

The hybrid beams were fabricated using Grade 50 and Grade HPS70 weathering bridge steels. The 70 ksi yield strength plate conformed to ASTM A709 97B Grade HPS70W standard specifications for high-strength low-alloy structural steel. The minimum requirements for this steel are: 90 ksi tensile strength, 70 ksi yield strength, and 19% elongation over a 2 inch gage length. Tables 4.1 and 4.2 of the report on this

first phase summarize the chemical composition, the tensile properties, and the charpy V-notch energies for this heat of steel. The A588W, 50 ksi yield strength plate conformed to ASTM A709 97B Grade 50W standard specifications for high-strength low-alloy structural steel. The minimum requirements for this steel are: 70 ksi tensile strength, 50 ksi yield strength, and 18% elongation over a 2 inch gage length. Tables 4.3 and 4.4 of the report on this first phase summarize the chemical composition, the tensile properties, and charpy V-notch energies for this heat of steel. All values satisfy the specification requirements. The mechanical properties listed in Tables 4.1 through 4.4 of the report on this first phase were verified in the laboratory during the course of this investigation by performing tensile tests and charpy V-notch tests on samples taken from the beams. All of the material testing at UWM was performed in accordance with ASTM test designation A 307-97a, “Standard Test Methods and Definitions for Mechanical Testing of Steel Products”.

1.2.1.3 Specimen Fabrication

The test beams were fabricated by PDM Bridge at their fabrication plant in Wausau, Wisconsin. To ensure a level of quality for the specimens comparable to that found in their highway bridges, the fabricator was required to follow the same fabrication techniques, workmanship, and inspection as required by the State of Wisconsin for fabrication of actual bridge members. Automatic submerged arc welding with a combination of Lincoln 780 weld flux and L-61 electrodes, was used to fillet weld the flanges to the web. Lincoln MiL 800 HPNi weld flux and LA-85 electrodes were used to butt weld the HPS70W steel plates together while Lincoln 860 weld flux and LA-75 electrodes were used to butt weld the Grade 50W steel plates together. All welds were

inspected using ultrasonic testing and approved by an inspector from American Engineering Testing, Inc. PDM Bridge also inspected the welds themselves using magnetic particle inspection.

1.2.1.4 Experiment Design

The purpose of this project was to obtain experimental data for the new HPS70W steel with hybrid details, which could be used to verify the given AASHTO fatigue lives. A group of full-size beams was subjected to constant amplitude, sinusoidal, cyclic loading and the results were used to construct the relevant S-N curve. Twenty-four full size beams with two different hybrid details were tested in four-point bending to obtain a region of pure bending in the beam. Twelve samples were categorized as 1G1 beams because they had hybrid HPS/A588W butt joints in their flanges. The remaining twelve samples were categorized as 1G2 beams because they had HPS/HPS butt joints in their flanges. In each group of twelve beams, four beams were tested at each of three designated stress range levels with a minimum stress range of 1.9 ksi in the extreme fiber of the beams. Tension-tension stress range levels of 24, 30, and 36 ksi at the extreme fiber of the beams, resulted in critical stress ranges of 19.7, 24.6, and 29.6 ksi at the fillet welds. The minimum stress range of 19.7 ksi was chosen based on the AASHTO fatigue limit of 16 ksi for Category B details. Lower values of stress range were not examined because the longer anticipated lives would have unnecessarily extended the testing time. The maximum stress range value of 29.6 ksi was chosen as a result of limitations on the jack capacity of the testing equipment. Each sample was tested in a laboratory environment until failure. Failure of each sample was defined by the development of a tension flange crack with a length equivalent to 50 to 60 percent of the flange width,

beyond which the fatigue life is normally less than 2 percent, as determined in this study. Since the number of cycles to failure at a given stress range varies widely with the severity of initial flaws produced during welding, the experiment was designed to include enough data points to permit a meaningful interpretation of the data. By testing 8 beams at each stress range, a reasonably accurate statistical distribution of data was obtained.

1.2.1.5 Test Equipment and Procedures

Fatigue tests of the welded beams were performed using a load-controlled MTS closed-loop loading machine with a maximum dynamic capacity of 110,000 pounds. All 24 of the simply supported beams were tested in four-point bending. Each test beam had a 17-foot 6-inch simple span with a 3-foot region of constant moment. Before any load was applied, all dimensions of each beam were measured, and the beam was carefully centered and aligned in the test frame. To check the alignment and stress induced by the applied load, two electrical resistance strain gages were bonded to the outside surface of each flange at the mid-span. By examining the strains at each gage location with the application of static load, it was checked whether or not the beam was properly aligned with respect to the load actuator. A single hydraulic load actuator applied the required load to a stiff spreader beam which distributed the load into two equal components applied at the beam's loading points. Constant amplitude, sinusoidal, cyclic loading was applied to each beam, resulting in a tension-tension loading in the bottom flange. The loading frequency for all beam specimens varied from 2.5 to 4.0 cycles per second.

Throughout the testing of each beam, the welds were carefully examined as frequently as possible for the detection and measurement of visible fatigue cracks. A hand-held magnifying glass with 10X magnification and magnetic particle inspection

methods were used to detect fatigue cracks. Once spotted, the growing cracks were periodically measured using a caliper.

1.2.2 Transverse Stiffeners

1.2.2.1 Test Specimens

The bridge also had transverse stiffeners fillet welded to the top flange and web of the trapezoidal shaped box girders. Therefore, tests were performed to verify that the fatigue strength of this hybrid HPS70W/A588 detail corresponds with other AASHTO Category C details. For ease of fabrication and small scale testing, steel plates were fillet welded to a tension plate. The samples consisted of a main plate ¾ x 3 x 18 inches long, made of HPS70W steel, to which four A588 steel plates, ¼ x 2 x 3 inches long, were attached using ¼ inch fillet welds. For the highest stress range, due to limitations on the actuator's dynamic capacity, ¼ inch had to be ground from each side of the entire stiffener sample to reduce the cross sectional area of the main tension plate. Therefore six of the samples had a main plate with the dimensions ¾ x 2 ½ x 18 inches long and the stiffener dimensions ¼ x 2 x 2 ½ inches. These small-scale specimens very closely simulate the stress conditions of a stiffener fillet welded to the flange or web of a beam.

1.2.2.2 Material

The materials used for these tests were the same as the beam tests discussed in section 1.2.1.2. The tensile properties, charpy V-notch energies, and chemical composition of the ASTM A709 97B Grade HPS70W steel is shown in Tables 4.1 and 4.2 of the report on this first phase. The tensile properties, charpy V-notch energies, and chemical composition of the ASTM A709 97B Grade 50W steel is shown in Tables 4.3 and 4.4 of the report on this first phase. All of the material testing at UWM was

performed in accordance with ASTM test designation A 307-97a, “Standard Test Methods and Definitions for Mechanical Testing of Steel Products”.

1.2.2.3 Specimen Fabrication

The transverse stiffener samples were fabricated by PDM Bridge at their fabrication plant in Wausau, Wisconsin. To ensure a level of quality for the specimens comparable to that found in their highway bridges, the fabricator was required to follow the same fabrication techniques, workmanship, and inspection as required by the State of Wisconsin for fabrication of actual bridge members. Semi-automatic submerged arc welding with a combination of Lincoln 780 weld flux and L-61 electrodes, was used to fillet weld the transverse stiffener plates to the main plate. All welds were inspected using ultrasonic testing and approved by an inspector from American Engineering Testing, Inc. PDM Bridge also inspected the welds themselves using magnetic particle inspection.

1.2.2.4 Experiment Design

The purpose of this portion of the project was to obtain experimental data which could be used to verify given AASHTO fatigue lives for transverse stiffener plates fillet welded to HPS70W steel. A group of small-scale laboratory samples were subjected to constant amplitude, sinusoidal, tension-tension, cyclic loading and the results were used to construct the relevant S-N curves. Each stiffener sample was composed of a main tension plate made of HPS70W steel with two, A588W steel plates welded to each side, in the transverse direction. Fillet weld terminations were included in the test samples. The stiffener sample details are shown in Figure 4.4 of the report in this first phase. Axial tension-tension stress cycles were applied to the main bar at stress range levels of

14, 20, 24, and 29 ksi with a minimum stress of 1.3 ksi. The minimum stress range of 14 ksi was chosen based on the AASHTO fatigue limit of 10 ksi for Category C details. Lower values of stress range were not examined because the samples tested at the 14 ksi stress range fell below the constant amplitude fatigue limit and never failed after applying 20 million cycles of load. The maximum stress range value of 29 ksi was chosen as a result of limitations on the jack capacity of the testing equipment. Each sample was tested in a laboratory environment until failure. Failure of each sample was defined by the development of a crack with a length equivalent to between 50 and 60 percent of the width of the bar, beyond which the fatigue life is normally less than 2 percent, as determined in this study. Since the number of cycles to failure at a given stress range varies widely with the severity of initial flaws produced during welding, the experiment was designed to include enough data points to permit a meaningful interpretation of the data. By testing six stiffener samples at each stress range above the experimental fatigue limit, and four stiffener samples below the obtained experimental fatigue limit, a reasonably accurate statistical distribution of data was obtained.

1.2.2.5 Test Equipment and Procedures

Fatigue tests of the stiffener samples were performed using a load-controlled MTS closed-loop loading machine with a maximum dynamic capacity of 110,000 pounds. All twenty-two of the stiffener samples were tested in axial tension. Before any load was applied, all dimensions of the samples were measured and each sample was carefully aligned within the hydraulic grips of the testing machine using inscribed center lines on the grips and on the specimen. A single hydraulic load actuator applied the required load to each sample. Constant amplitude, sinusoidal, axial tension-tension, cyclic loading was

applied to each sample at a load rate of 6.0 cycles per second. Since each sample had two pairs of stiffeners welded to the tension plate, each sample was used to obtain two data points on the experimental S-N curve. After the first pair of stiffeners, labeled "a" on each sample, had failed, the main plate was cut off near the fracture area, and the remaining portion of the sample was re-mounted in the testing machine and the second pair of stiffeners, labeled "b", were tested until failure.

1.2.3 Phase I Summary Findings

The primary objective of this phase of the study was to evaluate the effect of hybrid weld details on the fatigue strength of bridge members. Web-to-flange fillet welded connections, butt welded flange splices, and fillet welded transverse stiffeners were all examined using Grades HPS70W and A588W bridge steels. The following conclusions can be drawn from the fatigue test data and the regression analysis.

1.2.3.1 Plain Welded Beams

1. The fatigue test data for hybrid welded beams from this study correlated well with the previous data (4) for plain welded beams, that was used by AASHTO to create the Category B fatigue specifications for highway bridge design.
2. The cracks leading to failure in 23 of the 24 beams tested, initiated in the fillet weld connecting the web to the tension flange, most likely at weld flaws such as a gas pocket or wormhole.
3. Crack initiation at the flange tip occurred in only 1 of the 24 beams tested; however, this crack grew faster than the cracks in the fillet weld of the tension flange due to a higher stress intensity factor for the crack.

4. In many of the tests, cracks also formed in the fillet weld connecting the web to the compression flange. This can be attributed to the high tensile residual stresses that usually exist in the longitudinal fillet welded region.

1.2.3.2 Butt Weld Flange Splice

1. The fatigue test data for hybrid butt weld flange splices from this study correlates well with the previous data (4) for butt weld flange splices, that was used by AASHTO to create the category B fatigue specifications for highway bridge design.
2. None of the beams in the current study failed from a fatigue crack in the butt weld. All of the beams failed as plain welded beams, therefore, it is safe to categorize hybrid butt welded flange splices as AASHTO category B.

1.2.3.3 Transverse Stiffeners

1. The fatigue test data for hybrid transverse stiffeners from this study correlates well with the previous data (5) that was used by AASHTO to create the Category C fatigue specifications for highway bridge design.
2. All of the cracks leading to failure of the stiffener samples initiated at the weld toe of the fillet weld. By analyzing the fracture surfaces, it was seen that cracks initiating at the weld termination points contributed to the failure of about half of the samples.

The constant amplitude fatigue limit for the transverse stiffener samples appeared to fall above the 14 ksi stress range based on the 20,000,000 load cycles. Of the 4 tests run at a stress range of 14 ksi, none failed after 20,000,000 cycles of tension-tension loading.

Currently, the constant amplitude fatigue limit given by AASHTO for transverse stiffeners is 10 ksi.

1.3 Structural Monitoring Program

The Phase II of this study consisted of post-construction structural monitoring of Wisconsin's first HPS bridge structure. The Phase II study was later extended to include an investigation of load distribution for bending moment in the Land Bridge. Land Bridge was constructed along State Trunk Highway (STH) 131 in Vernon County on the state's west side on a stretch of highway between Ontario and LaFarge. The selected location for Wisconsin's first HPS bridge along STH 131 runs north-south, and at this location requires a clear span of 275 feet. Site topography and highway layout also required a slight sweep in the bridge from west to east. The bridge is a two hundred and seventy-five foot simple span bridge with two side-by-side trapezoidal shaped steel box girders. To maximize economy, HPS70W plates were used only for the bottom flanges, where tensile strength is the limit state for design, resulting in a hybrid girder design with HPS70W and A588W steel. Because of the length of the bridge, each girder was field spliced with three segments using HPS70W connection plates and high-strength A325M bolts. At each end of the trapezoidal box girders, bearing stiffener plates of Grade 50W steel are welded to the inside of the webs using fillet welds, and to the bottom flange using a double-bevel weld. Connection plates are welded to the inside of the web approximately every fourteen feet along the length of the bridge using fillet welds and have cross-bracing angles connected to them. T-sections are bolted to connection plates inside the girder, at the top of the web, and run diagonally in the horizontal direction along the length of the bridge to provide lateral support to the top flanges. Every

fourteen feet, connection angles are bolted to the outside of the web to support bridging angles between the two side-by-side girders.

1.3.1 Objectives

The monitoring program was intended to assess the in-service behavior of the constructed HPS bridge members, as well as to evaluate the overall response of the structure through monitoring strain, temperature, and displacement. The first phase of this project involved experimental testing to determine the fatigue life of HPS (and HPS/A588W) details under varying stress cycles in order to allow the S/N curves to be established for use with HPS. The laboratory testing was also able to verify that HPS details are able to, at a minimum, have fatigue properties consistent (or in excess of) the properties of conventional steel. With these experimental results established, there is a need to determine the in-service strains and subsequent stresses which are being experienced in the structure in order to apply the experimental testing and to enable a more accurate use of those results. Post-construction monitoring has added importance with this project as this was the first time HPS steel was used in a Wisconsin bridge. It is important that this structure is fully evaluated to ensure that all of the movements and reactions of the bridge coincide with those intended during design as there is a new material in use, as well as new details with the combining (welding) of the two types of steel. It is important that these in-service conditions are evaluated to verify or create new concerns regarding conditions that need to be considered in the design of these structures.

Another goal for this research program is to develop a thermal assessment of the structure and the way it moves and responds to thermal and environmental influences. Thermal movements and stresses are minimally considered in the design of bridge

structures. However, as has been proven in the past with structural failure investigations, thermal stresses and forces can be quite significant and detrimental to bridges. With the results of this testing, we would like to determine the significance of these thermal stresses and movements to show the significance of including these considerations into the design of bridge structures. In the design of bridges, much emphasis is placed on the stresses experienced due to live load traffic and the number of cycles at these stress levels. The fatigue life of the bridge is then estimated based on these live load traffic cycles (high-cycle fatigue). It is also prudent in these fatigue life estimates to include thermal stress cycles, which would constitute low-cycle fatigue of the bridge structure. The effect of these thermal stresses and movements could become significant in the design phase when considering the stress cycles being experienced due to thermal effects in a bridge, both in terms of the range of those stresses, as well as the number of cycles being experienced. With the results of this research, we would like to be able to develop a life cycle assessment for this bridge which would take into account not only the results of the stress cycles experienced due to traffic loads, but also the stress cycles experienced due to the thermal and environmental effects experienced by the bridge structure.

1.4 Load Distribution Study

Because of the limited number of past studies to investigate load distribution in curved box girder bridges and due to the unique characteristics and geometrical configuration of the Land bridge, there were unanswered questions regarding appropriate load distribution parameters that should be considered for the girders in the bridge. Both the AASHTO LRFD and Standard design specifications offer equations for determining load distribution factors for only straight box girders. The relevant equations in the

standard specifications are known to yield load distribution values that are excessively on the conservative side. The equations in the LRFD specifications are developed based on the premise that the calculated load distribution factors are closer to the real values experienced by the bridge girders. However, because of the bridge's unique characteristics and the limited applicability of the equations in the AASHTO specifications, it was deemed necessary to perform an investigation to determine appropriate load distribution values for the box girders in the bridge.

1.4.1 Objectives

Load distribution factors are calculated to determine the maximum possible level of load that could be resisted by a girder from all possible live loads in the bridge. The primary objective of this study is to determine the appropriate level of live load distribution based on the bending moment for the Land bridge. This objective is achieved by determining load distribution values through both field testing and performing a numerical simulation for the bridge structure. Additionally, the results from the field tests and the numerical analysis were compared with those calculated by equations provided by the AASHTO LRFD and Standard specifications.

CHAPTER 2

REVIEW OF LITERATURE

2.1 Review of Literature – Structural Monitoring

As the nation's infrastructure ages, methods for evaluating the condition of existing bridges have become ever more necessary. In the past twenty years, structural monitoring has become ever more commonplace as a tool for local and state agencies to not only evaluate the condition of their existing structures, but also to use the results as a tool to aid in the design of future structures. As technology has developed, the opportunities for structural monitoring have increased as these tools become more portable, affordable, and easy to operate. The uses and benefits of structural monitoring are many, as evidenced by the wide array of research that has been conducted utilizing structural monitoring techniques.

As Zhou (6) points out; state, county, and local jurisdictions that are responsible for maintaining and replacing the bridges in their bridge inventory are in need of new methods for condition assessment that can be used in combination with traditional visual inspection. As our federal interstate system recently surpassed fifty years of age, many of the bridges and structures, which make up this interstate system, are also reaching critical ages. These bridges are reaching ages and conditions at which the owners need to make important decisions pertaining to repair, rehabilitation, and possible need for replacement.

As use of the interstate system continues to grow, many of these bridges are experiencing increased traffic flows and increased truck weights. This coupled with the aging of the structures and the deterioration of components due to accumulation of a large

number of stress cycles, has created a need for additional tools for evaluating not only the current conditions of these structures, but also for ways of determining what useful life these structures have remaining. The determination of repair and rehabilitation versus replacement has become a critical decision as many steel bridges are reaching or have exceeded their original design life. Limited infrastructure funding may not allow all of these existing structures to be replaced, making it vital that bridge conditions are evaluated so as to address those structures in most need of repair or replacement.

One of the primary benefits of structural monitoring is to determine the actual service stresses and conditions experienced by a structural member. Design of structures and members for fatigue has been carried out for years. However, when designing for fatigue, the stresses being placed on members are based on analytical and empirical assumptions. Evaluating actual field conditions will show the true loads, stresses, and strains, due to traffic and possible damage. This will aid in evaluating the need for repair and/or replacement.

One of the leading examples of a commitment to investment and research in the structural monitoring field is in Connecticut. The University of Connecticut (UConn) and the Connecticut Department of Transportation (ConnDOT) began developing and implementing long term monitoring programs over two decades ago and have since monitored over 25 bridges. The goals of their monitoring program have been to learn how bridges behave, learn how monitoring can be used to supplement visual inspections, and to provide information needed for renovations and retrofit of existing bridges (7).

The following pages will look at previous structural monitoring research, focusing on the varying goals of the research, as well as the different approaches and applications used to produce the desired results.

As previously mentioned, John DeWolf and the University of Connecticut (UConn) have been leaders in the structural monitoring field. Since 1984, they have teamed with Connecticut Department of Transportation (ConnDOT) to use different monitoring approaches in the assessment of the state's infrastructure. This work has involved both short-term and long-term studies. The short-term studies typically provide information on connections, members, and diaphragms, with directed goals of evaluating localized stresses and damage for fatigue purposes. The long-term studies have been conducted to develop information on global behavior and to develop global monitoring approaches, which may be used for identifying structural deficiencies and damage.

Short-term studies focus on particular components or parts of the structure. Typically, they are done to assess the need for replacement or repair of a specific component or to determine if that component or portion of the bridge was behaving as designed. Short-term monitoring efforts have typically been based on strain monitoring, with some effort to integrate vibrational information with the strain data. These studies have generated data that have been used in localized evaluation of specific members or connections. Strain monitoring typically involves testing over a one to three day period. Most of their studies have involved the use of no more than eight strain gages, while some research has involved as many as 100 strain gages, however not all of them were monitored simultaneously.

During the life span of the typical bridge, the primary form of maintenance involves visual inspection. With this approach, however, not all areas or details are accessible, allowing some problems to go unrealized until they become more serious in nature. Subsequently, by this time the repair is typically much more expensive to make due to its urgency. Much of DeWolf and UConn's long-term monitoring has involved the use of accelerometers to determine vibrational information. The purpose of this is to evaluate the causes of what was perceived as excessive vibrations and to evaluate the overall structural integrity of the structure. Much of the long-term monitoring involves determining the actual stress levels experienced in the bridge members to provide histograms of data. These histograms of data can then be converted to provide fatigue life predictions. As will be seen in some of the following case studies, this has become a very useful tool, as it enables state and local agencies to determine the remaining fatigue life of bridge structures, or any of the parts within a structure. This can be very beneficial, whereas many times wholesale replacement of a structure is not practical, due to both the monetary costs and the difficulty of the disruption of roadways.

In their paper, DeWolf, Culmo, and Lauzon (8) finish with a case study in which analytical studies were carried out to determine how a series of bridge spans on one of the interstates in Connecticut should be renovated. Analysis demonstrated that all of the diaphragm connections would need replacement. After this, data was obtained from strain monitoring in the field, which determined that strains were lower than indicated by the analysis. As a result, only the center diaphragms were in need of repair, while the diaphragms at the quarter points were proven within acceptable limits by the in-service

field monitoring values. The estimated savings to the state due to this finding was approximately 2 million dollars in renovation costs for this multispan bridge (8).

As a follow-up to this research, Sartor, Culmo and DeWolf published another article, which details several more structural monitoring case studies, each with varying approaches, goals, and results (9). In their research, they point out that in analytical evaluations, it is not always possible to consider all variables and that to accurately study fatigue susceptibility of a bridge, the engineer must have the most realistic and precise information to make an accurate assessment. This is particularly important when the live load stresses used in fatigue life estimations are used in cubic equations. Furthermore, analysis using finite element models cannot mimic the wide variation of stress ranges that occur with day-to-day, conventional traffic on a bridge structure. Sartor, Culmo and DeWolf identify a few of these factors, which can produce a wide range of variables for determination of live load stress ranges:

- variability of truck designs,
- variability of truck loads (analytical evaluation of bridges assumes that trucks are fully loaded, not typically the case for in-service conditions),
- location of the load relative to the supporting structure,
- impact and dynamic effects (these factors are ever-changing due to roughness of bridge surface, smoothness of approach joints, and suspension of the trucks).

Of course, one cannot accurately account for all of these variables in a computer analysis; the only way is through field monitoring to determine actual stresses and distributions within the structure. The authors also point out the flexibility of the results

which can be obtained through field monitoring, which include: measurement of stress levels, distribution of loads, determination of deformational induced behavior, development of fatigue predictions, determination of whether or not repairs are required, and to assist in developing how any repairs should be made and to evaluate behavior following repair (9). All of the case studies performed as part of this research were short-term, carried out over a period of 1 to 2 days, employing a portable field monitoring system, which was easily installed. This system included a data acquisition unit, which was able to produce instantaneous results, allowing for adjustment of the monitoring approach, dependent on the results as they were evaluated.

Four case studies are presented which demonstrate the flexibility of structural monitoring and the varying approaches, goals, and results that can be obtained. All of the case studies were used to determine whether changes and/or repairs were necessary. The case studies included a wide range of bridge types, applications, and results, including:

- determining that corroded hangers in a 70-year-old drawbridge needed emergency repairs,
- determining that poor welds during fabrication were the cause of cracking in the vicinity of diaphragm connections in a 15-year-old steel girder bridge, and subsequently determining that repairs were not needed,
- proving that stress ranges in a 35-year-old interstate bridge were low enough so fatigue was not an issue, thus extending the life of the bridge,
- increasing the load rating of a 25-year-old bridge making it unnecessary to carry out expensive reinforcement details which were shown to be required through analytical efforts.

Through their research, the authors believe that the amount of data necessary to produce an accurate fatigue evaluation is not as significant as once thought. They feel that if the average daily truck traffic (ADTT) is known, the number of trucks needed to generate an accurate constant effective stress range and fatigue life of the element is about 200-300 occurrences. The authors feel that short-term structural monitoring is a cost effective tool to supplement the work of bridge inspectors and design engineers and that the cost of the system may be recouped many times over by proving that costly repairs to potential problems are not necessary and provide info that can assist in the management of a state's bridge infrastructure (9).

In 2000, Howell and Shenton III (2) developed an in-service bridge monitoring system (ISBMS) at the University of Delaware. The ISBMS was developed as a small portable system, which could be easily deployed for short term monitoring. The system was designed for operation on an as-needed basis for short periods of time and for use on ordinary highway bridges. As developed, the system was intended to assist with the following goals:

- assist in the load rating of a bridges,
- failure investigations,
- monitor bridge response as overloads crossed ,
- general health monitoring of the structure.

As used for in service live load traffic, the ISBMS has 3 primary methods of data collection; it records peak live load strains that exceed a specified threshold, the time

history program captures dynamic waveforms that exceed a specified threshold, and the rainflow program counts varying amplitude strain cycles.

As the bridge structure, or selected members, has gages applied for the purpose of this testing, the authors realize that this is also an opportune time to conduct a load test with a load truck of a known weight to see how a bridge performs. While this can be very beneficial in evaluating a bridge's performance between routine maintenance and inspections, this is not always feasible, as this typically requires closing the bridge to traffic, as well as the coordination of a test vehicle. Even still, a load test cannot produce the varying loads that an actual bridge experiences as pointed out in research by others including Zhou (6) and Sartor, Culmo, and DeWolf (9).

As the authors point out, if an accurate estimate of fatigue life is the desired outcome, load testing will not determine this and one will need to find the effective stress ranges the structure experiences under in-service loads. To accomplish this, continuous monitoring over a period of several weeks or months under site-specific traffic must be carried out. While some major bridges get continuous monitoring, the authors point out that these bridges make up but a fraction of the entire interstate system. They see this portable ISBMS as a way to provide monitoring of ordinary bridges, where permanent monitoring is not possible or even necessary, but intermittent monitoring would provide useful data about the condition of the bridge. This intermittent monitoring could provide quantitative data, which could become part of the bridge history log for comparison with future inspections to indicate any possible bridge deterioration. As others have also pointed out, the data from short-term monitoring can also be used to determine if effective stress ranges are higher or lower than those assumed for design, and thus

whether the fatigue life of the structure is greater or lesser than that originally indicated during design.

As a part of the joint effort of the University of Connecticut and the Connecticut Department of Transportation to develop and implement a long-term monitoring system on a network of bridges in the state of Connecticut, Chakraborty and DeWolf report on the monitoring of a three-span, multi-steel girder composite bridge (7). As part of this research, the structure was also analyzed using AASHTO Specs for comparison with the acquired field monitoring results. The authors identified the goals of their research to include:

- determination of the location of the neutral axis,
- evaluation of load distribution to the different girders,
- FE analysis to further study distribution,
- evaluate the influence of truck traffic and establish a baseline for long-term monitoring.

For the instrumentation of the bridge, the longer of the two end spans had 20 uniaxial strain gages mounted at mid-span. The gages were placed on the web of the conventional W-shaped sections, 2 inches above and below each of the adjacent flanges. All of the sensors were connected to an onsite computer for data collection, analysis, storage, and communication back to a central computer at the university. This system became operational in November of 2004.

The intent of this research was to collect and evaluate data from large trucks, which through data analysis (from field results) was determined to be at a threshold of 20 microstrain. This minimum strain level corresponds to trucks weighing approximately 20

kips and over. This lower bound on strain levels eliminated data and stress cycles associated with automobile traffic, which is not considered to contribute to the fatigue of structures. All of the strain gages were recalibrated daily to reset strain levels to zero, eliminating small changes and drifts in strain due to temperature fluctuations and time.

For this study, data which was collected for a half-month period indicated that traffic of lighter weight trucks (strain ranges of 25-45 microstrain) was about 1,600 to 1,750 cycles on the typical weekday, and 1,100 to 1,275 weekend. For heavier trucks (strain ranges of 45-70 microstrain), there were typically 100-125 cycles on weekdays. Fewer than 10 sets indicated strains above 70 microstrain on a typical day. Based on the acquired data, the maximum-recorded stress for a week was 2.94 ksi, which is 40% of the design stress for a single lane loading (the design stress for this bridge was 7.4 ksi). As indicated by the field data, design stresses are not typically achieved in this structure. Based on these results, the live load stresses designed for (as required in AASHTO) are significantly higher than the actual stresses experienced during the five-month monitoring period. Through their research, the authors cite their results as gaining a better understanding of the actual behavior of the bridge, determining that the actual strain and stress levels are well below those used in the design process (likely because the design process does not fully include redundancies, connection restraints, etc.), and gaining a better understanding of the way in which loads are distributed throughout the structure.

In his research from 2006, Zhou discusses three case studies of different applications and approaches to field monitoring. His observations and conclusions support those of others conducting similar research. As previous research has also found, Zhou found that fatigue analysis based on specification loads and distribution factors

typically underestimates the remaining fatigue life of existing bridges by overestimating live load stress ranges. Stress ranges determined from field strain measurements are typically significantly lower than the calculated ones due to participation of secondary members and floor (slab) systems that are usually neglected in analytical models. By performing field monitoring, the measured strains collected are able to reflect the actual load distribution in the structure as well as the weight, volume, and traffic patterns of in-service vehicular loads. Field measurement is also able to assess the affect of localized stress increases due to the secondary bending at truss joints, section losses due to corrosion, and other factors that cannot be included in analytical models. Field strain measurement is also able to take into account environmental effects, such as secondary stresses not accounted for in the typical analysis like frozen pins and frozen expansion bearings. The primary benefit of field monitoring is that it enables all of these factors to be included in the analysis of results while not requiring that any assumptions be made to account for these uncertainties.

Zhou found that in many cases only a small fraction of the stress range histogram is greater than the constant amplitude fatigue limit (CAFL), while the majority of the measured stress cycles are lower. Based on his experience, Zhou recommends that the measurement time period should be at least seven consecutive days to represent the basic unit of traffic repetition, while longer measurement periods obviously reduce the possibility of missing heavy vehicles and create a larger sample of in-service data.

2.2 Review of Literature – Live Load Distribution Factors

Load distribution factors have been used in bridge design since the 1930s. From 1930s to 1990's a set of simplistic formulas was used that consisted of a single parameter

"S-over" that was used for both shear and moment. These traditional S-over load distribution factor formulas are simple and easy to apply but can be overly conservative in some cases while unconservative in other cases. The National Cooperative Highway Research Program (NCHRP) set out to create a more accurate set of equations with the NCHRP Project 12-26 (10). The new set of equations created under NCHRP Project 12-26 were more accurate but also more complex and designers found these new equations difficult to use. A set of simpler and less complex set of live load distribution factor equations would help avoid any confusion by the design community. As such, the NCHRP performed a new study under project NCHRP 12-62 (11). This study included contributions from researchers at Tennessee Technological University and other institutions. The main purpose of this study is to shed light on the format of the live load distribution formulas to help develop more practical design formulas for the bridge community.

Project 12-62 used an automated process to compare live load distribution factors that were calculated using several simplified methods, in addition to a grillage analysis for over 1500 bridges. Data was used from four independent sources that included 809 bridges from the NCHRP 12-26 research, 24 bridges from the Tennessee Technological University, 653 bridges from several DOTs. The data from these bridges were entered into AASHTO Virtis, and 44 bridges were designed to push the limits of normal design parameters. The adjusted uniform distribution method (informally called Henry's Method) and an adjusted lever rule were chosen after a comparison to the grillage analysis was made. This limited the number of bridges being analyzed to just the ones form the NCHRP 12-26 and Tennessee Tech. Both methods can predict moment and

shear distribution factors. With calibration factors applied to improve the accuracy of both methods, they can predict load distribution factors more accurately (in most cases) than the current LRFD equations and without its range restrictions. This makes these methods simpler and more accurate than the current LRFD equations.

Several observations were made from the NCHRP 12-62 project. It found that the skew angle in bridges can affect both the live load moment and shear distribution factors. A skew angle below 30 degrees had a small effect on the distribution factor but when it was from 30 degrees to 60 degrees the live load moment distribution factor decreased while the live load shear distribution factor increased. The presence of diaphragms was shown to affect the live load distribution factors. The live load moment distribution factor decreased with support and intermediate diaphragms and the live load shear distribution factor increased with the addition of such diaphragms. Both effects were relatively small with the diaphragm configurations commonly used in bridge design. In the study, the stiffness of any barrier present in the bridge and any associated loads carried by it were neglected. It was found that as the vehicle was positioned away from the barrier or curb, both the live load moment and shear distribution factors decreased in a linear trend.

The current equations from the LRFD specifications (12) use girder spacing, span length, slab thickness, and beam stiffness to determine the load distribution factors. There are different formulas for the interior girders and exterior girders, for shear and moment, and for one-lane loaded and two-or-more lanes loaded. The formulas in the current LRFD specifications were developed based on using a trial and error type of curve fitting. Cai elaborated on these observations and identified the major parameters of

load distribution factors by using the theory of beam on an elastic foundation (13). In this approach, the bridge deck with a unit width and in the transverse direction is considered to be supported on the longitudinal beams that act as elastic springs. Using the beam on elastic foundation theory, Cai derived an equation that uses three constant coefficients as well as the girder length, girder spacing, girder stiffness, and slab thickness. The three constant coefficients in the equation ensure nonzero load distribution factors even when the spacing of the girders approaches zero; that the load distribution factors have a linear relationship with the girder spacing; and consideration of the effects of relative longitudinal stiffness and transverse stiffness on load distribution factors.

In order for Cai to assess the accuracy of his load distribution formula, he generated 3,600 sets of data for the cases when one lane was loaded, and when two or more lane were loaded., The same number of data sets were generated and examined for for shear load distribution. Cai varied the bridge parameters of span length, girder spacing, and slab thickness in order to obtain all the data sets for each case. He then used that data to determine the three coefficients used in his fourmula by curve fitting the data point. After comparing his proposed formula with the values obtained from the LRFD design specifications, Cai arrived at a maximum difference of about 7% and an average difference of about 1%.

Cai also considered the effects of intermediate diaphragms but found that the effect was only significant when the diaphragms were located near the bridge section being considered. Because of this, Cai derived a formula for the effect of diaphragms but recommended it as an optional equation for the designer. With the proposed formulas

from Cai, load distribution factors for moment and shear, exterior and interior girders, one lane loaded and two or more lanes loaded can be determined by considering only the three constant coefficients calculated appropriately. This would allow the many tables of the current LRFD codes to be reduced into one table defining the constant coefficients for the different applications. Although this study was based on a slab supported on plate girders, it could be extended to calculate load distribution factors for steel box girders.

In 1968, Fountain and Mattock analyzed a folded plate structure in order to study the lateral distribution of loads in a simple-span composite multiple box-girder bridge without intermediate diaphragms (14). Their findings formed the basis for the moment and shear load distribution factors for AASHTO Standard Specifications for Highway Bridges and the AASHTO LRFD Bridge Design Specifications. Their equations were only for the use of simply supported bridges with a span length between 15 m and 45 m (49 ft and 148 ft). However, both AASHTO Standard and AASHTO LRFD Specifications allow the use of such equations for spans reaching 150 m (492 ft) as well as for straight continuous span bridges. In 1978, Heins extended the work of Fountain and Mattock to cover curved bridges by developing a modification factor to account for the curvature in such bridges (15).

Samaan, Sennah, and Kennedy conducted an extensive parametric study, using the finite elements method, on 240 two-equal span continuous curved composite multiple box girder bridges (16). The objectives of their study were to examine the influence of the various parameters affecting the structural response, to establish a database for the distribution factors necessary for designing the bridge for the maximum longitudinal stresses and deflections, and to deduce empirical formulas for these factors. Based on the

findings from a 2004 sensitivity study by Samaan (17), it was known that the effects of concrete deck thickness, the presence of top lateral bracings at the level of the top steel flanges, and the span to depth ratio have little significance on the load distribution factors. Therefore, the parameters they considered were the effects of span length, span to radius of curvature ratio, the number of lanes, the number of box girders, the loading condition, the truck loading type, the web slope, and the presence of vertical cross bracings inside and between adjacent box girders.

Samaan, Sennah and Kennedy used the following assumptions during their parametric study.

- There is complete interaction between the concrete deck slab and the top of the steel flanges of the box girders.
- The materials, steel and concrete, are elastic and homogeneous.
- The effects of road superelevation, concrete curbs and railings are ignored.
- The concrete deck slab is uncracked in the positive moment region.
- The contribution of the cracked concrete deck slab to the cross-sectional stiffness at interior supports is negligible and can be ignored as suggested in the AASHTO Standard Specifications for Highway Bridges.
- The contribution of the reinforcing steel is taken into account and small deflection elastic theory is assumed.
- The bridges have a constant radius of curvature between support lines.
- Support lines assumed to be radial to the bridge centerline.

They also made the assumption that the cross-bracings and top chords in the diaphragms can be modeled as rectangular solid bars with the same cross section as the

back to back angles that are used in most bridges. This assumption was validated in the 2004 sensitivity study by Samaan.

From their study, Samaan, Sennah, and Kennady made several observations. It was found that there were no significant changes in the distribution factors with or without the presence of bracings between boxes. They also observed that when the ratio of span to radius of curvature was increased from 1 to 1.2, the live load distribution factors increased by 30% and 35% for a 40 m (131 ft) and a 100 m (328 ft) span length, respectively. From this study, they also found that the load distribution factors increased with the increase in the bridge span length. It was also found that when the number of boxe girders changed from 2 to 4, the load distribution factors increased by about 2% and that when the number of lanes increased from 2 to 4 the load distribution factors increased by about 30%. Another observation was that the web slope had negligible effect on the live load distribution factors. Samaan, Sennah, and Kennady also compared the results of the AASHTO Standard Specifications for Highway Bridges, the AASHTO LRFD Bridge Design Specification, and the Canadian Highway Bridge Design Code. The distribution factors from the AASHTO Standard Specifications for Highway Bridges were found to be somewhat higher than those of the other two. In conclusion, Samaan, Sennah, and Kennedy determined that the span to radius of curvature ratio, the number of lanes, the number of box girders, and the bridge span length are the most critical parameters affecting the load distribution factors for a box girder bridge. No direct comparison of the results of this study was made with those of AASHTO and the Canadian specifications by the authors.

CHAPTER 3

STRUCTURAL MONITORING PROGRAM and LOAD DISTRIBUTION STUDY

3.1 Bridge Description

Wisconsin's first HPS bridge structure, used for the monitoring portion of this study, was constructed along State Trunk Highway (STH) 131 in Vernon County on the state's west side on a stretch of highway between Ontario and LaFarge (Wisconsin Department of Transportation Structure B-62-187). The bridge runs north-south, and at this location requires a clear span of 83 meters (275 ft). The structure consists of side-by-side trapezoidal box girders, each 3,100 mm (10.17 ft) tall, 3,150 mm (10.33 ft) wide at the top and 1,600 mm (5.25 ft) wide at the bottom flange. Figure 3.1 shows a cross section of the bridge.

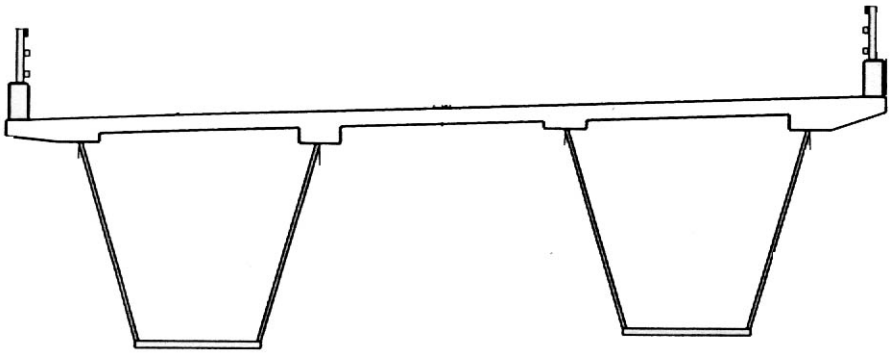

Figure 3.1: Section thru Bridge Looking North

Because of the length of the bridge, each girder was field spliced with three segments using Grade 485W (HPS70W, f_y= 70 ksi) connection plates and high-strength A325M bolts. The splice points occur at approximately third points of the span. The bottom flange of each of the girders is constructed of Grade 485W (HPS70W, f_y= 70 ksi) steel, 50 mm (2 in) thick for the middle portion and 44 mm (1.72 in) thick for the two outer portions. The remainder of the steel superstructure is constructed of Grade 345W

(Grade 50W, f_y= 50 ksi) steel. The webs are constructed of 22 mm (0.866 in) thick plate steel. The top flanges of each girder consist of 508 mm (20.0 in) wide plates varying in thickness from 75 mm (3 in) thick at the center to 63 mm (2.5 in) thick for approximately the first thirty feet of the outer portions to 40 mm (1.58 in) thick at the ends near the supports.

At each end of the trapezoidal box girders, bearing stiffener plates of Grade 345W (Grade 50W, f_y= 50 ksi) steel are welded to the inside of the webs using fillet welds, and to the bottom flange using a double-bevel weld (see Figure 3.9). Connection plates are welded to the inside of the web approximately every 4.25 meters (14 ft) along the length of the bridge using fillet welds and have cross-bracing angles connected to them (see Figure 3.2). T-sections are bolted to connection plates inside the girder, at the top of the web, and run diagonally in the horizontal direction along the length of the bridge to provide lateral support to the top flanges.

Figure 3.2: View Inside Bridge Girder

Every 4.25 meters (14 ft), connection angles are bolted to the outside of the web to support bridging angles between the two side-by-side girders (see Figure 3.3). Site topography and highway layout also required a slight sweep in the bridge from west to east as shown in Figure 3.4.

Figure 3.3: View Between Bridge Girders

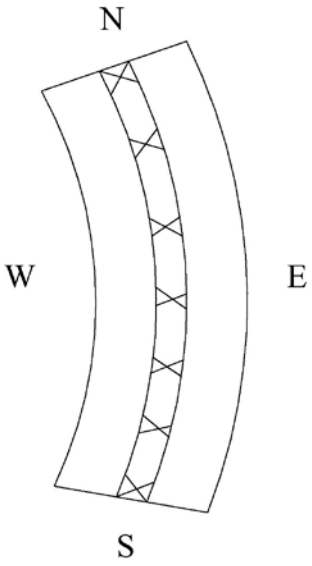

Figure 3.4: Plan Layout of Bridge

3.2 Structural Monitoring Equipment and Set-Up

To accomplish the goals of this project, various types of monitoring devices and sensors were used. Table 3.1 displays these devices and sensors and lists the products used for this monitoring project. The following pages present a brief description of how these products were selected and applied during this project.

Hardware and Sensors Used	
Data Acquisition Units	Campbell Scientific CR5000
Modems	USRobotics 56K V.90 External Modem
Modem Switcher Device	Blackbox Phone Line Manager FX121A
Electrical Resistance Strain Gages	Vishay/MicroMeasurements weldable 350-ohm resistance strain gage
Vibrating Wire Strain Gages	Geokon Model VK-4100/4150 Spot Weldable Strain Gage
Thermistors	Campbell Scientific Model 107 Temperature Probe
Linear Variable Differential Transformers (LVDT)	Sensotec Model JEC-AG DC/DC, Long Stroke (+/- 3.0 in)

Table 3. 1: Hardware and Sensors Used

3.2.1 Data Acquisition Unit

For monitoring the sensors and acquiring the required data, the research team used two Campbell Scientific CR5000 dataloggers. One datalogger would be placed inside of each of the two girders and would control and acquire data for all of the sensors in that girder. The research team chose these units for several reasons; they provided 20 input channels for sensors, each unit had a DC output for use with sensors requiring a voltage measurement (i.e., the LVDT's), the dataloggers came with a program allowing real-time monitoring, as well as remote downloading of data with a connected phone line

and modem. Each datalogger included a software to aid in the writing of specific codes to be executed for data acquisition. The programs run by the data acquisition units were written by the research team in BASIC language. The CR5000 also has a PCMCIA card slot, allowing for the insertion of a PC card to store the acquired data. While the research team downloaded data via the modem connection, all data was also stored to the PC card, ensuring that no data would be lost to possible errors in data transmission. This data was then available on-site for downloading, if necessary.

The dataloggers were powered from a ground power line, contracted by the university and installed by local utilities. Outlets were installed at the mid-span of each girder to provide power for the dataloggers and other measurement and communication devices. An outlet was also placed at the south end of the east girder to support lights and miscellaneous power needs.

One datalogger was placed at the mid-span of each girder to control all of the sensors for that girder. At each of these locations, the datalogger and other supporting hardware were placed inside of a box referred to as the command center. This box was made of plexiglass and surrounded with batt insulation. The purpose for the batt insulation was two-fold; 1) it electrically isolated all of the measurement devices from any interference which could have been caused by the electrical outlets or wires, the "antenna effect" of the steel girders, as well as any stray electrical interferences, and 2) it isolated the measurement devices thermally from experiencing the large thermal fluctuations experienced inside the girder. The need for this insulation around the command center became evident to the research team due to experiencing difficulties with acquired results early in the monitoring process. An overall drift was noticed in the

results of some of the data and it was determined through laboratory experimentation that this drift was due to thermal fluctuations of the datalogger itself. Further experimentation showed that maintaining a consistent temperature within the control center helped to minimize this effect. Figure 3.5 shows the command center in the east girder.

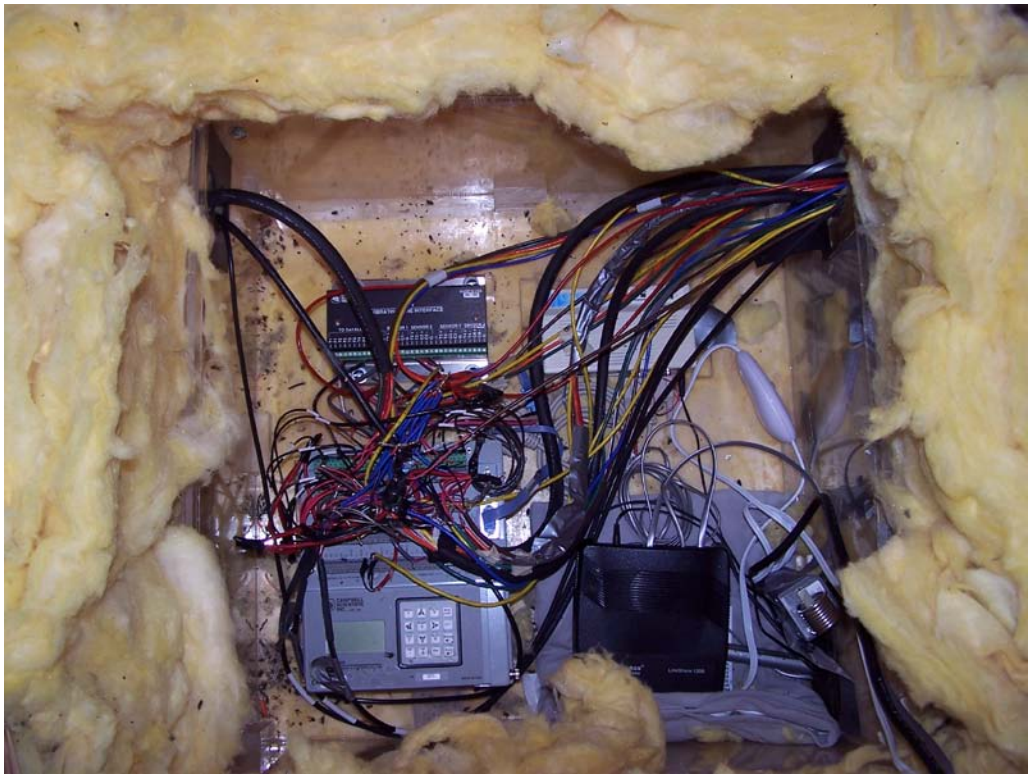

Figure 3.5: Data Acquisition Command Center

3.2.1.1 Preparation/Laboratory Work

Since the bridge site is almost 320 kilometers (200 miles) from the university, the research team performed laboratory experiments prior to the start of monitoring to simulate all of the conditions which could be experienced in the field. It became important to recognize and work out any problems before any sensors or devices were installed on the bridge. During these laboratory experiments, many possible problems

were intercepted and were able to be addressed. Some of these are worth mentioning as they explain why things were done as they were.

As previously mentioned, each of the command centers was wrapped in batt insulation. As part of the laboratory experimenting process, sensors were attached to the dataloggers and placed in cold, exterior conditions to simulate daily thermal swings. As this was done, the research team noticed that strain readings were displaying a daily overall shift or "floating" with the outside temperature even though at times the attached strain gages were in a controlled environment. This led the research team to modify two approaches to the monitoring process; 1) the temperature of the dataloggers themselves needed to be kept at a constant temperature, or as near as possible, and 2) the electrical resistance strain gage setup needed to be a ½ bridge configuration in order to employ one bridge of the strain gage to offset the temperature effects on the strain reading.

The temperature of the datalogger needs to remain a near constant as the connection of the strain gage to the datalogger and the datalogger itself was being affected by thermal swings of the sensor device. To accommodate this, the batt insulation was placed around the command center to help moderate the temperatures inside of the command center. A thermostat-controlled heating element was also added inside each of the command centers to keep all of the devices above 65 degrees Fahrenheit during the winter months for keeping the hardware functioning properly. Through the laboratory testing, the research team was able to determine that by keeping the temperature swings within the command center within reason, the strain readings obtained were minimally altered (within a range of approximately 4 microstrain) by the temperature swings of the datalogger.

Also determined through laboratory experiments was the necessity for the strain gages to have a ½ bridge configuration. It was recognized that initial strain readings, which employed a ¼-bridge configuration, were "floating" with the temperature changes, so it became necessary to utilize a ½ bridge configuration. This configuration employs two gages. In our case, one of those gages is the electrical resistance strain gage welded to the surface of the bridge steel, while the other gage is known as the "dummy" gage. This "dummy" gage is a similar strain gage attached to a similar but unloaded member that negates thermal strain effects in the active gage. In the case of the setup of the strain gages at the monitoring site, the "dummy" gages were welded to a 50 mm x 100 mm x 6.4 mm (2 in x 4 in x ¼ in) steel plates. Each plate of steel with the "dummy" gage attached to it was then located next to the active gage, resting directly on, but not attached to, the bridge steel so as to experience the same thermal shifts without experiencing any strain due to applied load.

With experimental testing completed to correct these issues, the research team was able to ensure that all of the strain readings obtained were producing accurate and valid results.

3.2.2 Strain Measurement

The primary focus of this study was to evaluate the range of stresses and displacements being experienced in the bridge girders due to 1) vehicular live load traffic and 2) daily and seasonal thermal effects. This information is critical in estimating the expected service life of the bridge. To accomplish this, a total of 32 electrical resistance strain gages (16 in each girder) were installed in a half-bridge configuration. Sixteen gages were chosen due to the fact that each datalogger had twenty available channels for

acquisition; two of which were required for measuring displacements with LVDTs and the two remaining channels were used for temperature measurement. The placement of the gages was chosen in order to enable a proper description of the stresses being experienced throughout various locations on the girder and to aid in determining the complex movements of the bridge. It was chosen that strain gages would be placed at each of the quarter-points and at mid-span of each girder. Figure 3.6 shows the locations of the 16 strain gages in each girder. Note that the numbering and locations of these gages are with respect to the reader facing north. At the first quarter-point, five strain gages were installed. Gages 1 and 5 were located on the underside of the top flange, approximately 2 inches from the top flange/web weld. Gages 2 and 4 were located on the bottom flange approximately 2 inches from the bottom flange/web weld. These locations were chosen as they would experience the maximum stresses, compressive or tensile, respectively, being experienced in the flanges. Gage 3, centered on top of the bottom flange, would give the maximum tensile strain experienced at the top of the flange plate at this quarter-point. Nine gages were installed at mid-span of each girder. A similar reasoning was applied in gage placement as for the quarter-span gages. However, at midspan, matching strain gages were placed on the adjacent web near the locations of those placed on the flanges. This was done to evaluate the transfer of stresses between web and flange, and also to get an estimate of the maximum strain (and subsequent stress) being experienced in the web/flange weld. At the final quarter-point, only two strain gages were placed due to the limited number of channels available in the dataloggers. Theoretically, the values obtained here should be the same as those at the first quarter-point, at least for vehicular traffic. It will be shown that this is not the case

for thermal stresses due to the differing locations on the girder as well as the relationship of location to bridge/girder geometry.

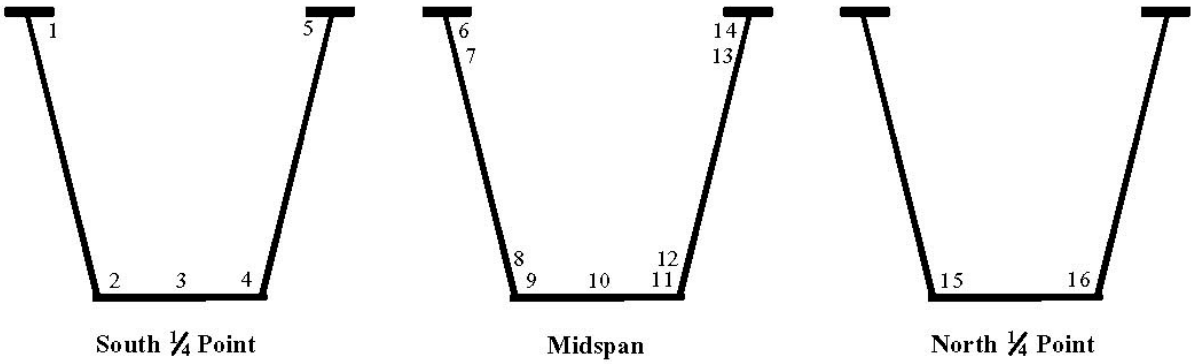

Figure 3.6: Strain Gage Numbering Conventions

All locations where electrical resistance strain gages were applied were carefully prepared by grinding off the paint, cleaning, and properly preparing the surface of the steel for strain gage application. Welded strain gages were employed for their long-term durability and accuracy as compared to epoxy adhered strain gages. After installation and testing, each of the strain gages was covered with a protective coating (Micro-Measurements Groups M-Coat F) to protect and isolate the gages from corrosion and electrical interference. This protective coating consists of a sequence of applications including sealant, aluminum foil tape, butyl rubber sealant, and neoprene rubber sheets. On top of this, each of the gages and their protective coating was then covered with a short length of angle iron to further prevent physical damage.

During installation, vibrating wire (VW) strain gages were also installed adjacent to gages 5 and 10 in each girder. The VW gages were used to verify the readings of the electrical resistance strain gages since VW gages are known to be extremely accurate

sensors. VW gages work well in static load applications; however, they do not work well with dynamic loads since it takes several seconds to obtain a strain reading with VW gages.

3.2.3 Deflection Measurement

In order to develop an understanding of how the structure reacted to live load traffic, as well as daily thermal cycles, it was necessary to study not only the thermal strains, and subsequent stresses being imposed on the structure, but also the movements caused by these loads. The two movements deemed necessary to evaluate for this study were vertical deflection at the mid-span and longitudinal expansion and contraction occurring due to daily thermal cycles. Obtaining both of these values would greatly help in understanding the complex movements of this bridge. To obtain these values, Linear Variable Differential Transformers (LVDT's) were utilized to determine the appropriate displacements.

3.2.3.1 Longitudinal Expansion/Contraction

The bridge girders are detailed in a simply supported fashion, with the south end of each girder being pinned down to its support, and the north end of the girder resting on a rocker (roller) support, which is expected to allow longitudinal movement. An LVDT was placed in each girder at the north end. As can be seen in Figure 3.7, a spring-loaded LVDT was attached to the end stiffeners of the bridge girder. The tip of the LVDT then rested against a plate which was fastened to the bridge abutment and extended into the bridge through a vent hole at the end of the girder. This LVDT was then able to determine the movement of the bridge girder with respect to the stationary abutment to

determine the expansion or contraction of each of the bridge girders due to thermal cycles.

Figure 3.7: Longitudinal Expansion/Contraction LVDT

3.2.3.2 Mid-Span Deflection

Measuring the deflection of the bridge girders at mid-span posed a challenge since the bottom of the girders are approximately 15 m (50 feet) above grade. This made it unreasonable to run a measurement device from the bottom of the girders to the ground below since it would be very difficult to isolate this device from the effects of wind over this distance, as well as possible damage to the device at ground level caused by animal and human interaction. Thus, it became necessary to develop a way to measure mid-span deflection from inside the bridge girders.

The research team employed a system which recognizes the fact that at the ends, or supports, of each girder, there is no vertical deflection occurring; so the mid-span deflection needs to be taken with respect to these end points. A system was employed (see Figures 3.8 and 3.9) in which a thin, stainless steel cable was attached near the top of the end stiffeners on the north end of each girder. This cable was then extended continuously to the south end of the bridge. Here, the cable is run through a pulley system that is again attached to the end stiffeners and dead weight is attached to this free end of the cable (see Figure 3.9). This produces a system in which there is always a constant tension on the cable. As the bridge expands and contracts, since the cable has a constant tension, the elevation of the cable at mid-span is not changing since it is supported at each end by the stationery abutments. As the girder deflects vertically due to live loading or due to thermal effects, the elevation of the steel cable does not vary. Since a stationary reference point now exists at mid-span, a vertical deflection may be taken as the difference between the bottom of the deflecting girder and the stationary steel cable. In order to measure this vertical deflection, a LVDT was hung from the steel cable, with the core of the LVDT bearing on a custom-fabricated track fastened to the top surface of the bottom flange of the bridge girder (see Figure 3.8). In contrast to the LVDT employed for measuring longitudinal expansion or contraction, the core (the inner, moving element) of this LVDT is freely moving and frictionless, which provides no resistance to movement. The core bears on the bottom flange of the girder due to gravity only. For this application, this is an important property so that the LVDT does not push back up on the steel cable, since this is our fixed datum point. The body of the LVDT now is stationery while the core is able to freely move up and down with the bottom of

the bridge girder. Since the bridge girder will also be experiencing longitudinal expansion and contraction, it became necessary for the mid-span deflection LVDT to be able to accommodate this movement (in the longitudinal direction, parallel to the girder span). In order to do this, the custom-fabricated track had a slot which accepted a roller that was attached to the core of the LVDT, allowing movement of the LVDT with bridge expansion and contraction while guiding the core of the LVDT and not allowing any lateral movement (perpendicular to the girder span).

Figure 3.8: Mid-Span Deflection LVDT

Since this was the first time the research team employed this method, great care was taken to ensure that it would provide meaningful and reliable results. A scaled-down, trial run of this setup was created in the Structural Laboratory at UWM. With this setup the research team was able to ensure that the LVDT would truly function in a frictionless manner, not causing the stainless steel cable to move up and down with the

deflections of the bridge. Creating a successful system under laboratory conditions to measure a 30 meter (100 ft) span, the research team was able to make minor modifications to install this system into the 83 meter (275 ft) bridge. The resulting system has performed exceptionally well and is very capable of measuring the deflection while not requiring any attachment to the ground at mid-span.

Figure 3.9: South End of Bridge Girder

3.2.4 Thermal Measurement

One of the major goals in this study was to attempt to quantify the thermal effects on this structure due to daily and seasonal temperature cycles. Early in the study, it became evident to the research team that this meant not only recording the air temperature each day, but more importantly, measuring the temperature of the steel itself. Outdoor ambient air temperature has lesser effect on the temperature of the steel; rather, the main factor is the presence of sunlight on the exterior surface of the bridge girder and

concrete deck. As seen in Figure 3.10, the bridge overhang casts a shadow on a portion of the face of the bridge girder for much of the day, depending on season and time of day. The research team considered this effect when placing the thermistors on the bridge steel to obtain steel temperature. A total of five thermistors were placed on the bridge to provide these measurements. The thermistors were placed on the interior surface of the bridge girder at mid-span, at approximately one-third of the height up from the bottom of the girder. This location was chosen so as to experience the maximum effects of the sunlight and to avoid experiencing any shadows due to the bridge overhang, while also distancing the thermistor from the "cold" bottom flange of the girder, which does not receive any sunlight. Thermistors were placed on both the east and west walls of each girder, to allow for a comparison of the temperature differential experienced due to sunlight exposure. One thermistor was also hung outside of the girder at mid-span, between the two girders. This was accomplished by hanging the thermistor out of a joint at a splice point of the girder. This thermistor would not experience any effects due to sunlight as it is hung between the two girders and does not experience any sunlight. The purpose of this thermistor is to get information regarding outdoor ambient air temperature to evaluate bridge movements due to average daily and seasonal temperature changes.

Figure 3.10: East Face of Bridge

Since the intention with using thermistors was to evaluate the temperature of the steel, great care was taken to avoid any outside effects compromising this information. The interior of the bridge girders has an epoxy paint coating for corrosion protection. This paint coating creates a thin insulation layer that makes actual steel temperature measurement difficult upon direct mounting of the thermistors on the painted surfaces. Accordingly, at locations where thermistors were to be applied to the girder, this paint layer was ground off to expose bare steel. The thermistor was then applied directly to the bare steel of the girder wall. In order to minimize the effects of the air temperature of the interior of the girder, each thermistor was then covered with an expanding foam insulation. The combination of these treatments provides an accurate reading of the temperature of the girder steel at these locations.

3.2.5 System Calibration

Prior to installing any sensors on the bridge, the research team performed testing and calibration to ensure that all sensors were yielding accurate results. Standard strain gages, weldable electric resistance gages, as well as vibrating wire strain gages were calibrated on a steel specimen mounted in a closed loop hydraulic testing machine with prescribed applied loads. It was verified that measured strain results matched those obtained through numerical computation. Thermistors were calibrated in incubation ovens and temperatures were also verified with independent thermocouples. The LVDT's were calibrated with standared shim plates of known thickness values to verify displacement measurement precision. The research team has also performed calibration of the LVDTs on occasional site visits.

3.2.6 Communications

To make remote communication with the data acquisition unit possible, each logger was connected to a telephone modem. A land phone line was installed at the bridge with connection to the command center of the east girder. At this point, the phone line was connected to a switch device; which was connected to both modems in the east and west girder command centers. This allowed the single phone line to communicate with the modem in either of the girders. Establishing communication with the dataloggers was a necessity due to the proximity of the bridge site in relation to the university. It allowed for real-time monitoring of both of the girders from the university, allowing the research team to perform occasional checks to ensure that the dataloggers and all sensors were running properly, alerting the research team to problems if real-time data displayed erratic or abnormal results; indicating a faulty or malfunctioning sensor.

Also, it allowed the research team to monitor the continuous presence of the electric power and the telephone line. In some instances, real-time monitoring results prompted the need for the research team to perform a site visit to repair or replace faulty sensors or devices. One other important benefit of the modem connection to the bridge was the ability to modify the program being run in the dataloggers. This was especially beneficial to the research team early on in the project when it was still being decided what data we were seeking and how that data was being collected (i.e., sensor scan rates, trigger values, etc.). Early in the project, modifications to the program were a common occurrence and the modem connection proved invaluable. As monitoring progressed and program parameters were fine-tuned, the scope of the monitoring goals was determined and the need to modify the programs diminished.

Since the bridge site was nearly 320 kilometers (200 miles) from the university, it was also important to establish communication to allow for the downloading of acquired data. If data was acquired and stored in the dataloggers until retrieval, there would be a possibility that sensors could be malfunctioning or not producing the desired data, and weeks to months worth of data could be lost in the time period it took for the research team to make a visit to the bridge to retrieve data and discover any problems. Establishing a modem connection between the bridge and the university allowed for scheduled downloads of acquired data and immediate analysis to ensure successful results. A schedule of bi-weekly remote data downloads was established to obtain data for analysis, as well as for general equipment observation.

3.2.7 Data Acquisition Methodology

As previously stated, the two primary goals of this research are to provide quantitative data and evaluation for the live load stresses and strains experienced by the bridge due to vehicular traffic, and to evaluate the stresses and movements experienced by the bridge due to both daily and seasonal environmental influences. As described in the following pages, the approach to acquiring data for these two purposes varied greatly. As described, both the vehicular and thermal goals of this project used varying sensors, data acquisition algorithms, and criteria in order to obtain the desired data.

3.2.7.1 Vehicular Data

In order to evaluate the effects of the vehicular live load traffic on the bridge, relevant strains in various parts of the girders were measured. As this bridge is simply supported, it was easy to estimate that the maximum tensile strain was occurring in the bottom flange of the girder at mid-span.

Early in the project, trial live load runs (both static and dynamic) were conducted with a control loaded truck provided by the Wisconsin DOT. For these runs, all sixteen of the strain gages were used in each of the girders. A sample of the data acquired from these trial runs is shown in Figure 3.11. Based on these field measurements, the research team was able to observe that the strain readings in gages 11 and 12 were similar (within 2-3 microstrain, 0.06 ksi) due to the truck loading. Thus, the research team was able to conclude that to evaluate the most critical fatigue detail categories in the bridge and in order to evaluate maximum strain cycles and frequency of occurrences for this research, only one gage needs to be used. That would be the gage experiencing the maximum strains and occurrences, which, in our case is gage 10. For the purposes of

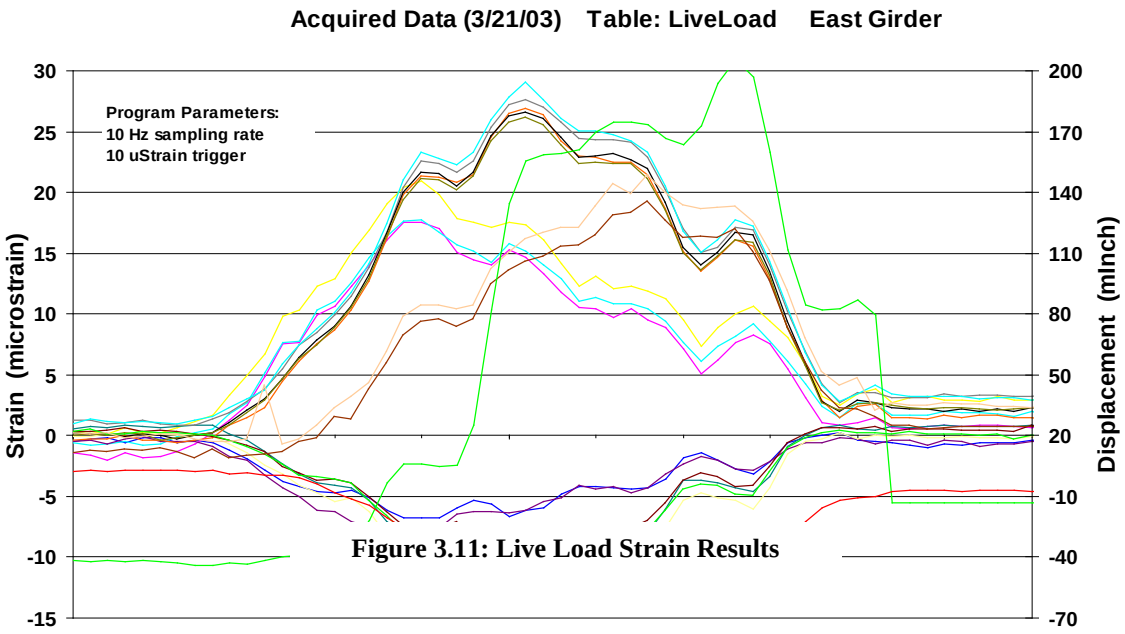

Figure 3.11: Live Load Strain Results

vehicular traffic, only gages 9, 10, and 11 were monitored. Since gages 9, 10, and 11 all have approximately the same strain readings, all three were monitored for redundancy and verification, while also providing backup data in case one of the gages was to produce faulty readings.

Since the purpose of the vehicular strain data was to record only the strains experienced due to vehicular live load traffic, one of the challenges was to find a way to remove the strains experienced in the steel due to thermal effects occurring at the same time as the live load occurrences. To accomplish this, the monitoring program was altered to "zero out" the strain reading on gages 9, 10, and 11 every five minutes to remove any gradual "drifting" of the strain readings due to thermal effects. Thus, all strain readings recorded by these gages would be due to live load traffic only.

To aid in recording strain cycles and frequency of occurrences, the research team utilized a rainflow cycle counting histogram which is run and reported directly by the CR5000 datalogger's data acquisition software. The research team was able to set the thresholds of the low and high strain cycles to be recorded by the program, as well as the

number of bins to divide into the range of the acquired strain data. It was chosen to use the minimum and maximum strain cycles as 25 and 195 microstrain, respectively. Between these values, data was divided into 19 bins, providing bins for every 10 microstrain. The minimum value of 25 microstrain was chosen since the corresponding stress is 0.725 ksi. Any values below this do not contribute significantly to reducing the fatigue life of the structure, and also there are many smaller recorded strain cycles created due to electrical "flutter" and due to typical small vehicular car traffic. This study aimed at focusing primarily on vehicular cycles due to larger truck loads. The maximum value of 195 microstrain was chosen since the corresponding stress is 8.55 ksi. In observing sample data early in this research, it was observed that no strain cycles could be expected to create a stress this high in the bridge structure. This rainflow data was then reported weekly, providing the number of cycles occurring in each of the strain cycle ranges for the given week. This weekly data was then manually compiled into monthly and yearly results, which will be presented later in this report.

3.2.7.2 Thermal Data

To evaluate the results of thermal effects on the bridge structure, the research team recorded the thermal strain being experienced relative to the displacements of each girder and the recorded steel temperature and outdoor ambient air temperature. Hereafter, this will be referred to as the "thermal response".

Early in the project, the research team sampled some continuous data acquisition to evaluate the thermal strains and movements occurring in the structure. This data included the observation of all sixteen of the strain gages to help gain an understanding of the where the greatest strains were occurring in each girder. Some of the data from these

trials is shown in Figure 3.12. As a result of this data, the research team was able to recognize that outdoor ambient air temperature was not so much the principle cause of the strains observed at various gages; rather, it was the presence of sunlight on the exterior surfaces of the bridge.

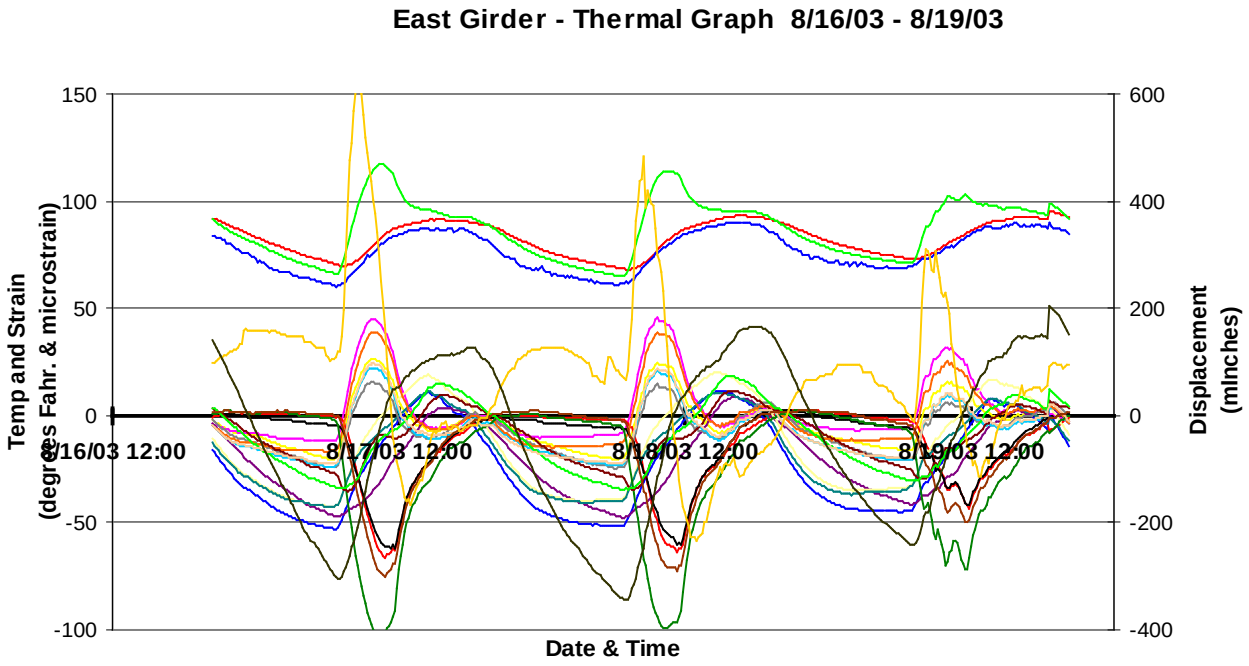

Figure 3.12: East Girder- Thermal Trial Results

On one of the early site visits to the bridge, the research team used an infrared thermometer to record the temperature of the steel from the inside of the girders at each of the strain gage locations, as well as some readings of the surface temperature of the concrete deck. Temperature readings were taken at 9 am, 12 pm and 2 pm. These results (displayed in Appendix A) were evaluated with respect to the continuous strain monitoring results previously referenced. As a result of these two exercises, the research team was able define the gages and measurements necessary to give a full representation and description of the effects of sunlight and thermal variations on the bridge structure.

For evaluating the “thermal response”, the gages monitored were gages 12 and 8 in the east and west girders, respectively. These gages were chosen as the “thermal” gages as they experience the greatest strains due to the presence of sunlight on the steel as they are the gages located on the outside face of each girder.

To evaluate the daily thermal response, gages 12 and 8 were used for the east and west girders, respectively. For this data, the goal was to not only consider the strains being experienced by the thermal gages, but to relate these values to the movements of the girder and the recorded outdoor ambient air temperature and the steel temperatures. For each of these measurement devices, a data point was recorded every 10 minutes. Since the goal of the data was to look solely at thermal effects, the strain and displacement readings were averaged over this 10 minute period. Due to the low volume of traffic on the bridge, this essentially removed the effect of any live loads on the reading as any live load that might occur over this 10 minute period would have adoration of only a few seconds. Clearly, this approach of averaging the strain value would not work as well on bridges which experience large amounts of traffic. In this case, an alternate approach would need to be used, such as signal processing, which would be able to filter out the shorter duration cycles (i.e., live load traffic), leaving the longer duration thermal cycles.

All of the data points reported within this 10 minute period were then averaged and this average value was then recorded in the data table. The recorded data points in this table include thermal strain, vertical deflection, longitudinal expansion/contraction, steel temperature on each face of the bridge girder, and the outdoor ambient air temperature. As presented later in this report, when these data points are displayed for

the duration of one month, they present a very thorough and concise description of the movements of the girders due to thermal effects.

3.3 Load Distribution Study, Equipment, and Set-Up

3.3.1 Strain Measurement

The primary focus of the load distribution study was to measure the strains (leading to stresses) and displacements that were experienced in the bridge girders when vehicular live load was being applied to the bridge. This information is the key to determining the live load distribution factors. In order to accomplish this, 30 electrical resistance strain gages (15 inside of each girder) were installed in the bridge girders. Two linear variable differential transformers (LVDTs) (one in each girder) were installed at the mid-span of the bridge to measure the displacement at the center of the bridge.

The electrical resistance strain gages were set up in a half bridge configuration with "dummy" gages. This configuration was used to offset the effects of fluctuating temperature and the length of wiring that was used to reach certain gages in the bridge. The configuration included two gages, one gage was adhered to the surface of the steel girder, while the other was used as a "dummy" gage. The "dummy" gage was a similar strain gage that was adhered to a small 50 mm x 100 mm x 6.4 mm (2 in x 4 in x ¼ in) steel plate. This steel plate with its "dummy" gage was then placed next to the active age but not attached to the bridge. This way, the "dummy" gage would measure the same interferences that the active gage was affected by and the effect could be subtracted and eliminated easily.

Strain gages were placed at or near the mid-span and quarter-span of each girder. Nine strain gages were placed at mid-span and six strain gages were placed at quarter-

span. The strain gages were placed in groups of three. The first group (MS1) was placed directly at the mid-span. The second group (MS2) was placed half-way between the mid-span and the first external bracing south of the mid-span. The third group (MS3) was placed at the first external bracing south of the mid-span. These three groups were approximately 1,542 mm (5.06 ft) apart. The fourth group of strain gages (QS4) was placed at the first external bracing north of the quarter-span. The fifth group (QS5) was placed directly at the quarter-span. These two groups were placed approximately 3,322 mm (10.90 ft) apart. Figure 3.13 shows the locations of the five strain gage groups.

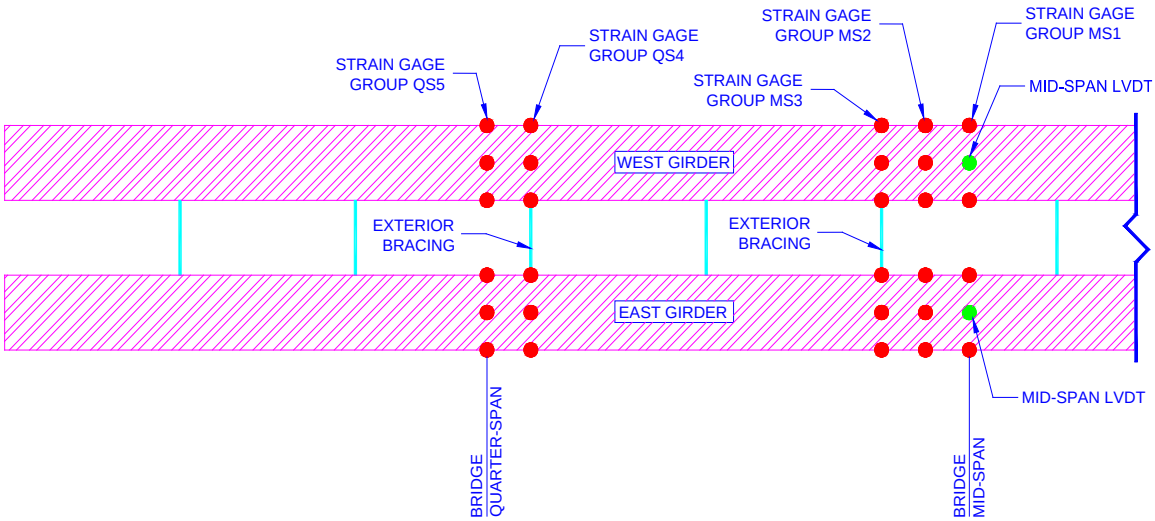

Figure 3.13: Strain Gage Group Locations

For each group, strain gages at the underside of the top flanges were approximately 50 mm (2 inches) from the flange/web weld line and the bottom flange strain gage in each girder was placed at the middle of the corresponding bottom flange. Figure 3.14 shows the locations of all of the gages. The locations of the strain gages were chosen so an accurate description of the stress at different points on the bridge can

be determined. The selected gage locations also allowed the effect of the external bracings to be determined for the live load distribution factors.

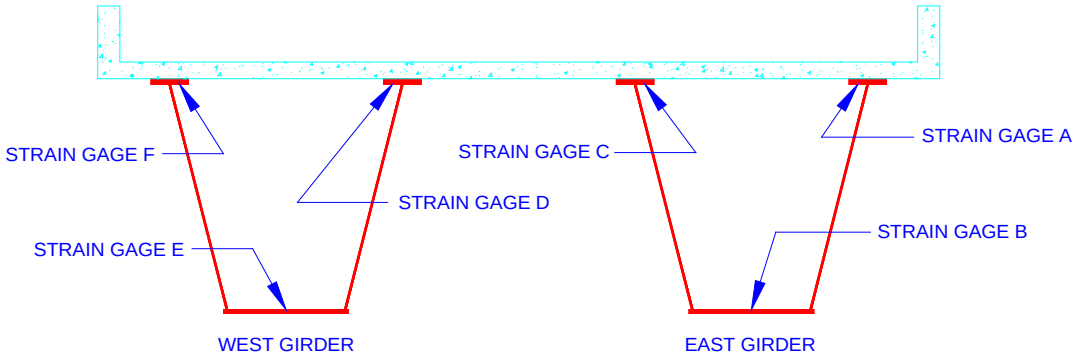

Figure 3.14: Strain Gage Numbering Convention and Locations

The strain gages that were applied directly at the mid-span and quarter-span locations were Vishay/MicroMeasurements weldable 350-ohm resistance strain gages. These gages were used to perform the bridge monitoring and were used to verify that all other gages were in proper working condition over long term. The strain gages applied at the other locations were Measurement Group epoxy adhered 120-ohm resistance strain gages. The area where each new strain gage was to be applied was first prepared by grinding off the paint, cleaning, and properly preparing the surface of the steel for the strain gage application. Epoxy adhered strain gages were used in most locations due to the short amount of time that the strain gages were going to be used.

3.3.2 Deflection Measurement

The mid-span deflection in each girder was measured following the same approach as that used under the structural monitoring study, as shown in the earlier sections in this chapter.

3.3.3 System Calibration

All data acquisition units and sensors were calibrated prior to the start of the field testing program following a similar approach to that used for the structural monitoring study, as shown in the earlier sections in this chapter.

3.3.4 Communication

To ensure synchronization of data acquisition, the two data acquisition units were linked together with a communication line. This link would allow the research team to start/stop the data acquisition units at the same time. This was important so all data from gages and LVTs was taken at the same time for each truck run. This allowed the research team to compare data from different sensors at specific times. The link between the data acquisition units was also used to zero out both units prior to the start of each test. This arrangement allowed the research team to operate the data acquisition units from inside of only one girder.

3.3.5 Data Acquisition

Live load distribution factors in the bridge were calculated based on the measurement of strains at different locations and converting those values to stresses and loads distributed to different girders in the bridge.

3.3.5.1 Sensor Relativity

Due to the geometrical configuration and corresponding boundary conditions in the bridge, it was decided to apply the strain gages only at the mid-span and quarter-span locations. At the mid-span location, three sets of gages were applied across the bridge's cross-section and two sets of gages were applied at quarter-span. Each set of gages

consisted of strain gages on all four top flanges and the two bottom flanges. The LVDTs where used at the mid-span of each girder to verify the effect of live loads on the bridge.

3.3.5.2 Truck Loading

With the assistance of the staff from the southwest regain of the WisDOT, the bridge deck was loaded with one and two test trucks during the field testing stage of this study. Fifteen different truck loading configurations were identified and used to verify the load distribution to each of the girders. These configurations were a combination of the trucks moving at a crawling speed and at highway speed to represent static and dynamic loading on the bridge, respectively. The truck weights were reported as the total truck weight and per axle. The front axle weights were 6.65 and 5.83 tons (13.3 kips and 11.66 kips) for trucks one and two, respectively. The rear axle weights were 11.65 and 13.72 tons (23.3 kips and 27.43 kips) for trucks one and two, respectively. The trucks' wheel spacing and tire contact surface were recorded and used in the analytical modal. The center-to-center wheel spacing at the front and rear axles was 1.83 and 2.0 m (6.0 and 6.67 ft), respectively. The front and rear wheel contact surface dimensions were 240x240 and 381x279 mm (9.5x9.5 and 15x11 inches), respectively. The distance between the front and rear axles for both trucks was 4.42 m (14.5 feet). Chalk lines were drawn on the bridge deck prior to driving the test trucks over the bridge to ensure the truck loads were in properly designated lanes. To ensure that the collected strain data was associated with only the truck loadings, all gages and LVDTs were zeroed out prior to every truck run.

CHAPTER 4

NUMERICAL ANALYSIS

4.1 Modeling Assumptions and Preparation

In order to determine the live load distribution factors for the Land Bridge, a 3-D numerical analysis was performed using a commercially available finite elements software (ANSYS). The following assumptions were made for the numerical analysis. Also, some initial assumptions were made in modeling the bridge using a CAD software (AutoCAD).

4.1.1 3-D Modeling with CAD

AutoCAD was used to model the bridge in 3-D. The bridge was modeled with no vertical curvature however the horizontal curvature and superelevation were considered per the bridge's design plans. The girders' top flanges, bottom flanges, webs and bearing stiffeners were also modeled per the bridge design plans. The lateral cross bracing inside and outside of the girders were modeled as rectangular members with the same equivalent area as the members shown on the design plans (See Figure 4.1). The interior and exterior web stiffeners that also served as connection plates for the cross bracings were modeled as rectangular plates with the same section modulus as the members shown on the bridge design plans (See Figure 4.1).

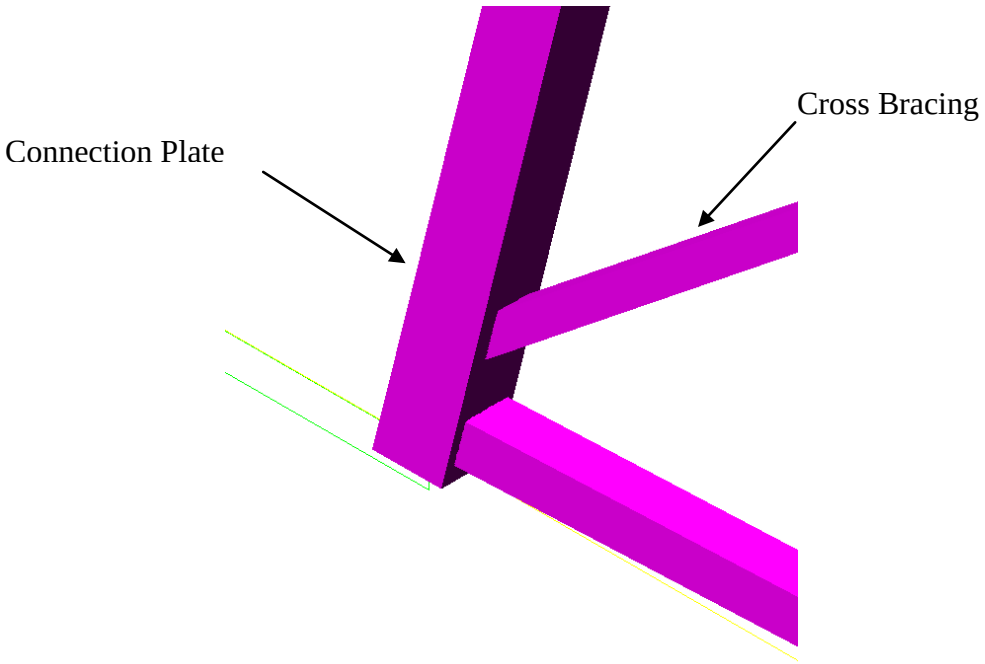

Figure 4.1: External Lateral Bracing 3-D Modeling

The horizontal interior bracings that run parallel with the flanges of the bridge girders were not modeled. The research team decided that these members were not effective in the finite elements model and that they were primarily used for stiffening the girders prior to the concrete deck placement and hardening. The concrete deck and parapets were modeled as plain concrete but the effect of the steel reinforcement was considered separately as it is discussed later under the ANSYS software section of this report. The steel railing that is attached to the concrete parapet was not included in the model as its effect was considered insignificant. The concrete haunches in the bridge deck were modeled with constant thickness and only varied at the locations were the top steel flanges varied in thickness.

Load bearing plates at each girder ends and on the bridge deck were included in the model to allow load transfer to the girders at the supports and at the locations of truck

wheels. A 1690 mm x 305 mm x 51 mm (66.5 in x 12.0 in x 2.0 in) plate was used at each end of the girders bearing plates (See Figure 4.2).

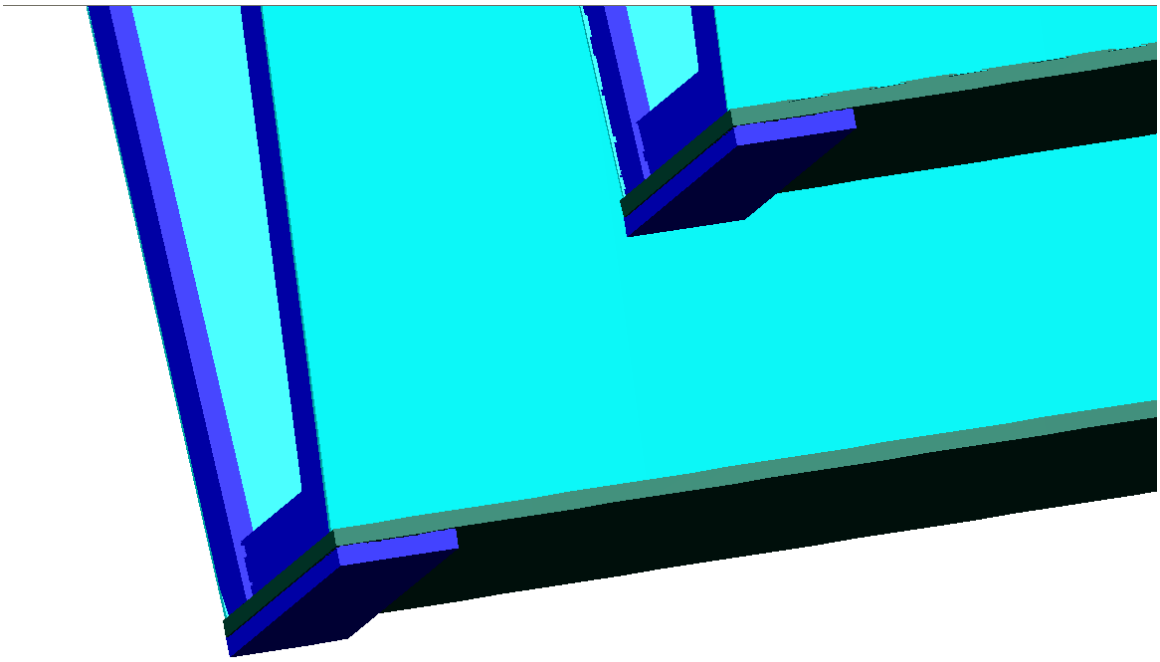

Figure 4.2: Bearing Plates

The load bearing plates on the bridge deck would allow the trucks' wheel load to be applied as a pressure load and not as a point load (See Figure 4.3). The front wheel load plates were modeled as 240 mm x 240 mm (9.5 in x 9.5 in) and the rear wheel load plates were modeled as a square 330 mm x 330 mm (13.0 in x 13.0 in) plates. The plate sizes were based on the actual surface area of the WisDOT trucks used in the field test. These plates varied in thickness due to the superelevation in the curved bridge. The truck wheel bearing plates were oriented on the bridge deck under two configurations. The first configuration allowed for up to three trucks to be placed on the bridge deck. Here, the first truck would be located 2 feet from the parapet wall on the east side of the bridge and each additional truck would be located at a distance of 4 feet from the previous truck.

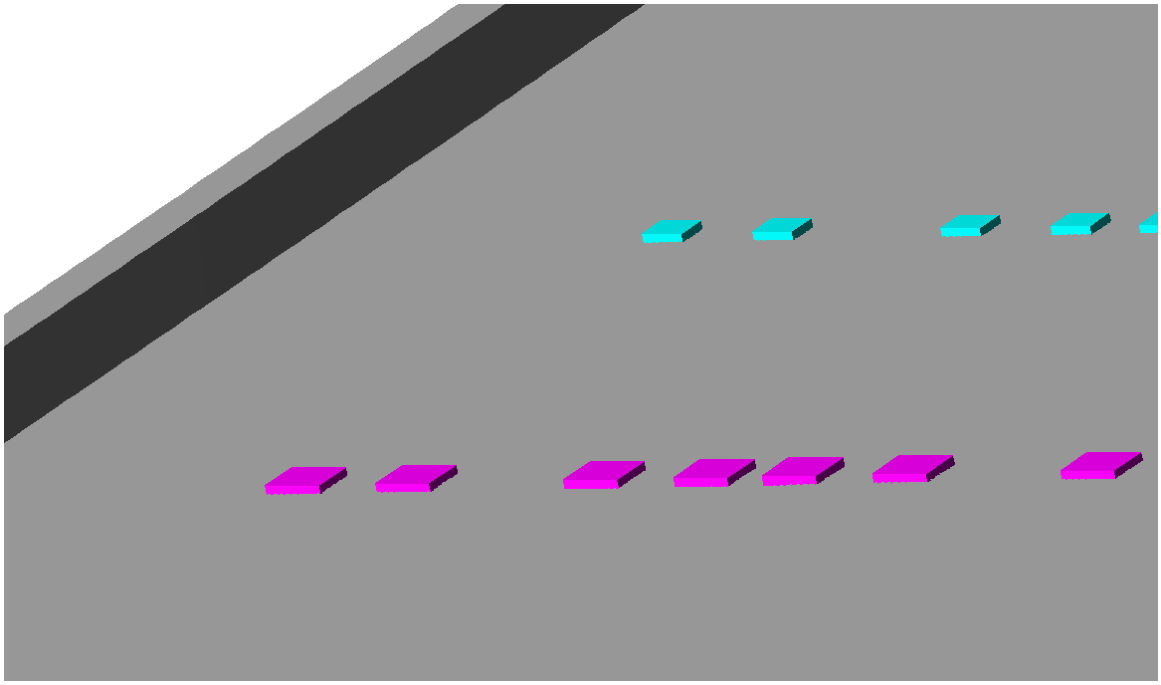

Figure 4.3: Front and Rear Wheel Loading Pads

The second configuration consisted of truck wheel load plates on the deck to allow placement of up to two trucks on the bridge deck. This configuration allowed a truck to be placed 2 feet from the centerline of the bridge on either side. This configuration accounts for the trucks driving in their respective drive lanes. Both of these configurations were placed at every eighth points on the bridge deck along the length of the bridge.

4.1.2 Finite Elements Modeling

One of the assumptions made for the finite elements modeling of the bridge was that the effect of steel reinforcement in the deck and concrete parapet was taken into account by proportionately increasing the modulus of elasticity of the concrete to yield the same effect from concrete with steel reinforcement. The increase was determined to be based on the cross sectional area of concrete in the deck, the area of longitudinal steel reinforcement and the ratio of the steel to concrete moduli. In order to accurately model

the composite action between the top flanges of the box girders and the concrete deck, the two member types were modeled as bonded (attached continuously). In order to increase the efficiency of the numerical analysis, the cross braces in the bridge were modeled as shell elements (See Figure 4.4). These elements were chosen with the same structural properties as the 3-D bracing elements. The bearing stiffeners at the end of each girder were also modeled as shell elements to improve the efficiency of the analysis (See Figure 4.4). Additional enhancement of the analysis efficiency was achieved by implementing the sweep meshing option of the software for the bridge deck, top flanges, webs, and bottom flanges to reduce the geometric degrees of freedom while maintaining the desired level of accuracy of the analysis. This sweeping option created a mesh consisting of rectangular elements with fewer nodes (See Figure 4.5).

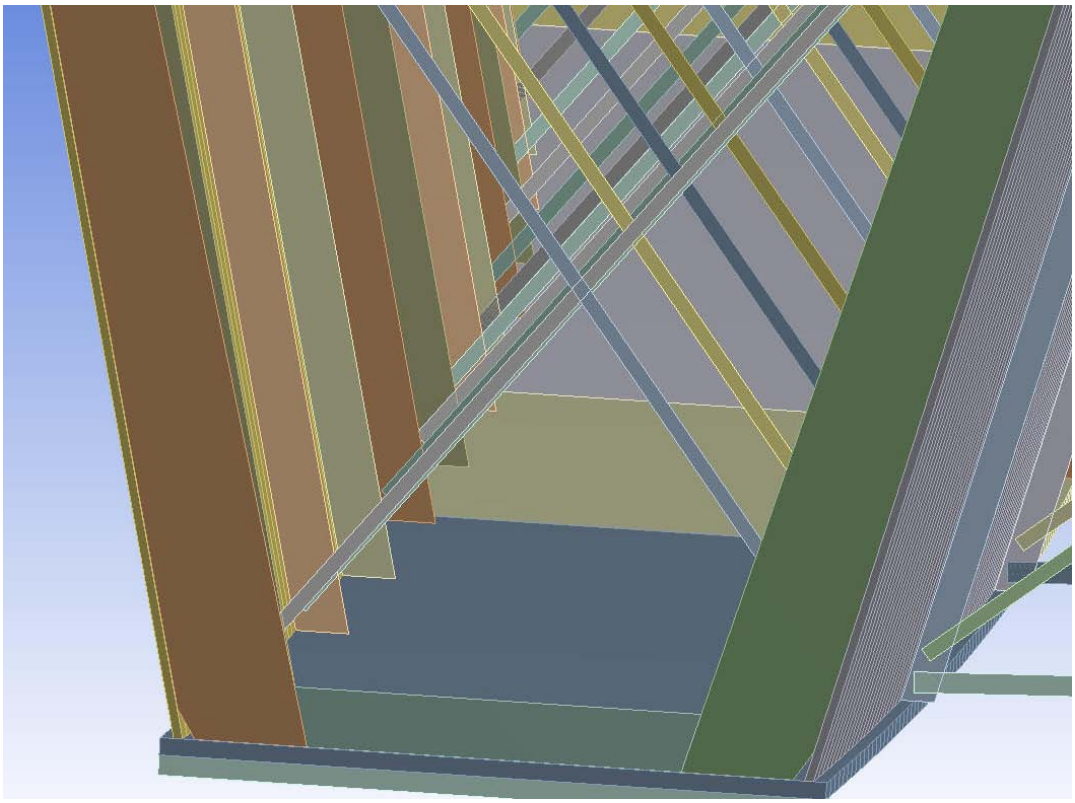

Figure 4.4: Shell Elements of the Lateral Bracings and Bearing Stiffeners

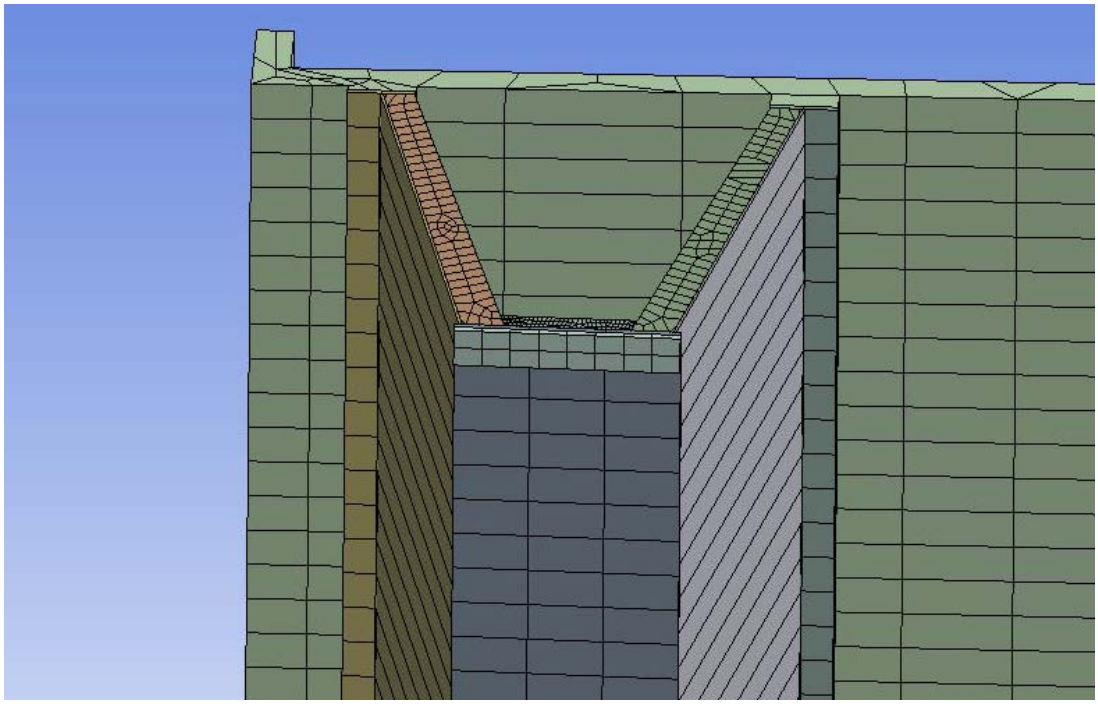

Figure 4.5: Meshing Using the Sweep Method

Established values of material properties were used for each element except for the concrete deck and parapet walls where the modulus of elasticity value was adjusted to take into account the effect of reinforcing steel. For the steel girders and cross bracing members, the value of the modulus of elasticity was used as 200 MPa (29,000 ksi). The modulus of elasticity value for concrete deck and parapet walls was adjusted to 31 MPa (4,500 ksi). To assure adequate rigidity, a large value of modulus of elasticity was chosen for the bearing pads that were modeled at the ends of each girder. The wheel load pads were given a small modulus of elasticity value to ensure that there would be no stiffening effect on the girders.

4.1.2.1 Boundary Conditions

To simulate the real conditions in the bridge, the finite elements model included appropriate boundary conditions at the end of each girder. At the north end of each box girder, a pin support with only free girder end rotation was introduced in the model. At

the south end of each girder, the imposed boundary condition in the model included only free end rotation and longitudinal displacement.

Probes, or results indicators, were introduced in the model at the locations of the supports to record reaction forces for a given load. Recorded reaction forces were used to verify the accuracy of the model under various loading conditions in the early stages of the numerical analysis to validate the accuracy of the assumptions and the analysis procedure.

4.1.2.2 Applied Loads

As discussed earlier in the discussion of the finite elements modeling, each front or rear truck wheel load was applied as a distributed load (pressure) over its appropriate load pad. The wheel loads and the corresponding pressure magnitudes used in the finite elements model were based on the averaged values from the two WisDOT trucks used during the field testing. It must be noted that the overall weight of the two trucks and their corresponding axle loads were nearly the same and the use of the averaged values was justified. Accordingly, pressure values of 482.6 kPa (70.0 psi) and 517.1 kPa (75.0 psi) were used for the front and rear wheels, respectively. The use of this approach, simplified the placement of more than one truck on the bridge deck for the purpose of the finite elements analysis (See Figure 4.6). In the figure, the square areas shown in red represent the wheels loads applied on the deck. The actual axle loads for both trucks were also used in separate finite elements analyses to verify the results through comparison with the field results.

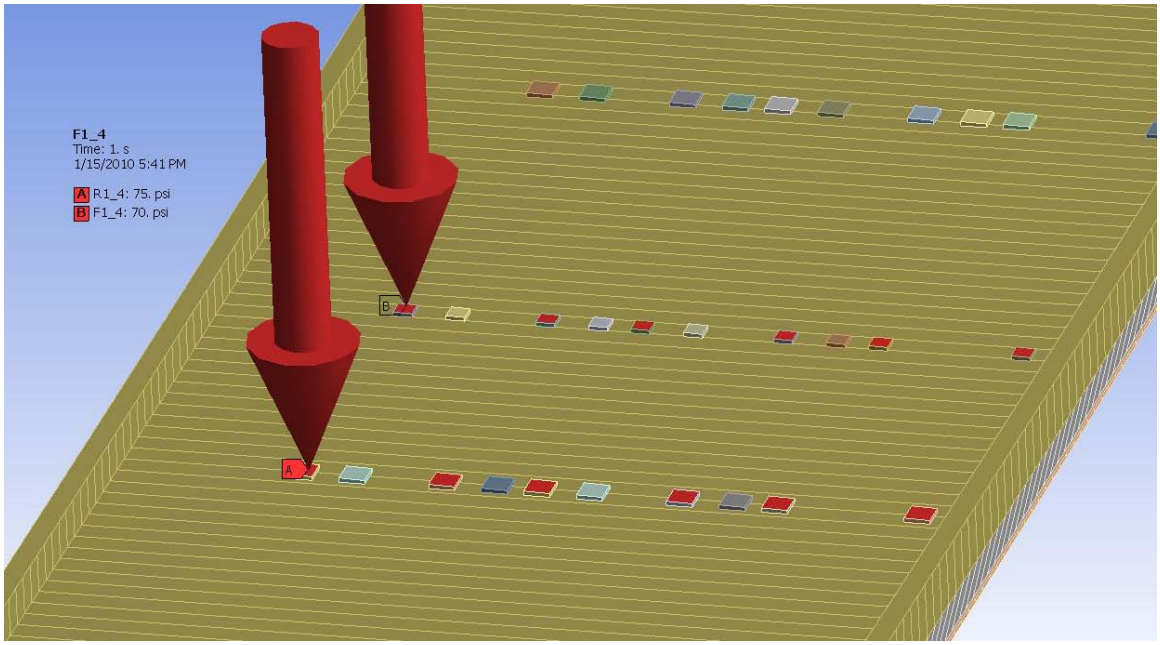

Figure 4.6: Axle Loads Applied on the Bridge Deck (3 Trucks)

CHAPTER 5

RESULTS AND DISCUSSION

Results from both the structural monitoring and live load distribution factor study are presented in this chapter of the report.

5.1 Structural Monitoring

Graphs and results presented in the following sections represent data collected at the bridge site between April 1, 2004 and August 31, 2008.

5.1.1 Live Load Cycles

Live load results for the first four years of data collection have offered good consistency. As can be seen in Figures 5.1 and 5.2, data for both east and west girders shows consistent results from year to year. No significant changes in the traffic load pattern were observed over the four years of monitoring. 100% of all traffic stress range results were within +/- 2 standard deviations of the corresponding mean value. It was found that 79% of all traffic stress range results were within +/- 1 standard deviation of the corresponding mean value. Comparisons of traffic load cycles between the east and west girders indicate that the east girder experiences more cycles than compared to the west girder in almost all stress ranges. This indicates that a majority of the traffic flow for this bridge is over the east girder, traveling north. Figure 5.3 displays a comparison of the average traffic stress cycles experienced in the typical year. Results show that a majority (approximately 95%) of the traffic stress cycles occur at the 9.0 MPa (1.3 ksi) stress range and lower, with the remaining stress cycles occurring in the 11.0 to 26.9 MPa (1.6 to 3.9 ksi) ranges.

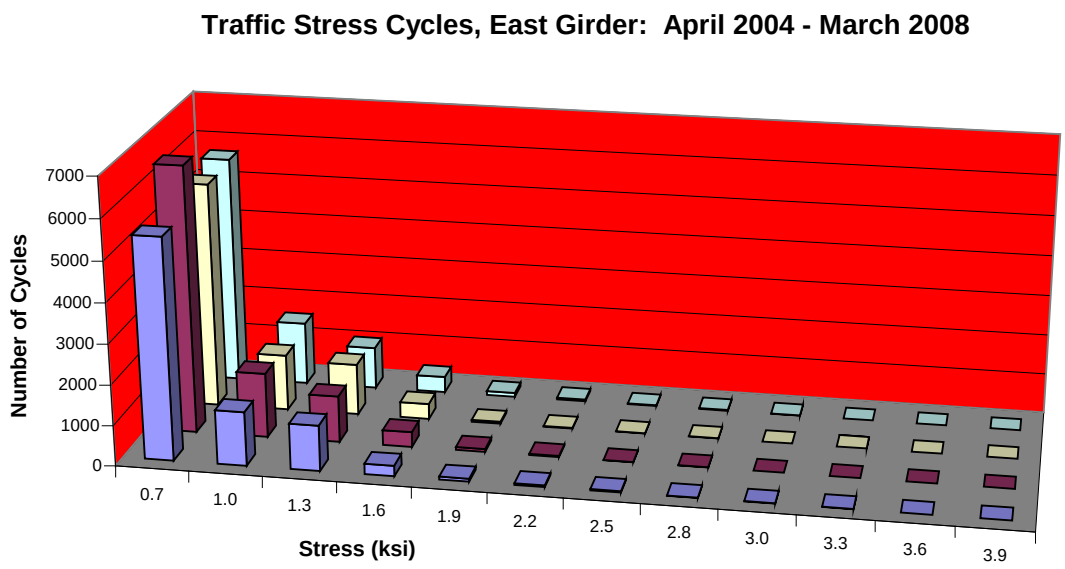

	0.7	1.0	1.3	1.6	1.9	2.2	2.5	2.8	3.0	3.3	3.6	3.9
Year 1	5475	1334	1124	262	74	42	32	9	6	6	0	1
Year 2	6615	1601	1149	372	74	30	8	4	1	1	0	0
Year 3	5606	1389	1271	382	49	18	6	7	0	2	0	0
Year 4	5687	1565	1038	397	99	47	24	21	4	2	0	0

Figure 5.1: Traffic Stress Cycles, East Girder: April 2004- March 2008

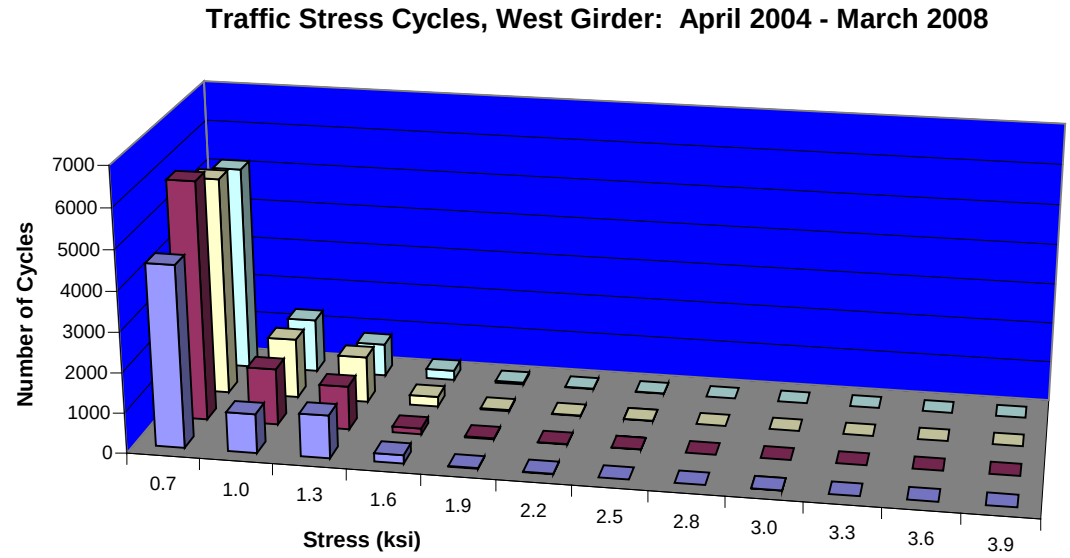

	0.7	1.0	1.3	1.6	1.9	2.2	2.5	2.8	3.0	3.3	3.6	3.9
Year 1	4528	975	1068	209	20	13	4	3	3	0	0	0
Year 2	5974	1406	1087	147	26	7	5	0	3	1	0	0
Year 3	5469	1493	1152	246	33	12	4	1	0	1	0	0
Year 4	5167	1342	819	240	47	14	7	0	2	3	0	2

Figure 5.2: Traffic Stress Cycles, East Girder: April 2004 – March 2008

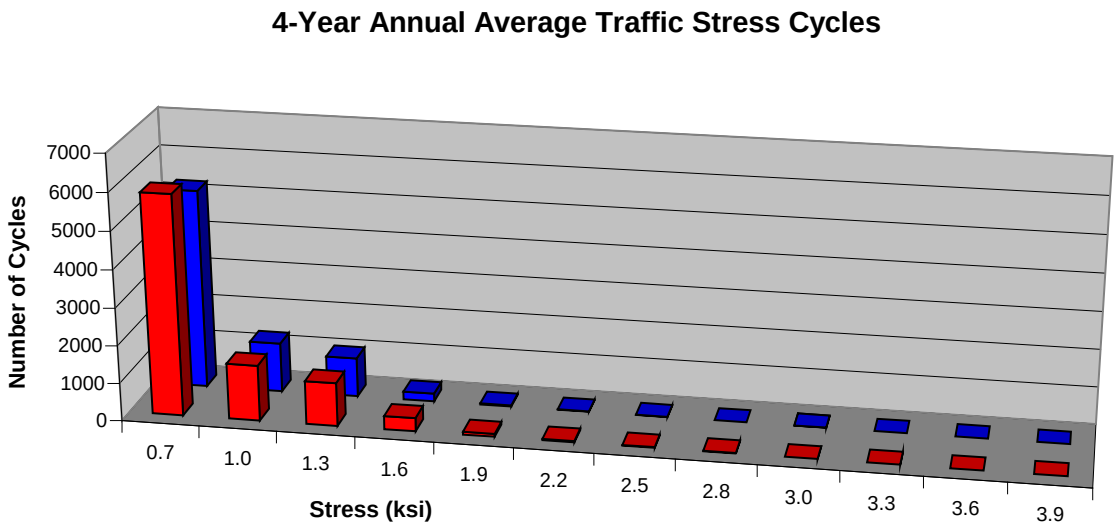

	0.7	1.0	1.3	1.6	1.9	2.2	2.5	2.8	3.0	3.3	3.6	3.9
East Girder	5846	1472	1146	353	74	34	18	10	3	3	0	0
West Girder	5285	1304	1032	211	32	12	5	1	2	1	0	1

Figure 5.3: 4-Year Annual Average Traffic Stress Cycles

5.1.2 Thermal Cycles

This study quantifies the effects of thermal cycles on the Land Bridge structure. As previously indicated, gages 12 and 8 were used to record "thermal" strains for the east and west girders, respectively. During each month of the 4-year monitoring program, thermal response data from gages 8 and 12 was integrated with those for girder displacements, girder wall temperature, and outside air temperature. Graphs similar to those shown in Figures 5.4 and 5.5 were prepared for each month.

Based on the thermal responses in the Land Bridge, the following observation is made regarding the stresses and movements of each of the girders within the typical cycle of one day. The east girder experiences maximum strain/stress at about 11 a.m., which is just past the point of maximum sun exposure to the east face of the girder. Minimum observed strain/stress in gage 12 occurs in the early a.m. hours. The maximum

longitudinal expansion of the east girder occurs at 7 a.m., which would correspond to the earliest occurrence of full sun exposure on the east face of this girder. The maximum contraction of the east girder occurs at 8 p.m. Typical daily values of expansion/contraction of the east girder range from 0.25 in to 0.75 in.

The mid-span deflection response of the east girder is more complex due to differential temperature values in the steel boxes and concrete deck during different hours in a typical day. At approximately 7 a.m., the east girder experiences a point of maximum downward deflection, due to temperature increase and associated expansion of the steel in the east girder while the concrete deck remains “cold”. During the following hours, the sun moves higher and causes a temperature increase in the concrete deck. At mid-day, when the sun is at its’ highest in the sky, the east girder is at its maximum upward deflection due to the temperature increase in, and expansion of, the concrete deck while there is a temperature reduction in the steel below the concrete deck. At about 4 p.m., the east girder again experiences a downward deflection, caused by and corresponding to the downward deflection of the west girder as it begins to receive full sun exposure on the west face of the girder. At approximately 8 p.m., the east girder again reaches a point of maximum upward displacement, which corresponds to the maximum downward deflection of the west girder. This phenomenon is likely due to the slight curvature, or sweep, in the bridge as shown in Figure 3.4. Typical daily ranges of this vertical movement of the east girder range from 6 to 18 mm (0.25 to 0.75 in).

The west girder experiences maximum strain/stress in gage 8 during the evening hours between approximately 5 p.m. and 8 p.m., which is just past the point of maximum sun exposure to the west face of the girder. Minimum observed strain/stress on gage 8

typically occurs in the early to mid-morning a.m. hours. The maximum longitudinal expansion of the west girder occurs at about 7 p.m., which would correspond to full sun exposure on the west face of this girder. The maximum contraction of the west girder occurs at about 7 a.m. Typical daily values of expansion/contraction of the west girder range from 6 to 18 mm (0.25 to 0.75 in).

The observed daily mid-span deflection of the west girder is explained as follows. At approximately 10 a.m., the west girder experiences a point of maximum upward deflection, caused by the warming up of, and expansion of, the steel in the east girder as well as the warming of the concrete deck. From about 10 a.m. on, the west girder begins to deflect in the downward direction. This seems to be unexpected as the west face of the west girder does not start receiving sun exposure, which would cause the downward deflection, until approximately 2 p.m. This is likely again caused by the sweep of the bridge. Between 6 p.m. and 8 p.m., the west girder experiences its maximum downward deflection, caused by full sun exposure on the west face of the girder. Typical daily ranges of this vertical movement of the west girder range from 6 to 18 mm (0.25 to 0.75 in).

To gain an understanding of the numbers of thermal stress cycles being experienced in the typical year, the strain cycles from each of these months were then converted to the corresponding stress ranges and presented in Figures 4.6 and 5.7 to present the thermal stress cycles experienced throughout the year. Note that the data presented for each of the years presents 365 data points, representing one stress cycle for each day.

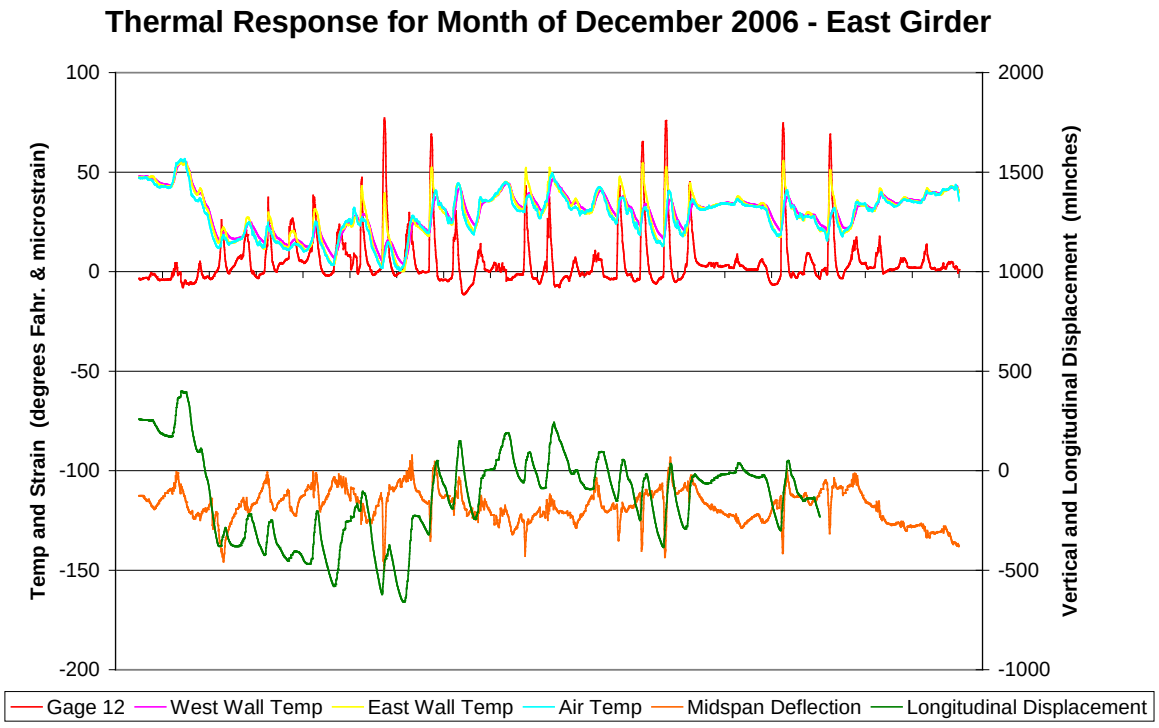

Figure 5.4: Thermal Response for Month of December 2006- East Girder

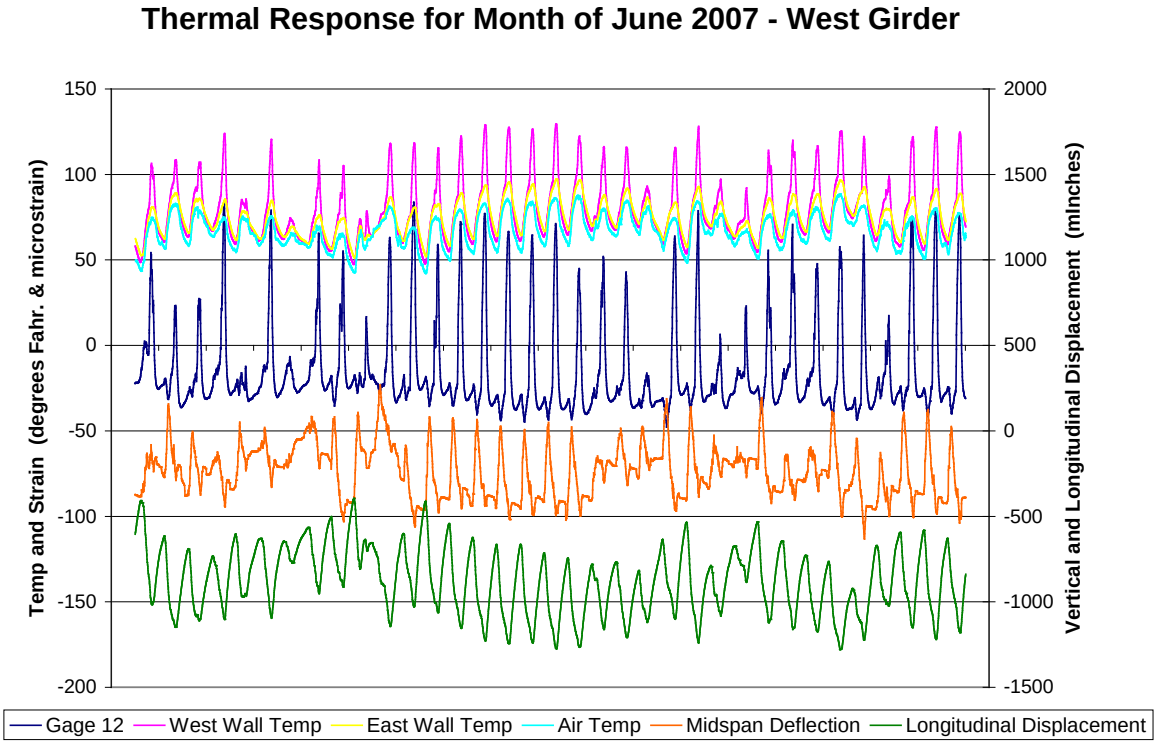

Figure 5.5: Thermal Response for Month of June 2007- West Girder

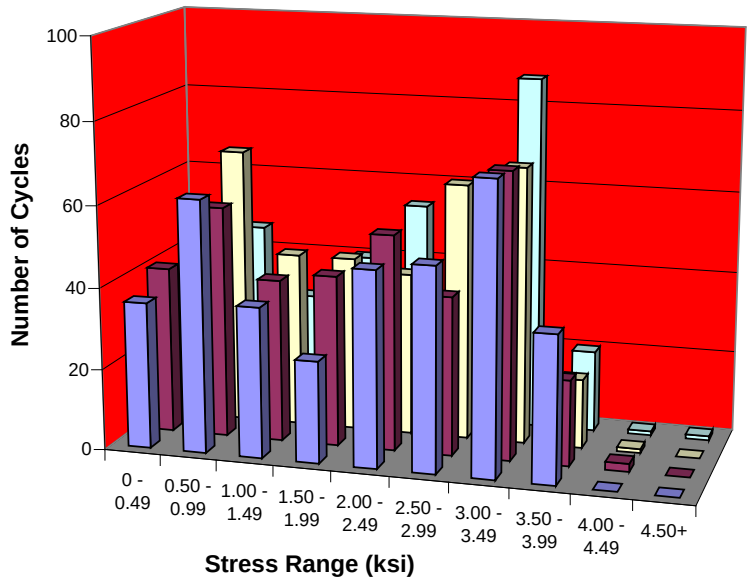

	0 - 0.49	0.50 - 0.99	1.00 - 1.49	1.50 - 1.99	2.00 - 2.49	2.50 - 2.99	3.00 - 3.49	3.50 - 3.99	4.00 - 4.49	4.50+
2005	36	62	37	25	48	50	71	36	0	0
2006	41	57	40	42	53	39	70	21	2	0
2007	22	68	43	43	40	63	68	17	1	0
2004/2008	40	46	29	40	54	48	87	20	1	1

Figure 5.6: Distribution of Yearly Thermal Stress Cycles, East Girder: 2004 - 2008

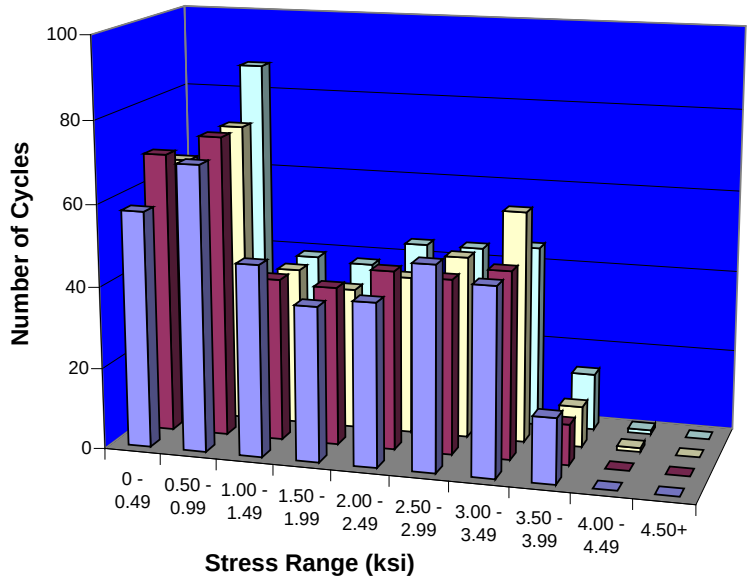

	0 - 0.49	0.50 - 0.99	1.00 - 1.49	1.50 - 1.99	2.00 - 2.49	2.50 - 2.99	3.00 - 3.49	3.50 - 3.99	4.00 - 4.49	4.50+
2005	58	70	47	38	40	50	46	16	0	0
2006	69	74	40	39	44	43	46	10	0	0
2007	65	74	39	35	39	45	57	10	1	0
2004/2008	53	87	39	38	44	44	45	14	1	0

Figure 5.7: Distribution of Yearly Thermal Stress Cycles, West Girder: 2004 - 2008

Figure 5.8 displays the average distribution of thermal stress cycles per year over a four-year period. As seen, the east girder experiences higher load level cycles in the 13.8 to 27.6 MPa (2.0 to 4.0 ksi) stress ranges than the west girder, while the west girder experiences more cycles in the lower stress ranges of less than 13.8 MPa (2.0 ksi). This can be attributed to the east-west orientation of the bridge structure. As such, the morning sun exposure of the east face of the east girder results in a rapid increase of temperature in the steel. This rapid change in steel temperature is due to the cool temperature in the steel during the night hours and it consequently creates large strain cycles. On the converse side, the west girder stress range cycles occur in the lower stress ranges due to the fact that the temperature of the steel in the west girder increases more gradually, creating smaller strain cycles. While most of the data and graphs presented seem to indicate that the larger strain cycles occur when there is a large difference between air temperature and steel temperature, the actual cause of the larger strain cycle is the rate of change of steel temperature. These figures were based on air temperature simply for ease in comparison and description.

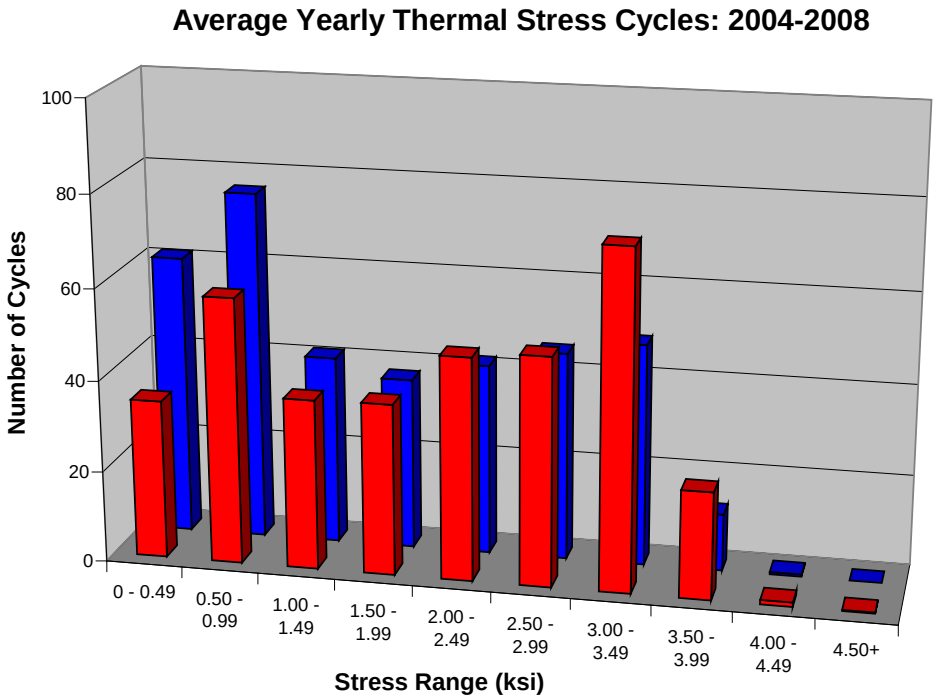

	0 - 0.49	0.50 - 0.99	1.00 - 1.49	1.50 - 1.99	2.00 - 2.49	2.50 - 2.99	3.00 - 3.49	3.50 - 3.99	4.00 - 4.49	4.50+
East Girder	35	58	37	38	49	50	74	24	1	0
West Girder	61	76	41	38	42	46	49	13	1	0

Figure 5.8: Average Yearly Thermal Stress Cycles: 2004 - 2008

Figures 5.9 and 5.10 are scatter plots of the observed daily stress ranges and the wall temperatures observed plotted with respect to the daily air temperature range. These plots show the 4-year data for every day recorded through August 31, 2008.

As seen in Figure 5.9 for the east girder, both the stress ranges and the wall temperature ranges vary linearly with air temperature range. The stress range typically varies by 6.9 MPa (1.0 ksi) for each 10-degree range of air temperature (i.e., a 30-degree range of air temperature typically produces a 20.7 MPa (3.0 ksi) thermal stress range). It was found in this study that the wall temperature range was typically 62% higher than the air temperature range.

Figure 5.10 shows similar results for the west girder. Both the stress ranges and the wall temperature ranges again vary linearly with air temperature range. The stress range typically varies by 5.5 MPA (0.8 ksi) for each 10-degree range of air temperature (i.e., a 30-degree range of air temperature typically produces a 16.5 MPa (2.4 ksi) thermal stress range). Here, the wall temperature range was typically 84% higher than the air temperature range.

The reason behind some of the variations and scatter seen in these graphs is that many environmental factors influence these recorded results. For example, some days with very high temperatures may have a large amount of cloud cover throughout the day, and thus the bridge does not experience much direct sunlight exposure. Similarly, some days which may have cooler air temperatures and clearer skies will experience fairly constant air temperatures, while steel temperatures will vary greatly throughout the day based on the sunlight which radiates on the bridge structure.

Figures 5.9 and 5.10 present a simple way to evaluate what magnitude of stress ranges and wall temperature ranges can be expected in the Land Bridge on any given day based on the air temperature range that is anticipated.

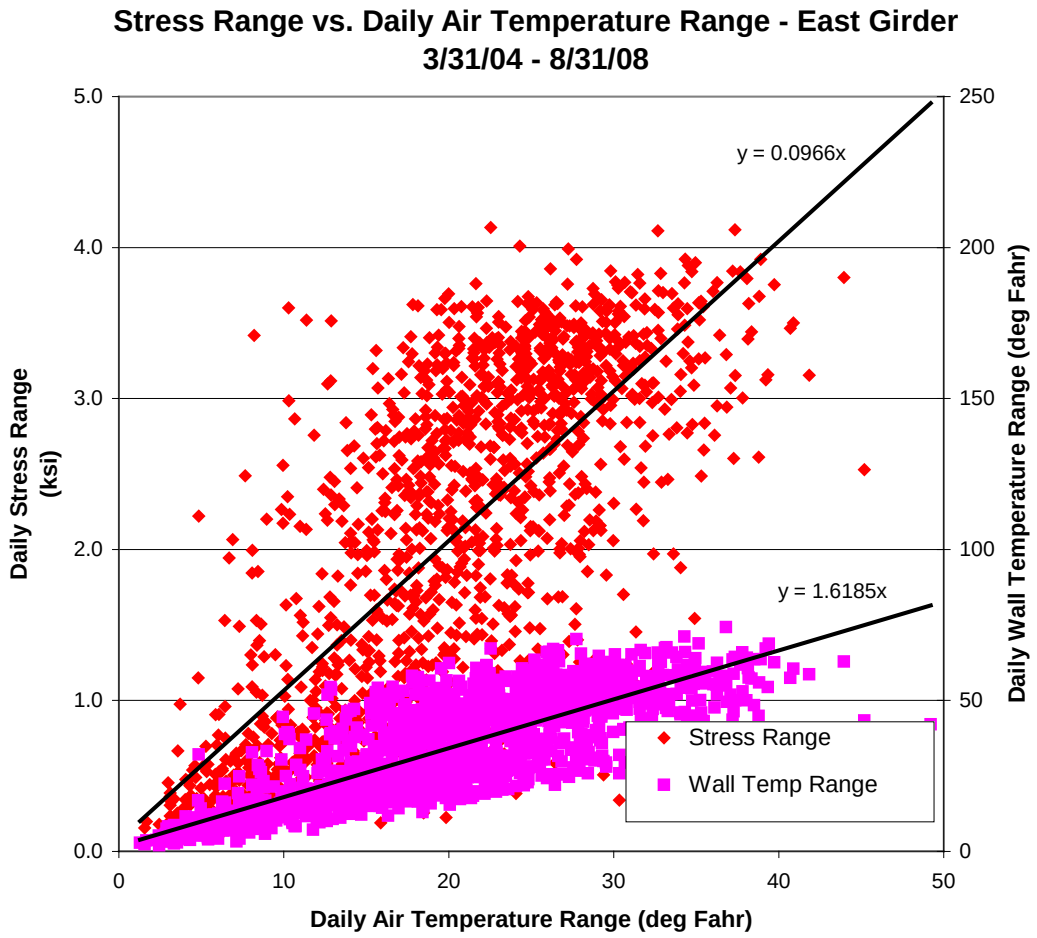

Figure 5.9: Observed Daily Thermal Effects vs. Daily Air Temp. Range- East Girder

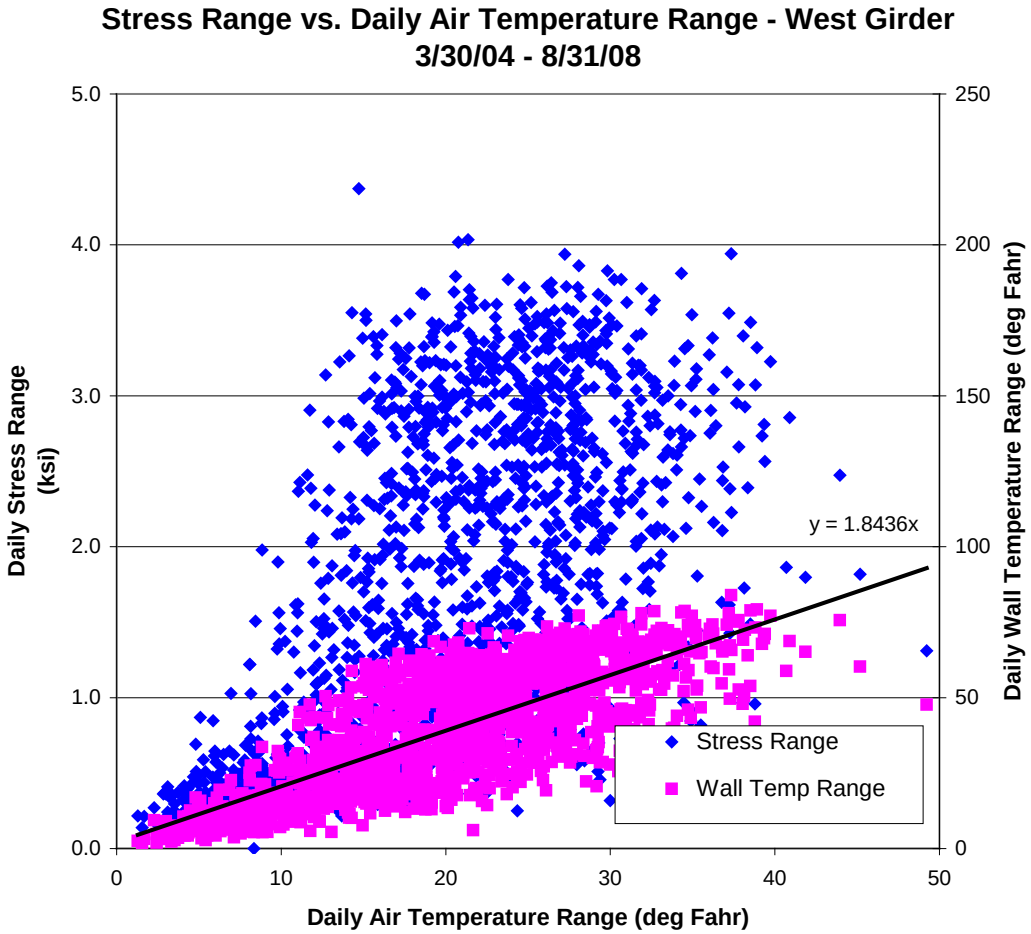

Figure 5.10: Observed Daily Thermal Effects vs. Daily Air Temp. Range- West Girder

Figures 5.11 and 5.12 are scatter plots of the observed displacement ranges and the wall temperatures plotted with respect to the daily air temperature range. These plots show the 4-year data for every day recorded through August 31, 2008.

As seen in Figure 5.11 for the east girder, both the longitudinal displacement and the mid-span deflection ranges vary linearly with air temperature range. For each 10-degree change in the temperature, the change in the longitudinal displacement range is 4.3 mm (0.17 in), i.e., a 30-degree range of air temperature produces a 12.9 mm (0.51 in) longitudinal displacement range. The value of the mid-span displacement range for each 10-degree temperature change is 5 mm (0.2 in).

Figure 5.12 shows similar results for the west girder. Both the longitudinal displacement and the mid-span deflection ranges again vary linearly with air temperature range. For each 10-degree change in the temperature, the change in the longitudinal displacement range is 4.8 mm (0.19 in). The value for the mid-span displacement range is 3.6 mm (0,14 in).

Figures 5.11 and 5.12 present a simple way to evaluate what magnitude of displacement ranges can be expected in the Land Bridge on any given day based on the air temperature range anticipated.

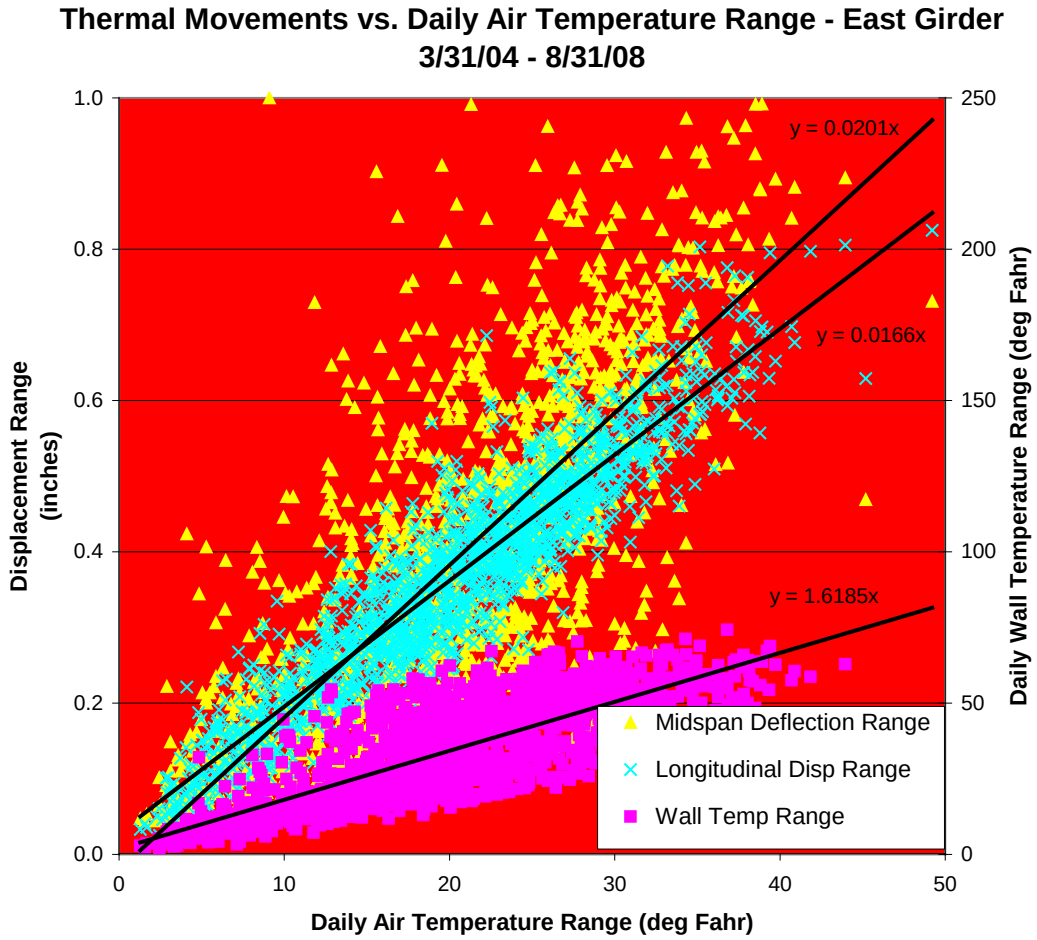

Figure 5.11: Thermal Movements vs. Daily Air Temp. Range- East Girder

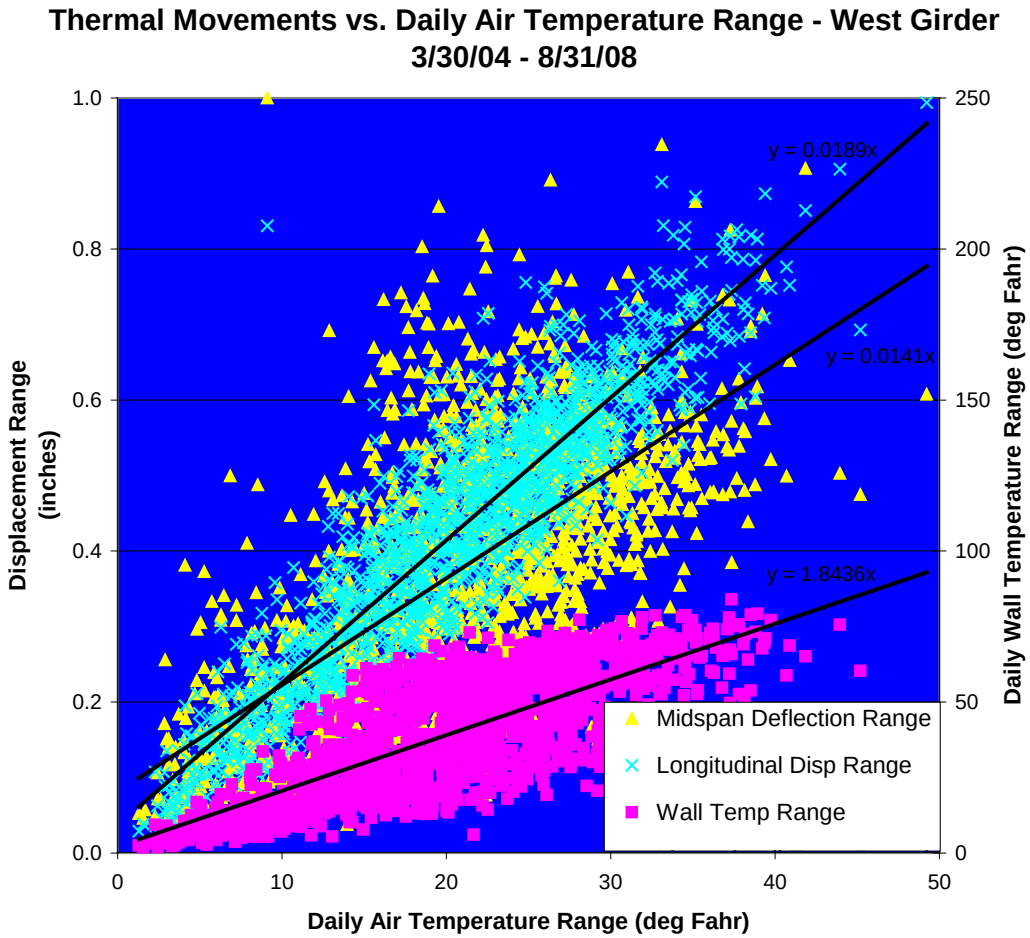

Figure 5.12: Thermal Movements vs. Daily Air Temp. Range- West Girder

5.2 Load Distribution Factor Study

Results for load distribution factors in the Land Bridge are presented here from both a field testing program as well as a numerical simulation based on using a commercially available finite elements software (ANSYS). The results were compared with those from the AASHTO LRFD and standard specifications. In this study, the distribution factors are determined and discussed only for moment.

5.2.1 Distribution Factors from Field Tests

5.2.1.1 Truck Loading Configurations

The research team used several different truck loading configurations to determine moment distribution factors in the Land Bridge. It was found that the maximum distribution factor for the bridge would occur when all the design lanes in the bridge were loaded. Although the bridge is designed for only two lanes of traffic for its normal service life, it was loaded for the purpose of this study as having three lanes of traffic. This was done since there is adequate deck width for three lanes of traffic due to an existing shoulder at each side of the bridge. During the field testing program, only two trucks were available and they were used in 15 different configurations as shown in Appendix C. In order to achieve three loaded traffic lanes, the research staff superimposed the results from two different loading configurations that included a single truck on one side of the deck and a double-truck configuration on the opposite side. For the east girder, the loading combination is shown in Figure 5.13. Alternatively, one could combine truck runs 9 and 6 to obtain similar, but slightly more conservative, results. For the west girder, an appropriate truck loading combination can be selected in the same way as shown in Figure 5.14. As shown in Figure 5.13, the single truck configuration includes a truck that is placed 609.6 mm (2 ft) clear from the west wall barrier. This results in a distance of 2874.3 mm (9.43 ft), instead of 1219.2 mm (4 ft), between this and the adjacent truck from the loading configuration 9. As such, the calculated load distribution factors for the bridge are expected to be slightly smaller than the actual values. Calculation of the load distribution factor from the alternate truck loading combination, as described above, will yield results that are slightly larger than the actual values.

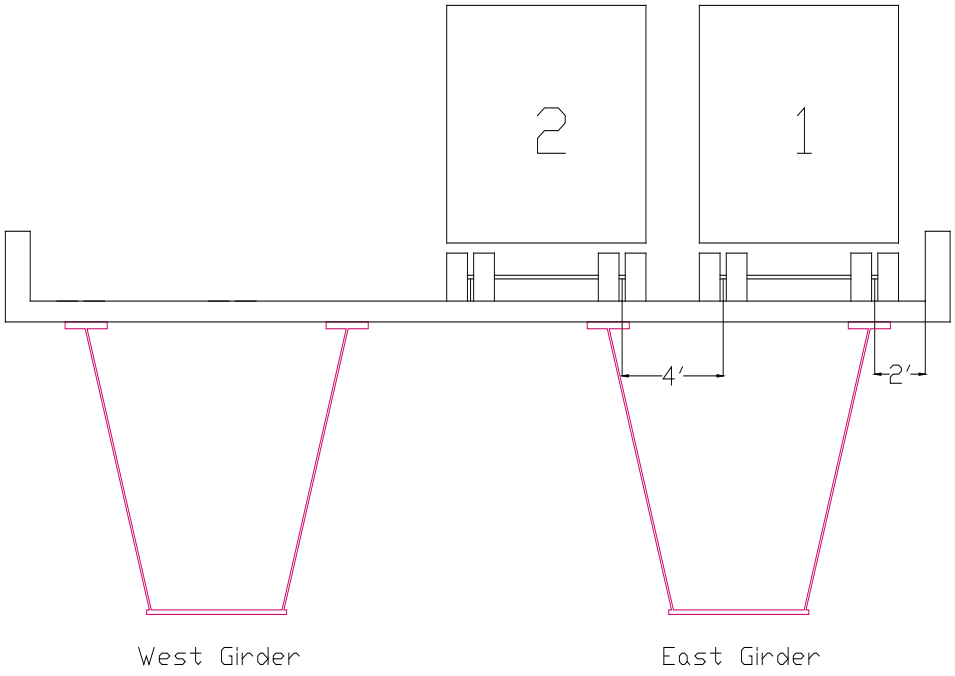

A) Truck Run #9: Loading the first two design lanes for the east girder.

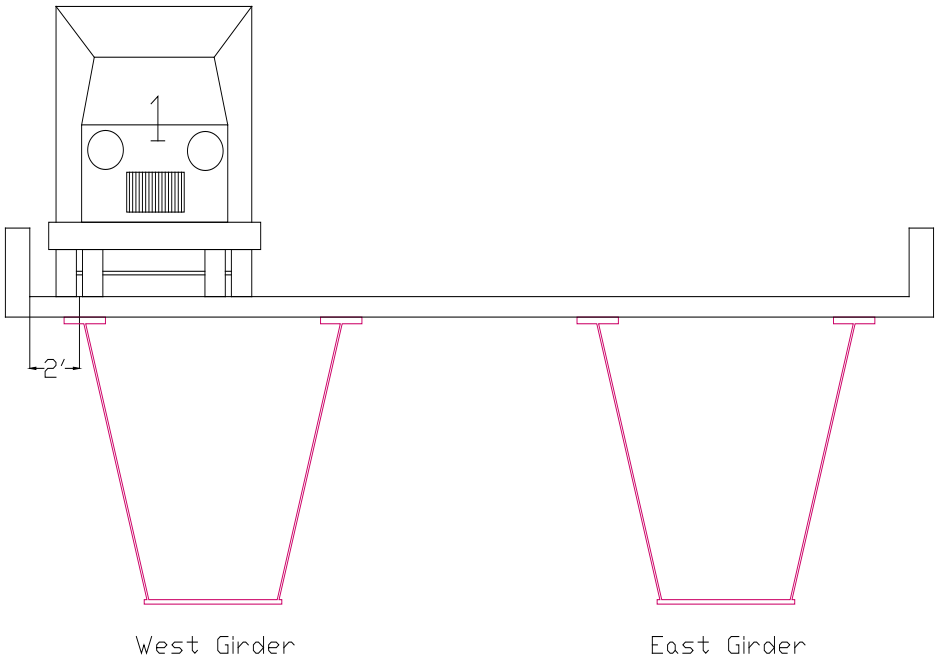

B) Truck Run #2: Loading the third design lane for the east girder.

Figure 5.13: Three Design Lanes for the Maximum Load Over the East Girder

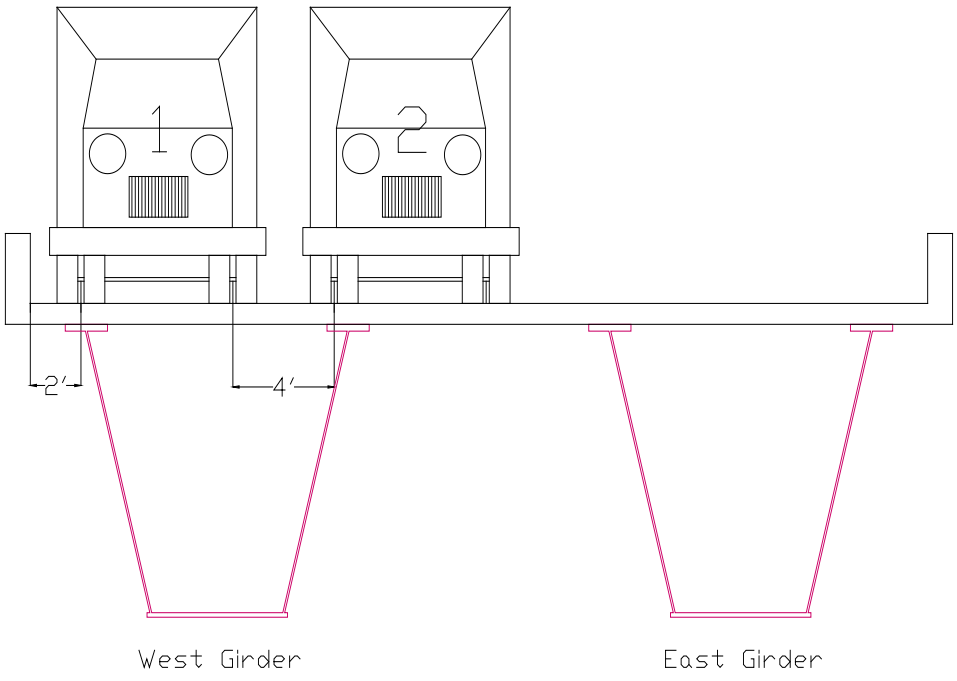

A) Truck Run #10: Loading the first two design lanes for the west girder.

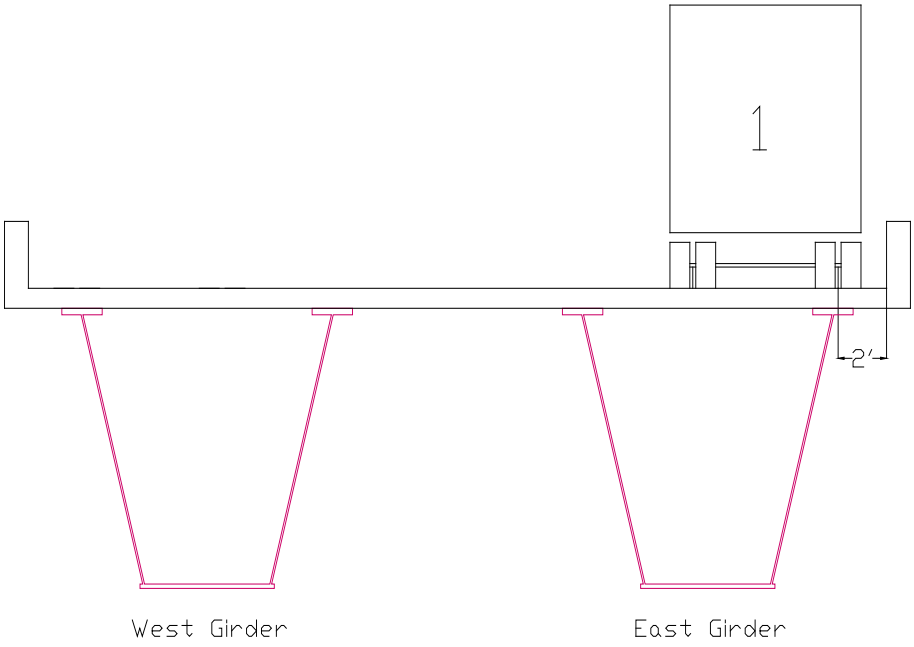

B) Truck Run #1: Loading the third design lane for the west girder.

Figure 5.14: Three Design Lanes for the Maximum Load Over the West Girder

5.2.2 Strain Measurements and Calculations of Distribution Factors

Strains in the top and bottom flanges of the box girders in the bridge were measured and recorded as described in chapter 3. These strains were then converted into stresses under the assumption of linear elastic behavior for the girders. Figure 5.15 shows graphs of stress values for strain gages A through F in the east and west girders at the mid-span for truck loading configurations 2 and 9. The beginning and end points for each girder are identified in the graphs as 0 and 72, respectively. The stress values resulted from truck loading configurations 2 and 9 were superimposed to achieve full loading on the bridge deck. The moment distribution factor for positive moment in the bottom flange of the east girder was calculated by multiplying the ratio of the stress in the flange to the total stress in both bottom flanges by the number of trucks for each loading configuration. A similar approach was used to calculate load distribution factors for the top flanges and also in the west girder. Tables 5.1 and 5.2 show stress values at all strain gage locations in the top and bottom flanges, percentages of corresponding stresses, and the maximum live load moment distribution factors for the east and west girders at mid-span. The stress values and load distribution factors in the tables are calculated for conditions where the truck loads were located at each $1/8^{th}$ of the span length. Load distribution factors are calculated in the same fashion for the east and west girders for the quarter-span, as shown in Appendix E.

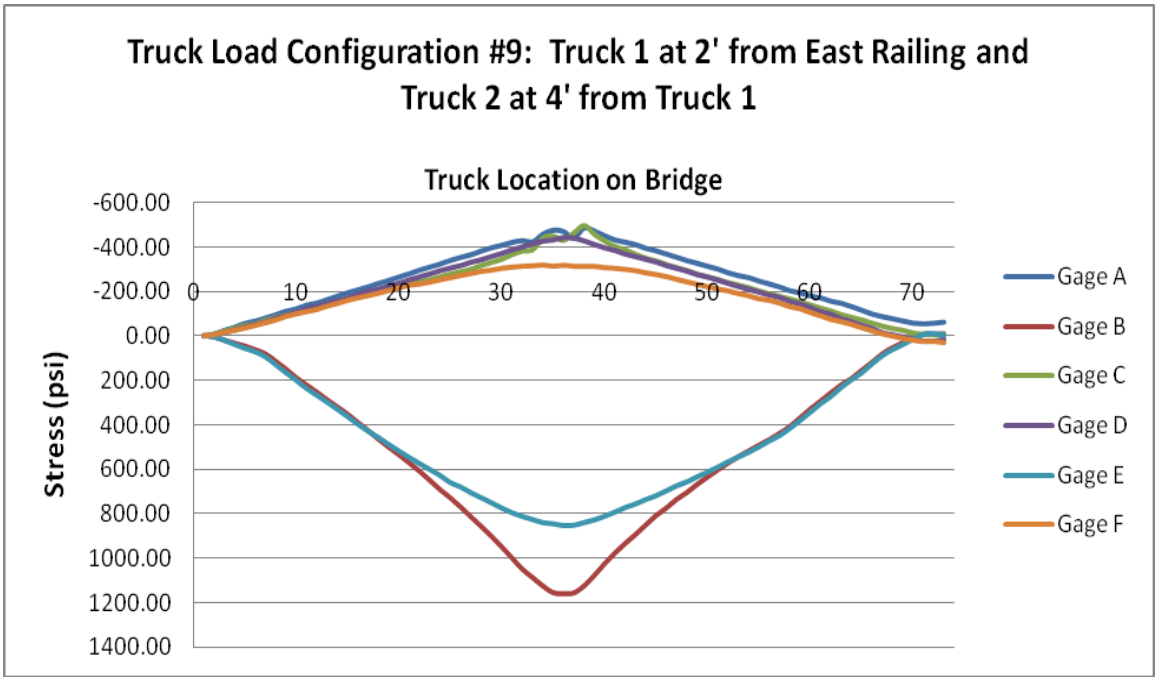

A) Truck Run #9: Mid-span stress in the first two design lanes for the east girder.

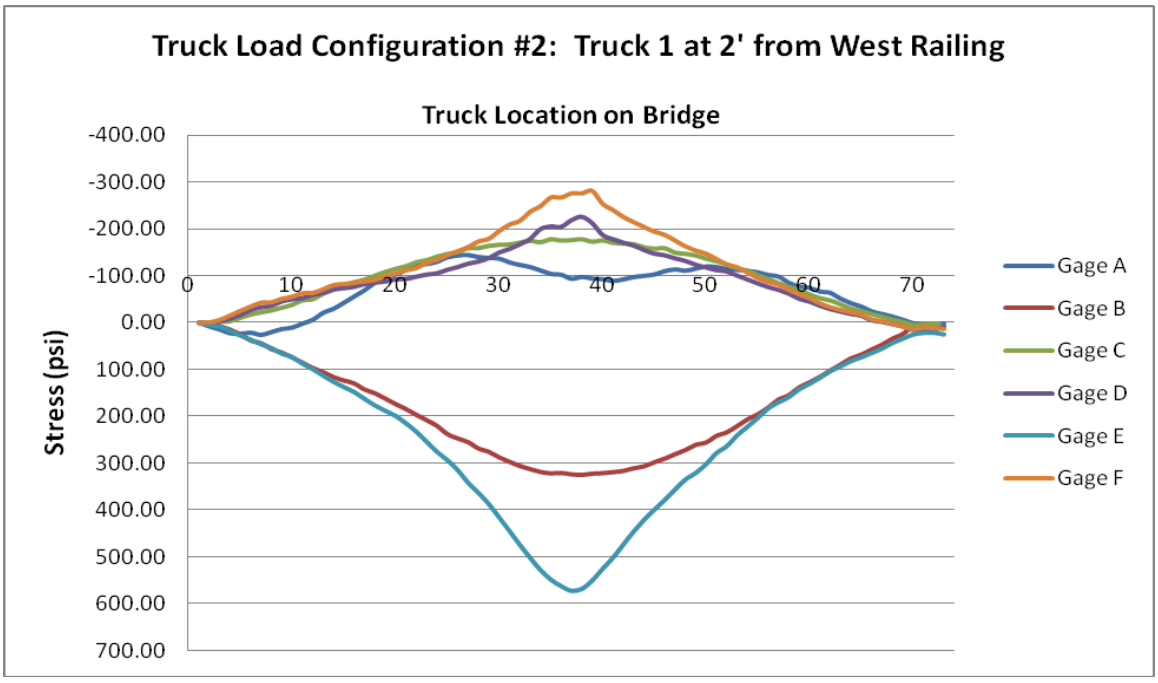

B) Truck Run #2: Mid-span stress in the third design lane for the east girder.

Figure 5.15: East Girder Mid-span Stresses for Three Design Lanes

East Girder from Truck Runs #2 and #9								
Top Flange								
Load at Span Location	Number of Lanes Loaded	Stress Values at Gages					% of Stress	Distribution Factor
		A	C	D	F	Total		
1/8	2	-122	-107	-105	-98	-433	53	1.37
	1	-11	-37	-50	-56	-154	31	
1/4	2	-251	-218	-224	-205	-897	52	1.57
	1	-97	-108	-88	-99	-392	52	
3/8	2	-384	-318	-342	-292	-1335	53	1.55
	1	-139	-159	-131	-173	-602	50	
1/2	2	-441	-465	-439	-314	-1659	55	1.44
	1	-93	-176	-219	-275	-763	35	
5/8	2	-355	-308	-304	-255	-1223	54	1.54
	1	-113	-149	-138	-175	-575	46	
3/4	2	-235	-191	-183	-160	-769	55	1.65
	1	-101	-93	-77	-87	-357	54	
7/8	2	-117	-73	-48	-36	-273	69	2.03
	1	-34	-24	-15	-17	-91	64	
							Average =	1.59
							Max =	2.03
							Min =	1.37
							Standard Deviation =	0.20
Bottom Flange								
Load at Span Location	Number of Lanes Loaded	Stress Values at Gages					% of Stress	Distribution Factor
		B		E		Total		
1/8	2	189		201		390	48	1.47
	1	74		74		148	50	
1/4	2	500		488		988	51	1.47
	1	162		189		351	46	
3/8	2	856		726		1582	54	1.51
	1	268		364		632	42	
1/2	2	1154		849		2003	58	1.51
	1	324		573		897	36	
5/8	2	734		672		1406	52	1.48
	1	281		357		638	44	
3/4	2	467		472		939	50	1.49
	1	181		184		365	50	
7/8	2	155		167		322	48	1.44
	1	68		74		143	48	
							Average =	1.48
							Max =	1.51
							Min =	1.44
							Standard Deviation =	0.02

Table 5.1: East Girder Field Distribution Factors at Mid-span for Truck Runs #2 & #9

West Girder from Truck Runs #1 and #10								
Top Flange								
Load at Span Location	Number of Lanes Loaded	Stress Values at Gages					% of Stress	Distribution Factor
		A	C	D	F	Total		
1/8	2	-85	-107	-101	-114	-408	53	1.42
	1	-83	-51	-43	-33	-211	36	
1/4	2	-182	-229	-211	-235	-857	52	1.45
	1	-154	-104	-102	-80	-440	41	
3/8	2	-267	-347	-341	-383	-1339	54	1.51
	1	-216	-151	-162	-118	-647	43	
1/2	2	-313	-383	-425	-437	-1557	55	1.53
	1	-237	-183	-180	-128	-729	42	
5/8	2	-271	-263	-235	-277	-1046	49	1.40
	1	-208	-140	-144	-108	-601	42	
3/4	2	-177	-149	-134	-154	-613	47	1.38
	1	-126	-80	-90	-72	-367	44	
7/8	2	-55	-22	-18	-19	-115	32	1.09
	1	-44	-23	-28	-26	-121	44	
							Average =	1.40
							Max =	1.53
							Min =	1.09
							Standard Deviation =	0.14
Bottom Flange								
Load at Span Location	Number of Lanes Loaded	Stress Values at Gages					% of Stress	Distribution Factor
		B		E		Total		
1/8	2	236		231		467	49	1.51
	1	59		64		124	52	
1/4	2	524		547		1071	51	1.50
	1	175		157		332	47	
3/8	2	755		921		1676	55	1.51
	1	367		260		628	41	
1/2	2	800		1071		1872	57	1.50
	1	541		294		836	35	
5/8	2	618		654		1271	51	1.48
	1	312		254		566	45	
3/4	2	412		394		806	49	1.48
	1	177		177		354	50	
7/8	2	99		103		202	51	1.53
	1	87		92		179	51	
							Average =	1.50
							Max =	1.53
							Min =	1.48
							Standard Deviation =	0.02

Table 5.2: West Girder Field Distribution Factors at Mid-span for Truck Runs #1 & #10

Since maximum stresses occur at the bottom flanges of the box girders in the Land Bridge, the primary consideration is given to the bottom flanges for the purpose of calculating load distribution factors for bending moment. As shown in Tables 5.1, 5.2, as well as in Appendix E, the mid-span live load distribution factors for the bottom flanges of the east and west girders from the field tests have been calculated as having values close to 1.50. At the quarter-span, the distribution factor for the east girder was about 7 percent larger than that for the west girder.

5.2.3 Distribution Factors from the Numerical Simulation

5.2.3.1 Finite Elements Model Verification

In order to verify the accuracy of the results from the numerical simulation, a comparative study was performed where the results from the finite elements analysis of the bridge were evaluated against the results from the field testing under similar conditions. The truck loading configuration 15, with two trucks each located 3 feet from the deck centerline, was chosen for the comparative study. This loading configuration was chosen due to the symmetry of the applied load with respect to the positions of the girders in the bridge. It is understood that the inherent curvature in the bridge and the corresponding torsional effect would influence the results so a perfect symmetry in the results could not be achieved. During the field testing exercise, the trucks were placed and kept for a short period of time at the quarter-span, mid-span, and three-quarter-span positions and strain values at all gages were measured and recorded. Corresponding stresses were calculated based on the measured strain values. Figure 5.16 shows the static stress values from all of the strain gages installed at strain gage location MS1, at the mid-span of the bridge. Strain gage locations identified as MS1, MS2, and MS3 were at or

near the mid-span of the bridge and strain gage locations QS4 and QS5 were at or near the quarter-span of the bridge. These locations were described in more detail in chapter 3. As shown in the figure, maximum stresses occurred in the mid-span bottom flange that indicated the significance of calculating the moment distribution factor values for the bottom flanges of the girders in this bridge. Appendix D includes similar stress graphs for a selected number of truck loading configurations that were used to calculate load distribution factors in the bridge.

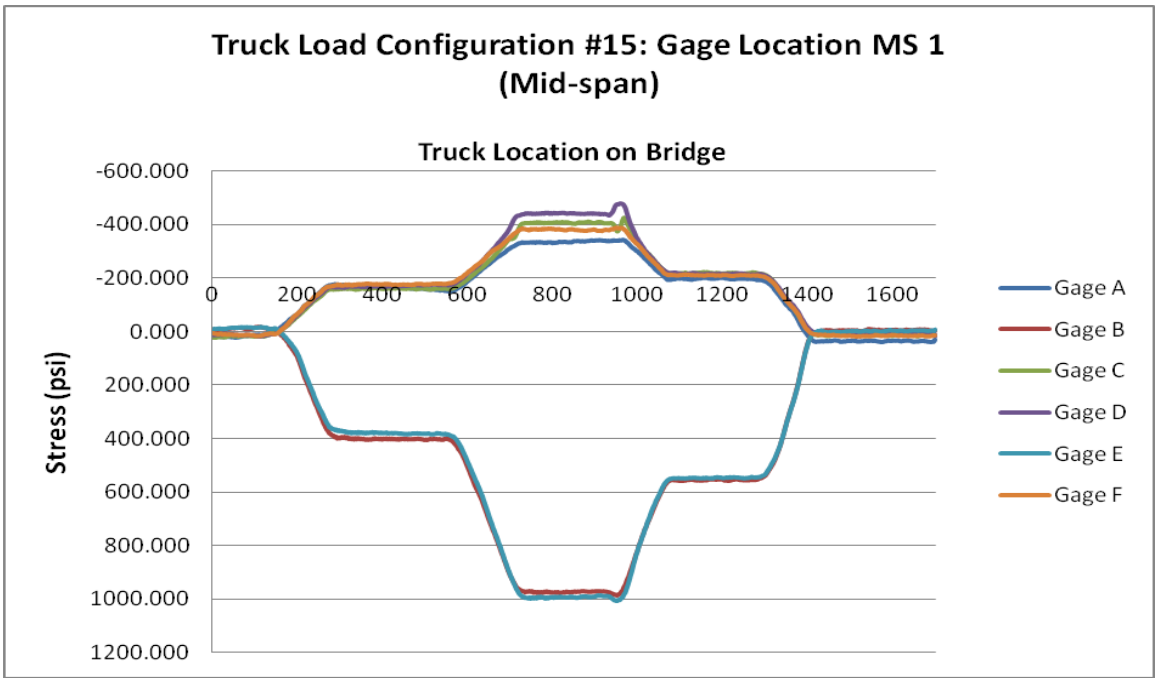

Figure 5.16: Stresses at theMid-span for Truck Load Configuration #15

The stress values calculated from the measured strains were then compared with stresses at the same points on the bridge but obtained from the numerical analysis. Table 5.3 shows the comparison of the results from the field testing and numerical analysis. It can be seen from the table that the stress values from the two methods were relatively close for the identical points on the bridge. In addition, the ratios between the stress values for the top flanges of the east and west girders as well as those for the two bottom

flanges are similar when a comparison of the results from the field test and numerical analysis is made.

Truck Configuration #15: Stress Comparison with Truck at Mid-span										
								Ratio Between Gages		
	Location	Gage A	Gage B	Gage C	Gage D	Gage E	Gage F	A & C	D & F	B & E
Field Results	MS 1 (Mid-span)	-365	979	-422	-454	999	-394	0.864	1.152	0.980
	MS 2	-383	1060	-483	-477	1054	-433	0.794	1.101	1.005
	MS 3	-396	1037	-398	-444	1078	-438	0.996	1.014	0.962
	QS 4	-238	691	-321	-324	673	-268	0.741	1.207	1.026
	QS 5 (Quarter-span)	-197	539	-227	-194	502	-203	0.869	0.954	1.073
Numerical Results	MS 1 (Mid-span)	245	1101	350	282	1098	270	0.700	1.044	1.003
	MS 2	230	945	260	223	933	249	0.885	0.896	1.013
	QS 5 (Quarter-span)	142	620	157	130	598	149	0.904	0.872	1.037

Table 5.3: Stress Comparison between Field and Numerical Results

5.2.3.2 Calculations of Distribution Factors From Numerical Simulation

The moment distribution factors from the results of the numerical analysis were calculated in a similar fashion to those calculated from the field tests. The bridge loading in the numerical analysis included three trucks with the same characteristics as those used in the field testing program. The first truck was positioned 609.6 mm (2 ft) clear from the barrier wall over the east girder. The next two trucks were placed side-by-side and at a distance of 1219.2 mm (4 ft) from each other. This resulted in a maximum effect for the load distribution factor applied to the east girder. The truck loads were placed at each eighth point along the bridge span and the corresponding stresses in the top and bottom

flanges at both the mid-span and quarter-span were calculated for the same points that strain gages were installed during the field testing program. Figure 5.17 shows an example of the mid-span stress values for both the top and bottom flanges of the bridge girders. These stresses were evaluated for all of the relevant loading conditions at both the mid-span and quarter-span and the corresponding distribution factors were calculated.

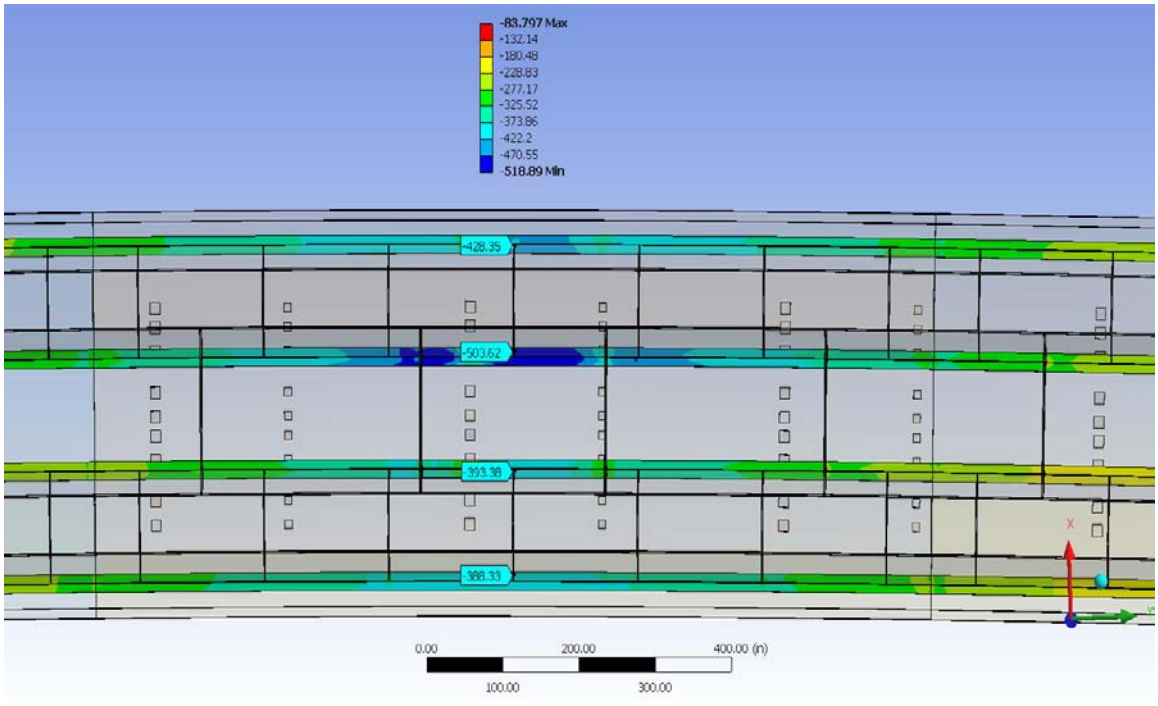

A) Top Flange Stresses at the Mid-Span.

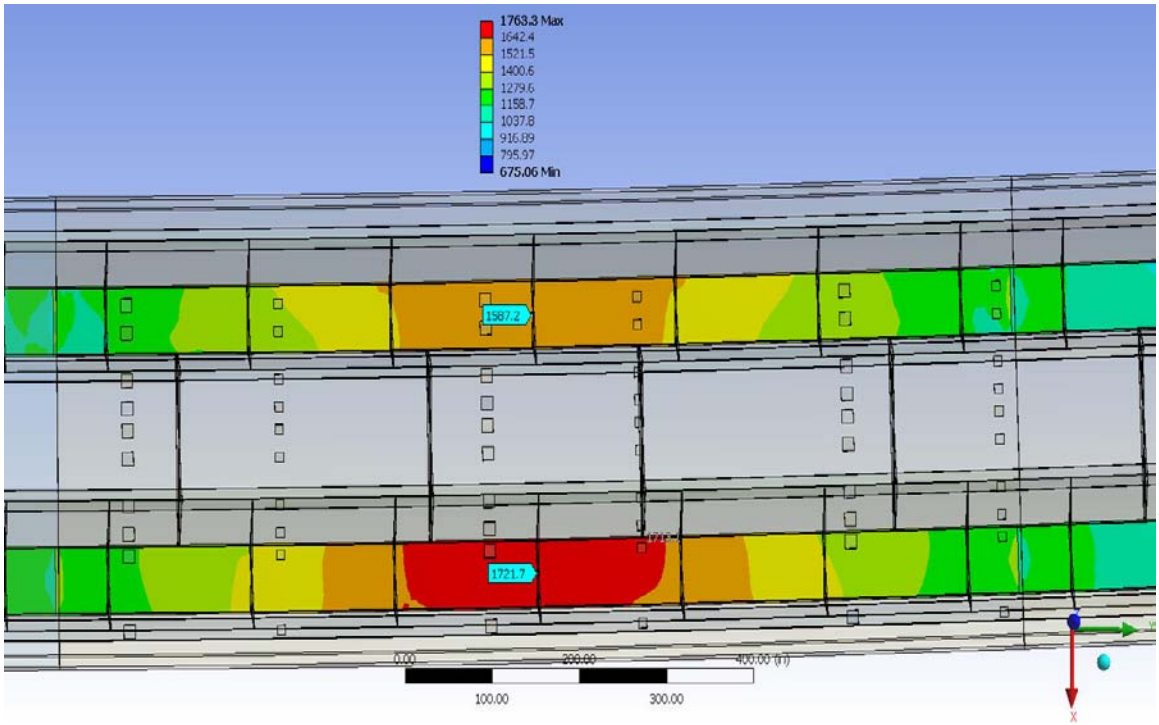

B) Bottom Flange Stresses at the Mid-span.

Figure 5.17: Top and Bottom Flange Stresses from the Numerical Analysis

The mid-span stresses at the locations of the installed strain gages for both east and west girders are presented in Table 5.5. In order to calculate the values of load distribution factors for the top flanges of the east girder, first the ratio of the total stresses in the top flanges of the east girder (at the locations of gages A and C) to the total stresses for the top flanges of both girders (at gages A, C, D, and F) were calculated. This is shown as "% of Stress" in the table. The corresponding distribution factor is then calculated by multiplying the number of loaded lanes or trucks on the bridge by the calculated ratio. The distribution factors shown in Table 5.5 include those at the bridge's mid-span with trucks positioned at each eighth point along the span length. The distribution factor values for the bottom flange of the east girder, as shown in Table 5.5, were calculated following a similar approach to that for the top flanges. Distribution factors at the quarter-span of the bridge were also calculated and shown in Appendix E. Considering the results for both the mid-span and quarter-span locations, it can be observed that the calculated distribution factors for the top flanges are somewhat greater than those for the bottom flanges. However, due to much higher level of stresses at the bottom flanges of the box girders in the Land Bridge, it is clear that the primary consideration should be given to the distribution factors for the bottom flanges. It can be seen from the results that there is little variation in the values of the distribution factors calculated at both the mid-span and quarter-span for the bottom flanges as the positions of the loads are varied along the span length. The same observation is made for the top flanges of the east girder when the distribution factors are considered at the mid-span. However, a more significant variation of the results is observed when the distribution factors are considered at the quarter-span.

East Girder Mid-span								
Top Flange								
Load at Span Location	Number of Lanes Loaded	Stress Values at Gages					% of Stress	Distribution Factor
		A	C	D	F	Total		
1/8	3	-112	-119	-94	-102	-427	54	1.62
1/4	3	-222	-239	-190	-212	-863	53	1.60
3/8	3	-334	-359	-292	-318	-1303	53	1.60
1/2	3	-420	-514	-395	-382	-1711	55	1.64
5/8	3	-332	-359	-290	-315	-1296	53	1.60
3/4	3	-225	-240	-187	-206	-858	54	1.63
7/8	3	-116	-121	-90	-96	-423	56	1.68
							Average =	1.62
							Max =	1.68
							Min =	1.60
							Standard Deviation =	0.03
Bottom Flange								
Load at Span Location	Number of Lanes Loaded	Stress Values at Gages					% of Stress	Distribution Factor
		B		E		Total		
1/8	3	433		433		866	50	1.50
1/4	3	880		872		1752	50	1.51
3/8	3	1352		1300		2652	51	1.53
1/2	3	1775		1626		3401	52	1.57
5/8	3	1345		1295		2640	51	1.53
3/4	3	873		870		1743	50	1.50
7/8	3	426		434		860	50	1.49
							Average =	1.52
							Max =	1.57
							Min =	1.49
							Standard Deviation =	0.02

Table 5.4: Stresses and Distribution Factors at the Mid-span for the East Girder - Numerical Analysis

5.2.4 Comparative Study of Live Load Distribution Factors

Results of distribution factors from the field and numerical simulation were compared to those determined from the appropriate design equations presented in the AASHTO Standard Specifications for Highway Bridges and the AASHTO LRFD Bridge Design Specification. The load distribution factor equation listed in the standard specifications is:

$$W_L := 0.1 + 1.7R + \frac{0.85}{N_w} \qquad \text{(Eq. 5.1)}$$

Where:

W_c = Roadway width between curbs or barriers

$N_w = W_c / 12$ (Reduced to the nearest whole number)

$R = N_w$ / Number of box girders

And the LRFD equation is:

$$DF := 0.05 + 0.85\left(\frac{N_L}{N_b}\right) + \left(\frac{0.425}{N_L}\right) \qquad \text{(Eq. 5.2)}$$

Where:

N_L = Number of Design Lanes

N_b = Number of Beams

The equations in both specifications allow calculations of live load distribution factor values for straight steel box girders through considering the number of design lanes and the number of box girders in a bridge. No equations are presented in either specifications for box girder bridges with curvature. Also, it is noted that the equations in both specifications do not include appropriate parameters to take into account the effects of interior vs. exterior girders. Figure 5.18 shows values of live load distribution factors obtained from the field testing, numerical simulations, AASHTO standard specifications, and AASHTO Standard specifications for both the top and bottom flanges at the mid-span and quarter-span.

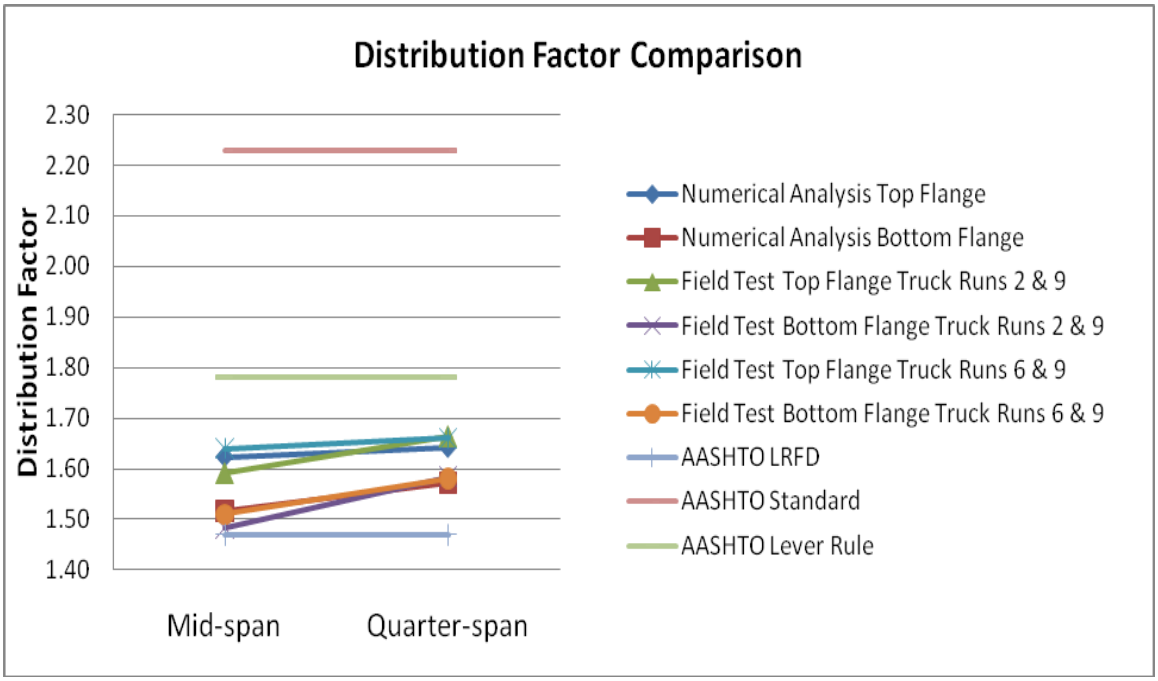

Figure 5.18: Distribution Factors from Field Tests, Numerical Simulation, AASHTO LRFD, AASHTO Standard Specifications, and the Lever Rule

It can be seen from Figure 5.18 that AASHTO Standard Specifications yield over-conservative values for live load distribution factors. It is noted that the calculated values from the standard specifications are about 30% higher than those determined from the field testing and numerical simulation of the Land Bridge. On the other hand, live load distribution factors determined from the AASHTO LRFD Specifications have been found to be about 12% smaller than those from the field tests and numerical simulation. It is noteworthy that the comparison of the field testing and numerical simulation results with those from the AASHTO specifications was done with the consideration that the existing AASHTO equations are only for straight box girder bridges. However, the present AASHTO equations were assumed to be valid for the purpose of this study since the curvature in the Land bridge was not significant. As shown in Figure 5.18, the live load distribution factors from both the field tests and the numerical simulation were found to

be larger at the quarter-span than those at the mid-span. Since the distribution factor values for only moment were the focus of this study, the effect of larger values at the quarter-span was not investigated as a part of this study. However, if load distribution factors for shear are being considered, the larger values at locations closer to the span ends should be considered for the purpose of design.

CHAPTER 6

CONCLUSIONS AND RECOMMENDATIONS

The primary objectives of this study were to perform a long-term structural monitoring program and to investigate the characteristics of live load distribution among the box girders of the Land Bridge.

The structural monitoring program included an evaluation of in-service behavior of the constructed HPS bridge members through monitoring strain, temperature, and displacement. Due to the curved geometry of the bridge structure, it was recognized that an in-depth assessment of the response of the structure due to the daily temperature changes was important to be made. Special temperature response measurement techniques were used in this study to determine the thermal response of the structure independent of other in-service loads.

The load distribution investigation included a field testing program, a numerical simulation study, and comparison of the results with those obtained from the new AASHTO LRFD specifications and AASHTO standard specifications. The AASHTO LRFD specifications is known to provide a more accurate representation of the live load distribution factors, but in both AASHTO specifications (LRFD and Standard) the curvature of the bridge is not taken into account as a parameter in the calculations of load distribution factors . Live load distribution factors were considered for only the bending moment in this study.

The following conclusions are drawn from the structural monitoring program and the live load distribution study.

6.1 Conclusions – Structural Monitoring Program

1. The data indicates relatively small magnitudes and occurrences of live load stress cycles. The majority (approximately 95%) of the 8,000 to 9,000 traffic load cycles recorded per year occurred at the stress range level of 6.9 MPa (1.3 ksi) or smaller. The remainder of the traffic load cycles occurred in the 11.0 to 27.0 MPa (1.6 to 3.9 ksi) stress ranges. The recorded data was very consistent, indicating that unless there are any major future changes in traffic flow, this data could be used to accurately predict the fatigue life of the structure.
2. As described in earlier chapters of this report, load cycles due to thermal loads were observed independent of other in-service loads. These thermal stress cycles proved to be more significant than in-service live loads in terms of magnitude, while producing a limited quantity of cycles. The east girder experienced greater loads in the 13.8 to 27.6 MPa (2.0 to 4.0 ksi) stress ranges than the west girder. The west girder experienced a greater number of cycles in the lower stress range levels of less than 13.8 MPa (2.0 ksi).
3. No significant change in the traffic load pattern was observed over the four years of monitoring. All traffic stress range results were within +/- 2 standard deviations of the corresponding mean value. It was also found that 79% of all traffic stress range results were within +/- 1 standard deviation of the corresponding mean value.
4. The resulting data from this research can be used as a tool to estimate the fatigue life of the structure. Based on the results of this research, the bridge structure should have infinite life since the maximum stress ranges were less than 27.6 MPa

(4.0 ksi). This stress range level is less than one-half the constant-amplitude fatigue threshold given by AASHTO fatigue specifications for highway bridge design for Category B details which is 55.2 MPa (8.0 ksi).

6.2 Conclusions – Live Load Distribution Study

1. It has been shown in this study that there is a reasonably good agreement between the results from the field testing and the 3-D numerical simulation.
2. Available literature suggests that the provisions of the new AASHTO LRFD specifications yield more accurate values of live load distribution factors than those from the AASHTO standard specifications. However, in the case of the Land Bridge, the AASHTO LRFD specifications resulted in an under-conservative value for the load distribution factor when compared with the results obtained from both the field testing and numerical simulation. On the other hand, the AASHTO standard specifications yielded over-conservative results for load distribution factors when compared to results from both the field testing and numerical analysis.

The following recommendations are offered based on the findings from the structural monitoring program and live load distribution study.

6.3 Recommendations

1. It was found that the contribution of thermal effects can be more significant than the influence of the traffic load on the bridge. Design standards currently in place do not consider the effect of these thermal stresses. Depending on the geometrical configurations, these considerations could greatly impact the design of future structures. Accordingly, it is recommended that further research be conducted on

larger, more heavily traveled structures. One such structure that would be a good candidate for further live load/thermal response research would be the newly constructed Marquette Interchange in Milwaukee, Wisconsin. The new Marquette Interchange bridge structures can offer an excellent opportunity by serving as an effective laboratory for investigating the true response of these structures due to in-service live loads and more importantly due to thermal effects. Conducting structural monitoring research on real structures provides great benefits to the design community in determining in-service conditions. This can lead to better estimations of fatigue life when actual stresses, due to both live load and thermal loads, are considered.

2. Findings from this and other limited studies indicate the significant effect of bridge curvature on the values of live load distribution factors for curved box girder bridges. AASHTO standard specifications and LRFD specifications do not currently take into consideration the effect of the bridge curvature in calculations of live load distribution factors for curved box girder bridges. As such, design engineers calculate either over-conservative or under-conservative load distribution factors when using theses specifications. To overcome this limitation, it is recommended that a new study be initiated with the objectives of further evaluating the effects of bridge curvature on the load distribution factors calculated for box girder bridges. The study should include one or more suitable bridges for field testing and numerical simulation. The newly constructed Marquette Interchange bridges or other suitable Wisconsin bridges could be included in the study. The numerical simulation study should be extensive and it

should cover a broad range of design variables. The study should aim to develop practical design equations and aids for the design engineers.

REFERENCES

1. Alex Wilson (ArcelorMittal USA, AISI, SAG, CAG). (October 2007). "Steel Bridge Update: Research, Availability & Choices." *Powerpoint Presentation*. Washington D.C.
2. Howell, D.A., and Shenton III, H.W., (2006). "System for In-Service Strain Monitoring of Ordinary Bridges." *J. Bridge Eng*., 11(6), 673-680.
3. American Association of State Highway and Transportation Officials (AASHTO). (2002). *Standard Specification of Highway Bridges*, Washington D.C.
4. Lucas, J.M., Berred, A., and Louis, C., *Thermal actions on a steel box girder bridge*, Proceedings of the Institution of Civil Engineers: Structures and Buildings., SB2, 175-182.
5. Roeder, C.W. (2003). "Proposed Design Method for Thermal Bridge Movements." *J. Bridge Eng.*, 8(1), 12-19.
6. Zhou, Y.E., (2006). "Assessment of Bridge Remaining Fatigue Life through Field Strain Measurement." *J. Bridge Eng*., 11(6), 737-744.
7. Chakraborty, S., and DeWolf, J.T., (2006). "Development and Implementation of a Continuous Strain Monitoring System on a Multi-Girder Composite Steel Bridge." *J. Bridge Eng.* 11(6), 753-762.
8. DeWolf, J.T., Culmo, M.P., and Lauzon, R.G., (2006). "Connecticut's Bridge Infrastructure Monitoring Program for Assessment." *J. Infrastructure Systems.*, 4(2), 86-90.
9. Sartor, R.R., Culmo, M.P., and DeWolf, J.T., (1999). "Short-Term Strain Monitoring of Bridge Structures." *J. Bridge Engineering*., 4(3), 157-164.
10. Zokai, T., Osterkam, T. A., and Imbsen, R. A. (1992). "Distribution of Wheel Loads on Highway Bridges." *NCHRP Rep.* 12-26/1, Transportation Research Record, Transportation Research Board, Washington, D.C.
11. Puckett, J. A., Mertz, D., Huo, X. S., Jablin, M. C., Peavy, M. D., and Patrick, M. D. (2006). "Simplified Live Load Distribution Factor Equations." *NCHRP Rep.* 12-62, Transportation Research Record, Transportation Research Board, Washington, D.C.
12. American Association of State Highway and Transportation Officials Load and Resistance Factor Design (AASHTO LRFD). (2007). *Bridge Design Specifications*, AASHTO, Washington D.C.
13. Cai, C. S. (2005). "Discussion on AASHTO LRFD Load Distribution Factors for Slab-on-Girder Bridges." Practive Periodical on Structural Design and Construction, 10(3), 171-176.
14. Mattock, A. H., and Fountain, R. S. (1967). *Criteria for Design of Steel-Concrete Composite Box Girder Highway Bridges*, United States Steel Corporation, Pittsburgh.
15. Heins, C. P. (1978). "Box girder bridge design –start-of-the-art." *AISC Eng. J.*, 2, 126-142.
16. Samaan, M., Sennah, K. M., Kennedy, J. B. (2005). "Distribution Factors for Curved Continuous Composite Box-Girder Bridges." *J. Bridge Eng.*, 10(6), 678-692.
17. Samaan, M. (2004). "Dynamic and Static Analysis of Continuous Curved Composite Multiple-box Girder Bridges." PhD dissertation, Univ. of Windsor, Windsor, Ont., Canada.

APPENDIX A

SAMPLE OF MONTHLY THERMAL RESPONSE GRAPHS

The graphs shown in Appendix A are an example of those prepared for each month of structural monitoring. Graphs from 2006 have been presented as they are representative of the yearly data which was observed. Data is presented for both the east and the west girders.

As previously mentioned in the body of this report, this research program evaluated load cycles due to thermal loads of the structure independent of other in-service loads. Thermal stress cycles proved to be more significant than other in-service loads in terms of magnitude, while producing a limited quantity of cycles. The east girder experienced greater loads in the 2.0 to 4.0 ksi stress ranges than the west girder. The west girder experienced a greater number of cycles in the lower stress range levels (less than 2.0 ksi).

The following graphs aid in understanding the thermal movements and stresses of each of the girders. For a full description of the thermal response of the girders to these atmospheric variations, see Chapter 4. Observing these graphs, it is clear that with an increase in temperature of the steel (i.e., solar gain), there is an increase in the thermal strain and subsequent stress. Days without many solar gains (cloudy days) become very evident when viewing these graphs. These graphs also indicate that for both longitudinal displacement and midspan deflection, while there is a slight amplification due to solar gains, the range of air temperature primarily controls them.

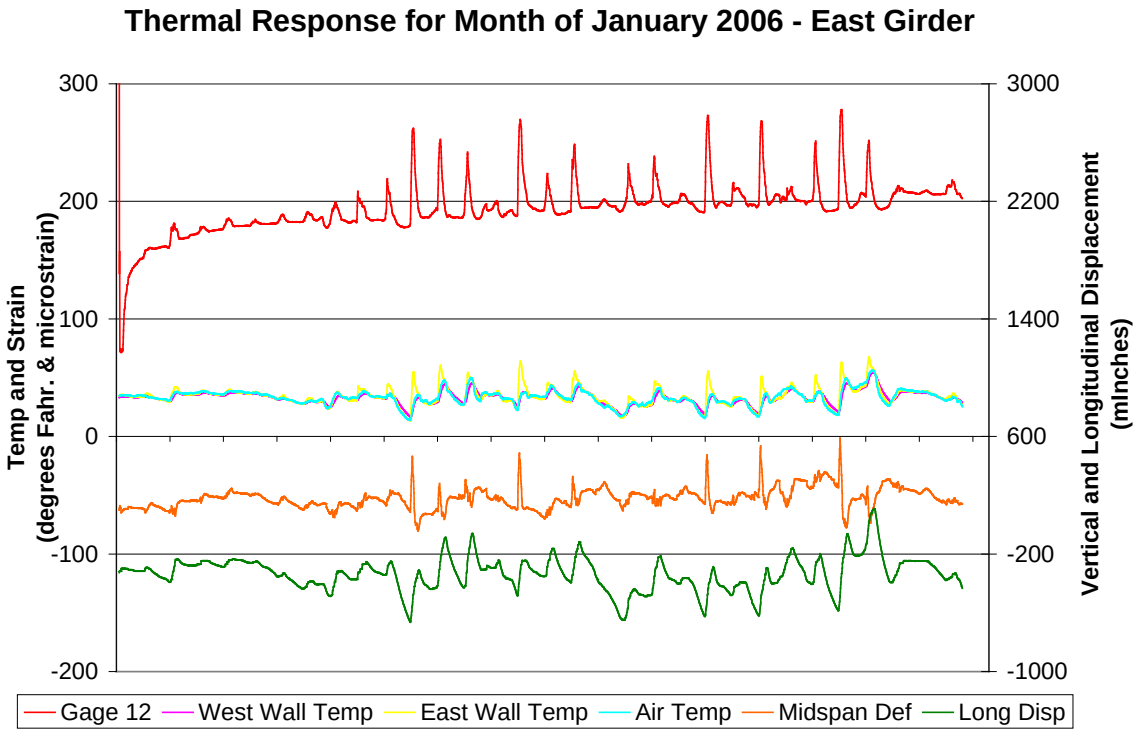
Thermal Response for Month of January 2006 - East Girder
Temp and Strain (degrees Fahr. & microstrain)
Vertical and Longitudinal Displacement (mInches)
300
200
100
0
-100
-200
3000
2200
1400
600
-200
-1000
Gage 12
West Wall Temp
East Wall Temp
Air Temp
Midspan Def
Long Disp

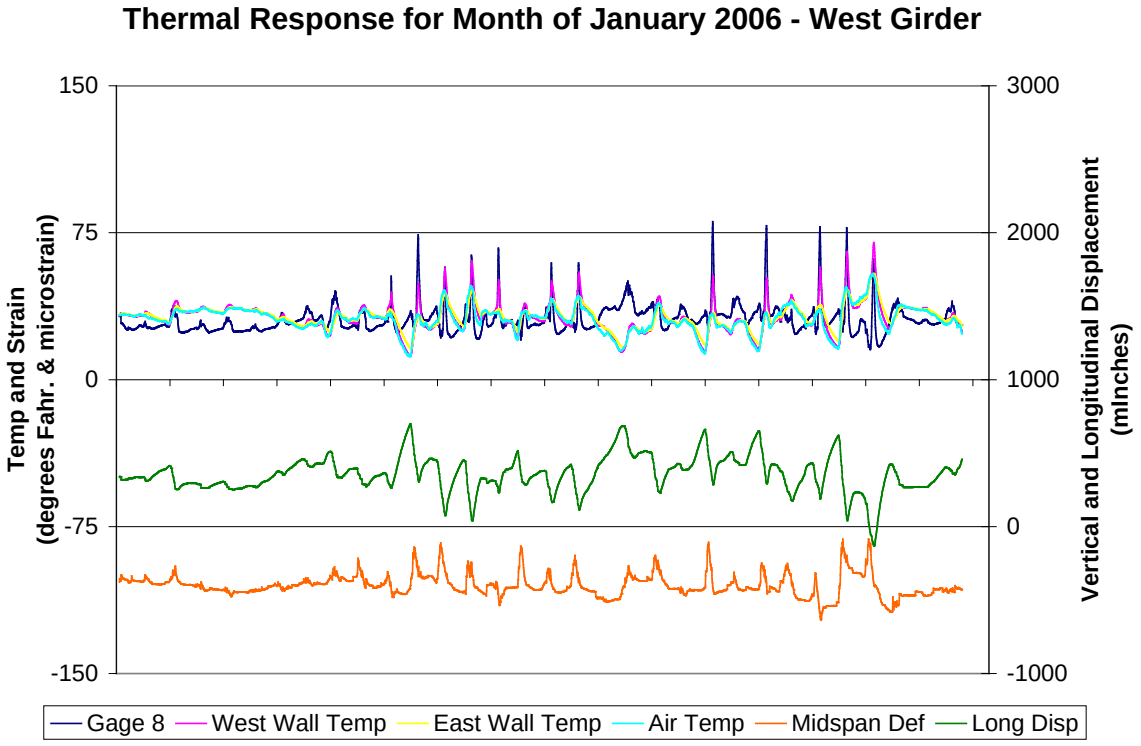
Thermal Response for Month of January 2006 - West Girder
Temp and Strain (degrees Fahr. & microstrain)
Vertical and Longitudinal Displacement (mInches)
150
75
0
-75
-150
3000
2000
1000
0
-1000
Gage 8
West Wall Temp
East Wall Temp
Air Temp
Midspan Def
Long Disp

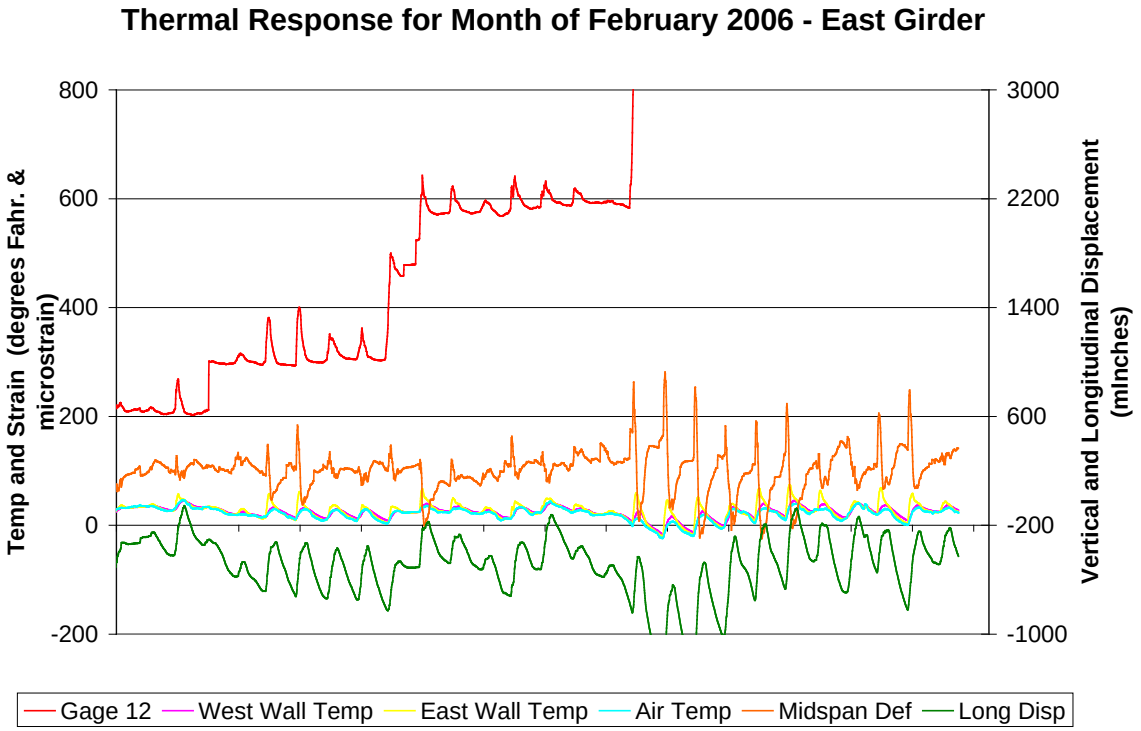
Thermal Response for Month of February 2006 - East Girder
Temp and Strain (degrees Fahr. & microstrain)
Vertical and Longitudinal Displacement (mInches)
800
600
400
200
0
-200
3000
2200
1400
600
-200
-1000
Gage 12
West Wall Temp
East Wall Temp
Air Temp
Midspan Def
Long Disp

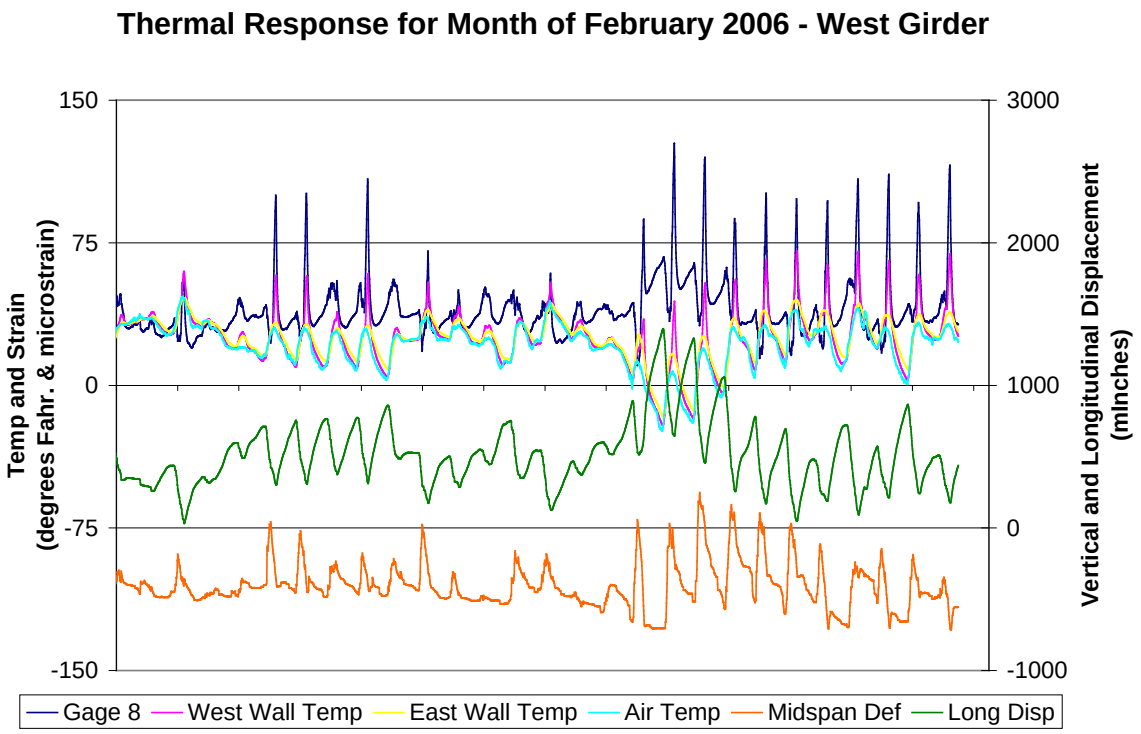
Thermal Response for Month of February 2006 - West Girder
Temp and Strain (degrees Fahr. & microstrain)
Vertical and Longitudinal Displacement (mInches)
150
75
0
-75
-150
3000
2000
1000
0
-1000
Gage 8
West Wall Temp
East Wall Temp
Air Temp
Midspan Def
Long Disp

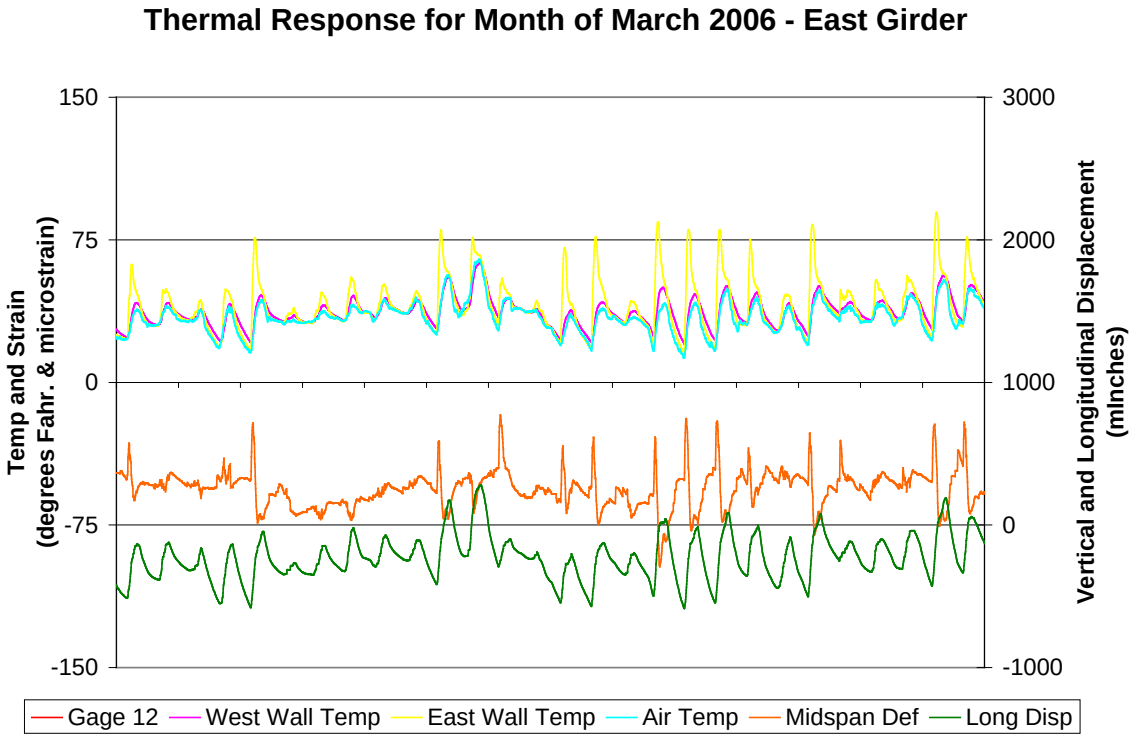
Thermal Response for Month of March 2006 - East Girder
Temp and Strain (degrees Fahr. & microstrain)
Vertical and Longitudinal Displacement (mInches)
150
75
0
-75
-150
3000
2000
1000
0
-1000
Gage 12
West Wall Temp
East Wall Temp
Air Temp
Midspan Def
Long Disp

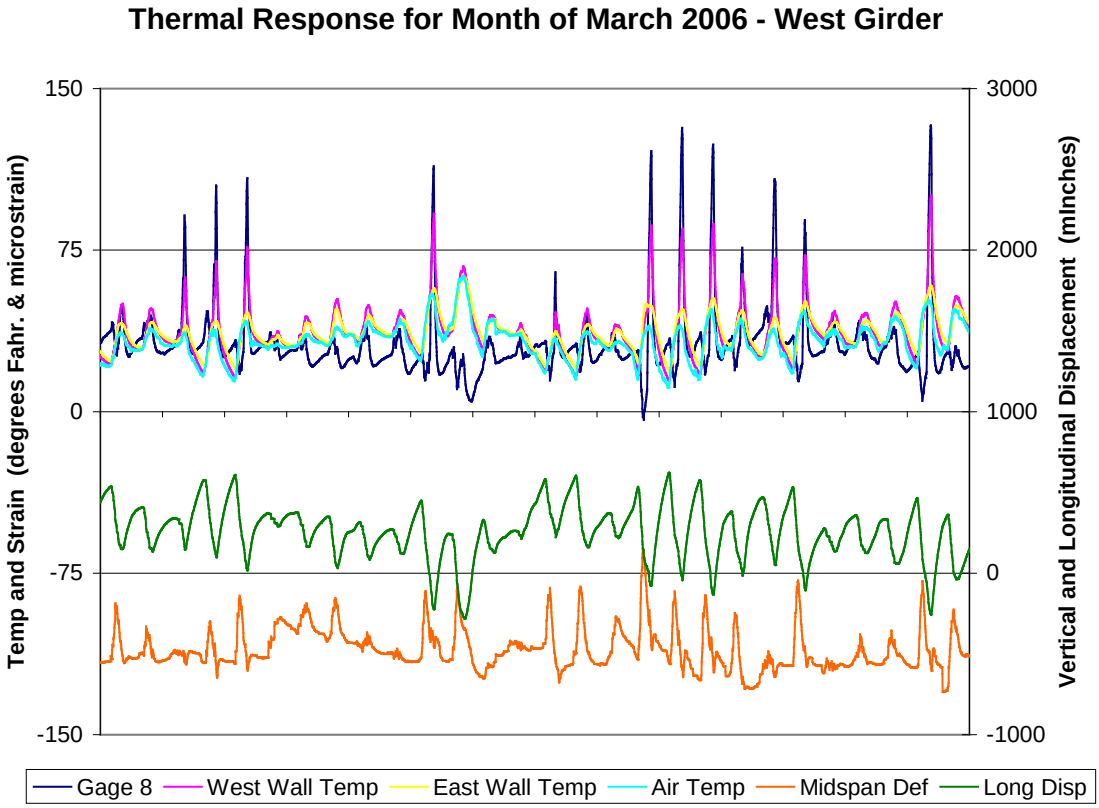
Thermal Response for Month of March 2006 - West Girder
Temp and Strain (degrees Fahr. & microstrain)
Vertical and Longitudinal Displacement (mInches)
150
75
0
-75
-150
3000
2000
1000
0
-1000
Gage 8
West Wall Temp
East Wall Temp
Air Temp
Midspan Def
Long Disp

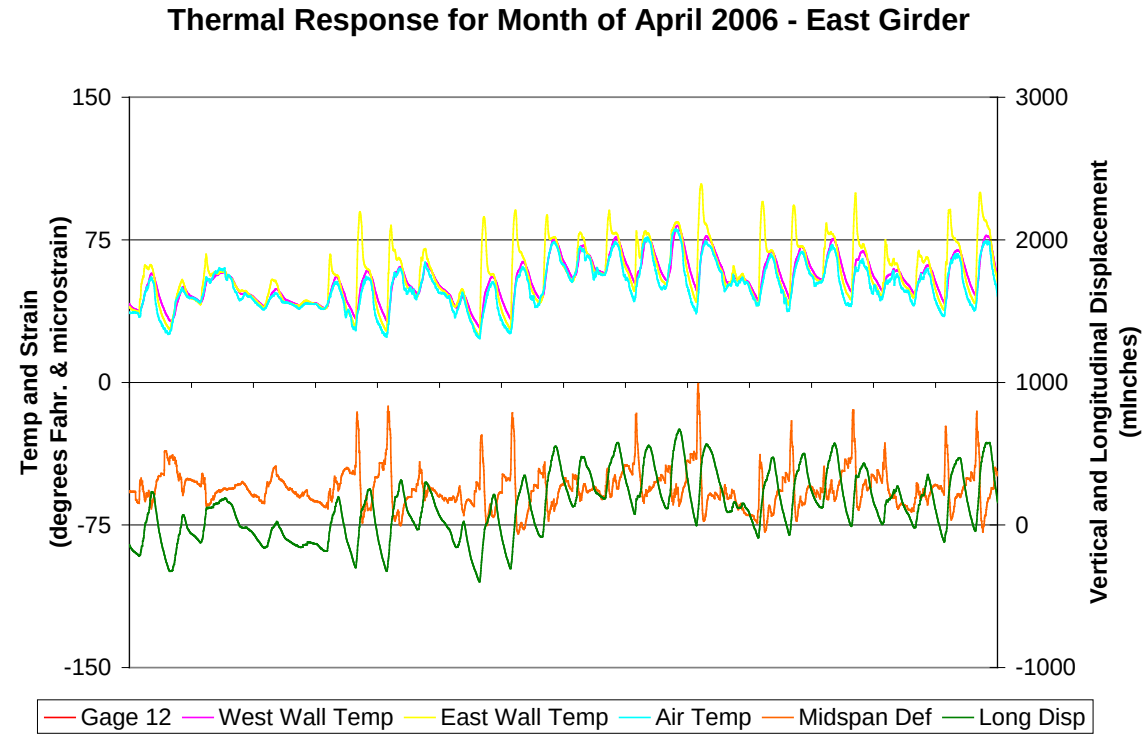
Thermal Response for Month of April 2006 - East Girder
150
75
0
-75
-150
3000
2000
1000
0
-1000
Temp and Strain
(degrees Fahr. & microstrain)
Vertical and Longitudinal Displacement
(mInches)
Gage 12
West Wall Temp
East Wall Temp
Air Temp
Midspan Def
Long Disp

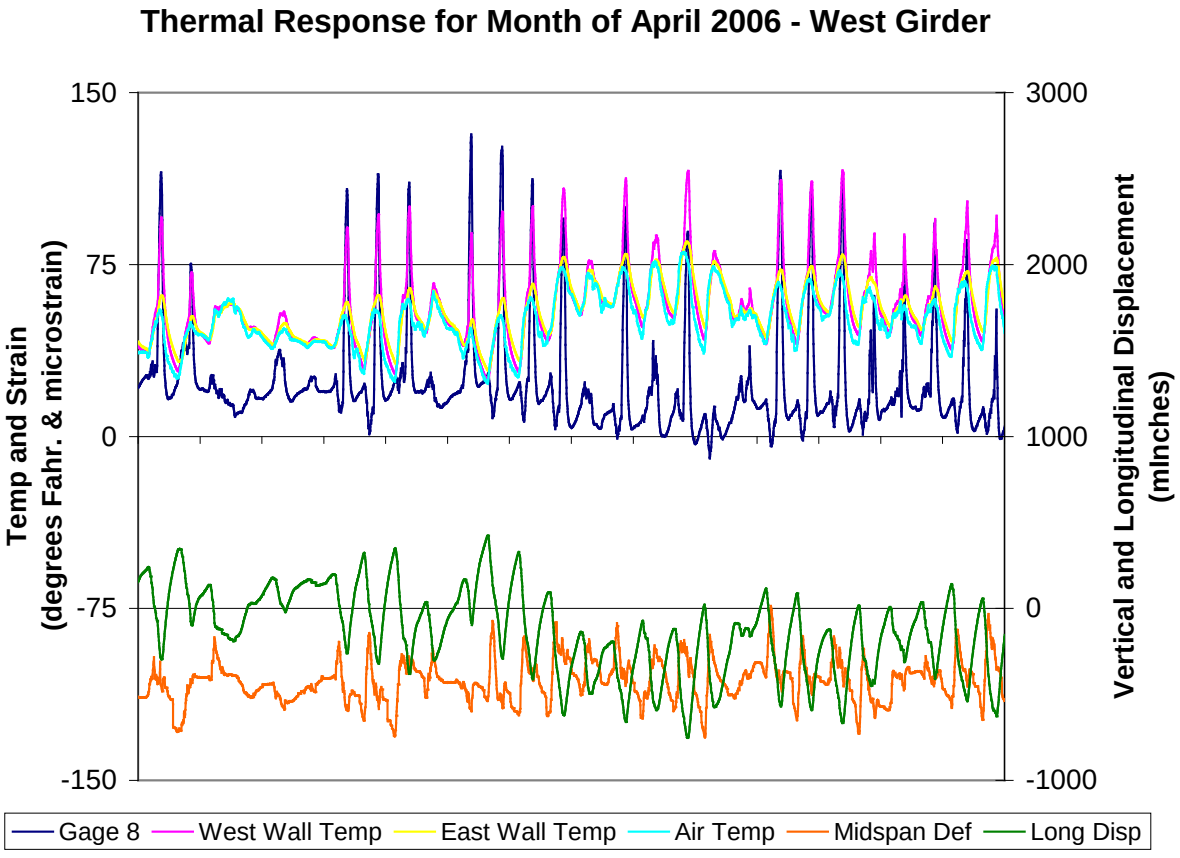
Thermal Response for Month of April 2006 - West Girder
150
75
0
-75
-150
3000
2000
1000
0
-1000
Temp and Strain
(degrees Fahr. & microstrain)
Vertical and Longitudinal Displacement
(mInches)
Gage 8
West Wall Temp
East Wall Temp
Air Temp
Midspan Def
Long Disp

Thermal Response for Month of May 2006 - East Girder

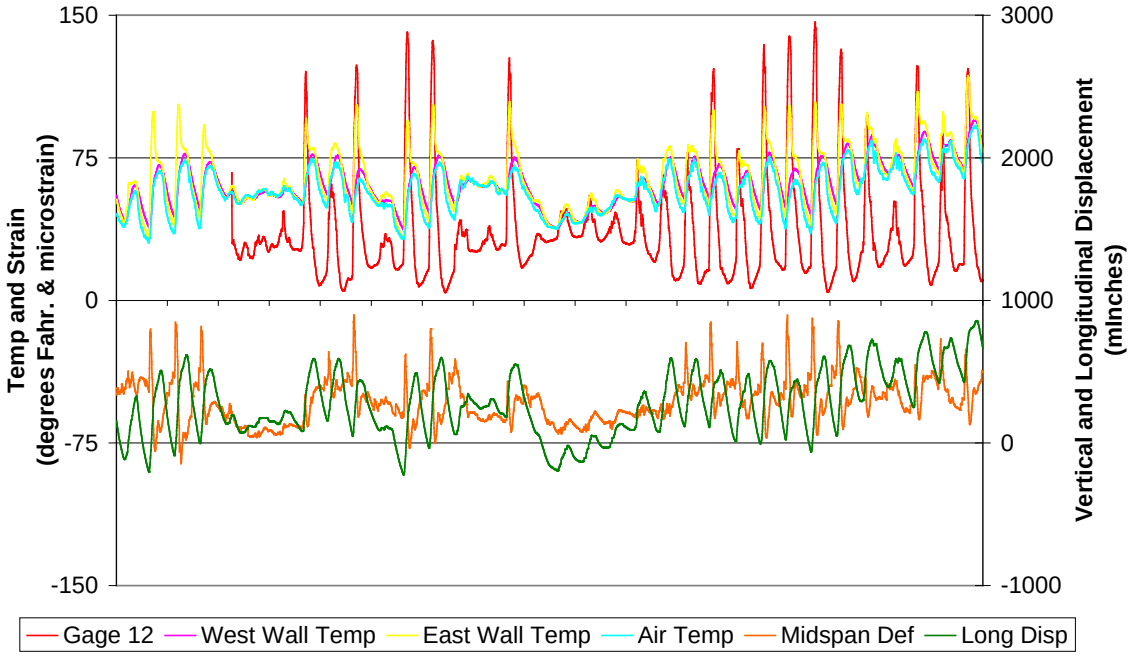

Thermal Response for Month of May 2006 - West Girder

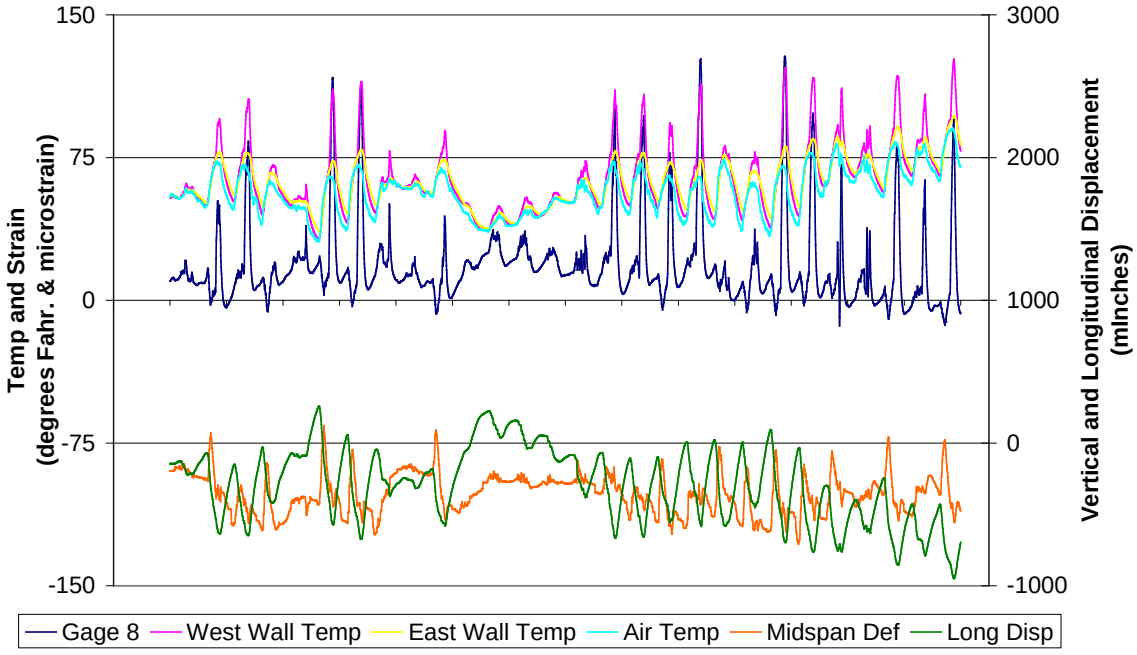

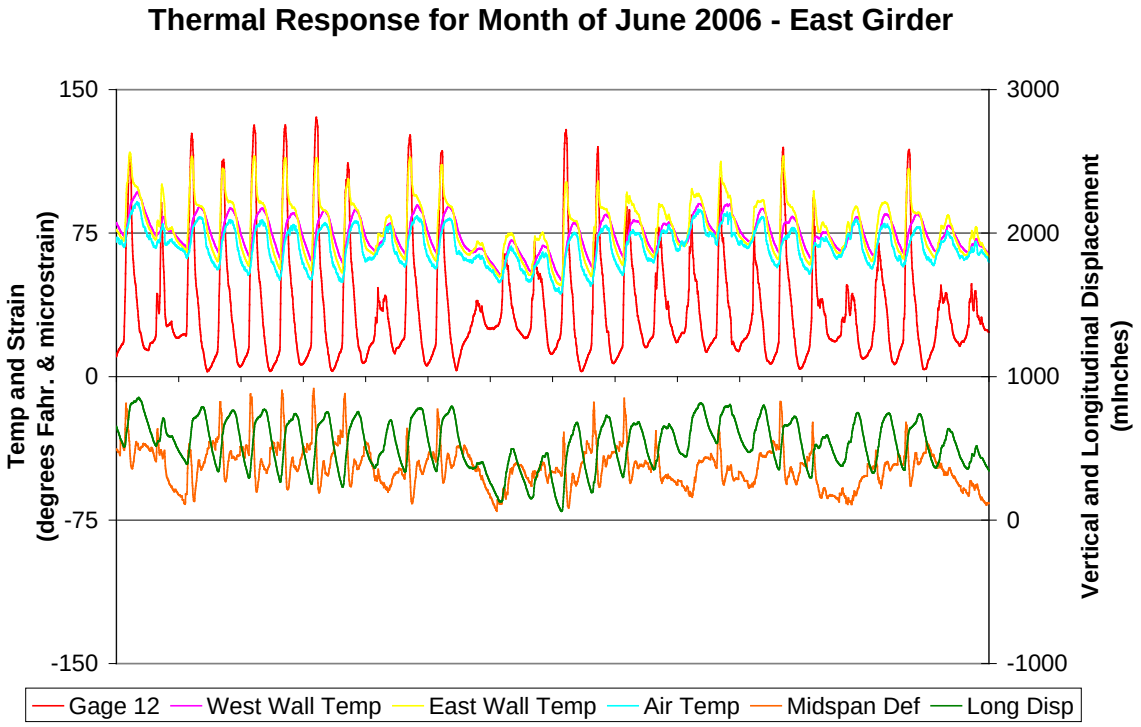
Thermal Response for Month of June 2006 - East Girder
150
75
0
-75
-150
3000
2000
1000
0
-1000
Temp and Strain
(degrees Fahr. & microstrain)
Vertical and Longitudinal Displacement
(mInches)
Gage 12
West Wall Temp
East Wall Temp
Air Temp
Midspan Def
Long Disp

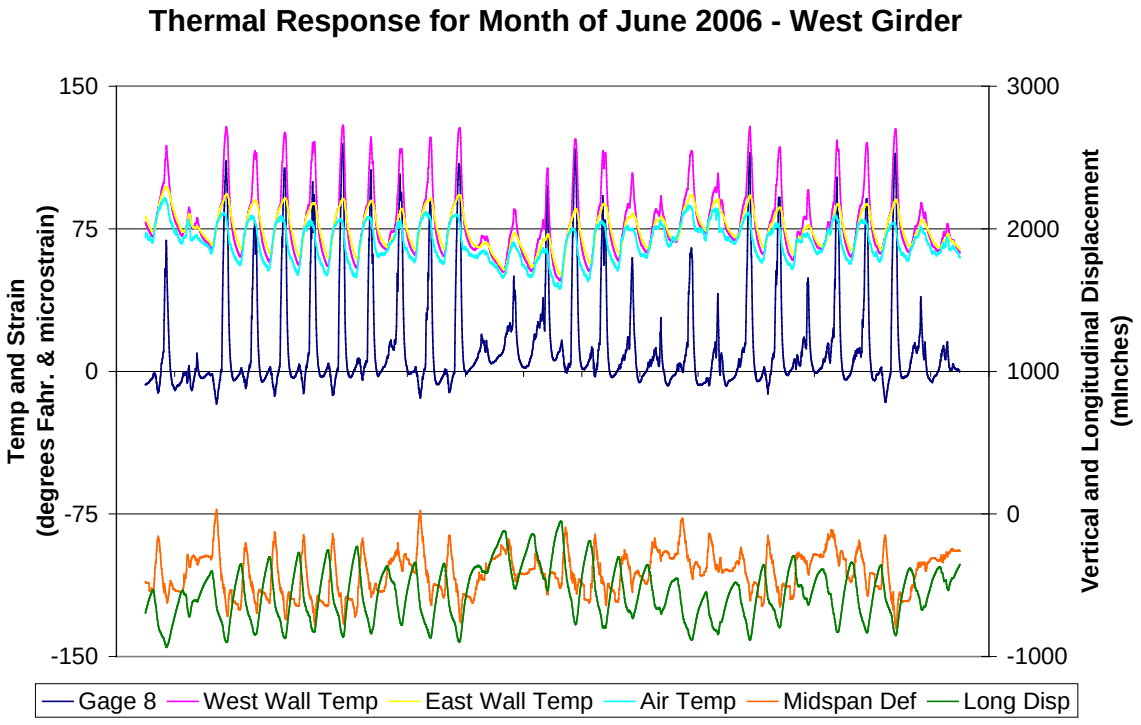
Thermal Response for Month of June 2006 - West Girder
150
75
0
-75
-150
3000
2000
1000
0
-1000
Temp and Strain
(degrees Fahr. & microstrain)
Vertical and Longitudinal Displacement
(mInches)
Gage 8
West Wall Temp
East Wall Temp
Air Temp
Midspan Def
Long Disp

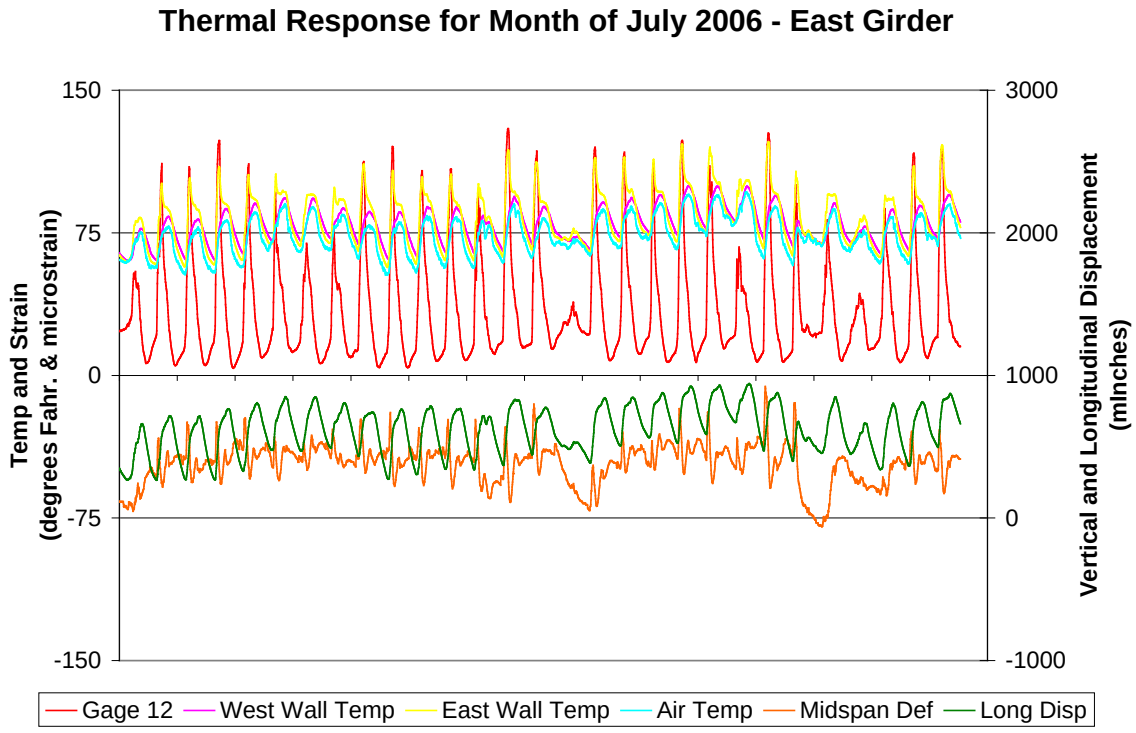
Thermal Response for Month of July 2006 - East Girder
Temp and Strain (degrees Fahr. & microstrain)
Vertical and Longitudinal Displacement (mInches)
150
75
0
-75
-150
3000
2000
1000
0
-1000
Gage 12
West Wall Temp
East Wall Temp
Air Temp
Midspan Def
Long Disp

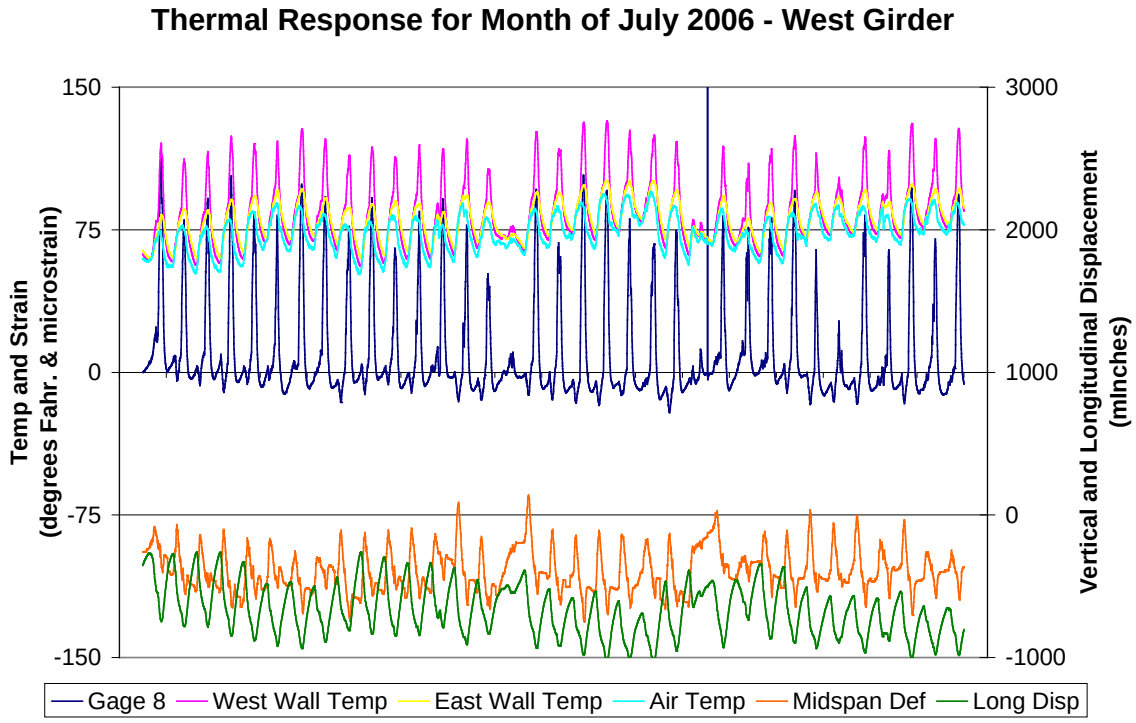
Thermal Response for Month of July 2006 - West Girder
Temp and Strain (degrees Fahr. & microstrain)
Vertical and Longitudinal Displacement (mInches)
150
75
0
-75
-150
3000
2000
1000
0
-1000
Gage 8
West Wall Temp
East Wall Temp
Air Temp
Midspan Def
Long Disp

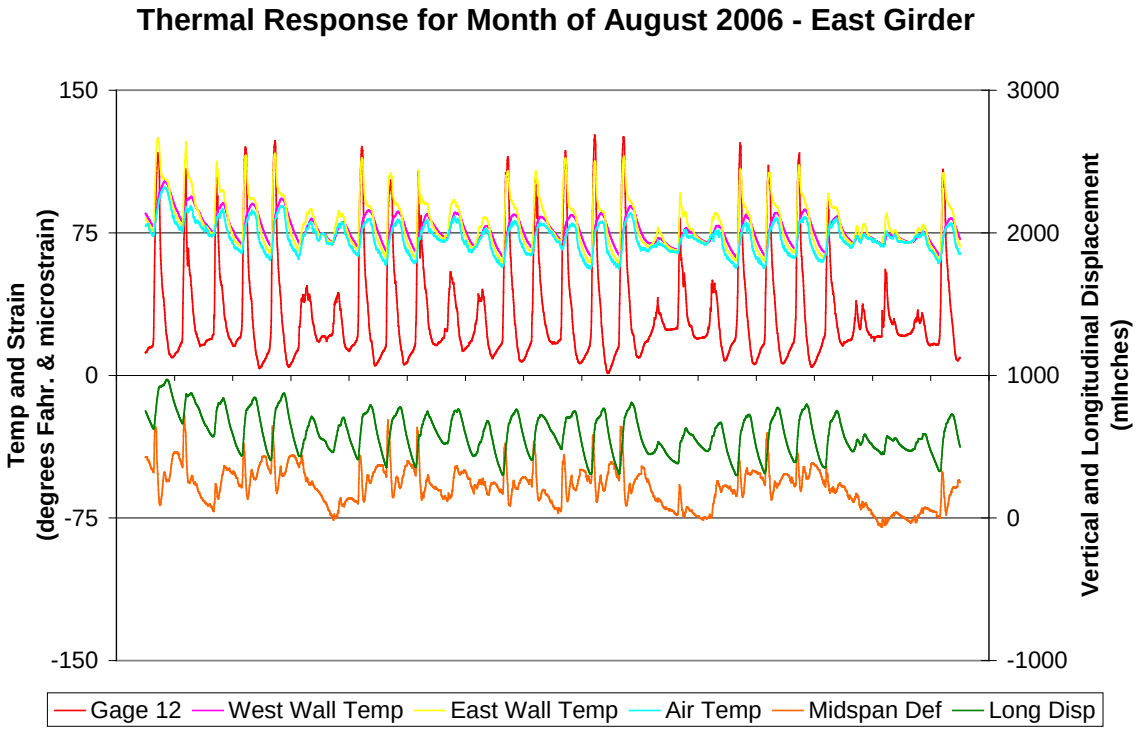
Thermal Response for Month of August 2006 - East Girder
Temp and Strain (degrees Fahr. & microstrain)
Vertical and Longitudinal Displacement (mInches)
150
75
0
-75
-150
3000
2000
1000
0
-1000
Gage 12
West Wall Temp
East Wall Temp
Air Temp
Midspan Def
Long Disp

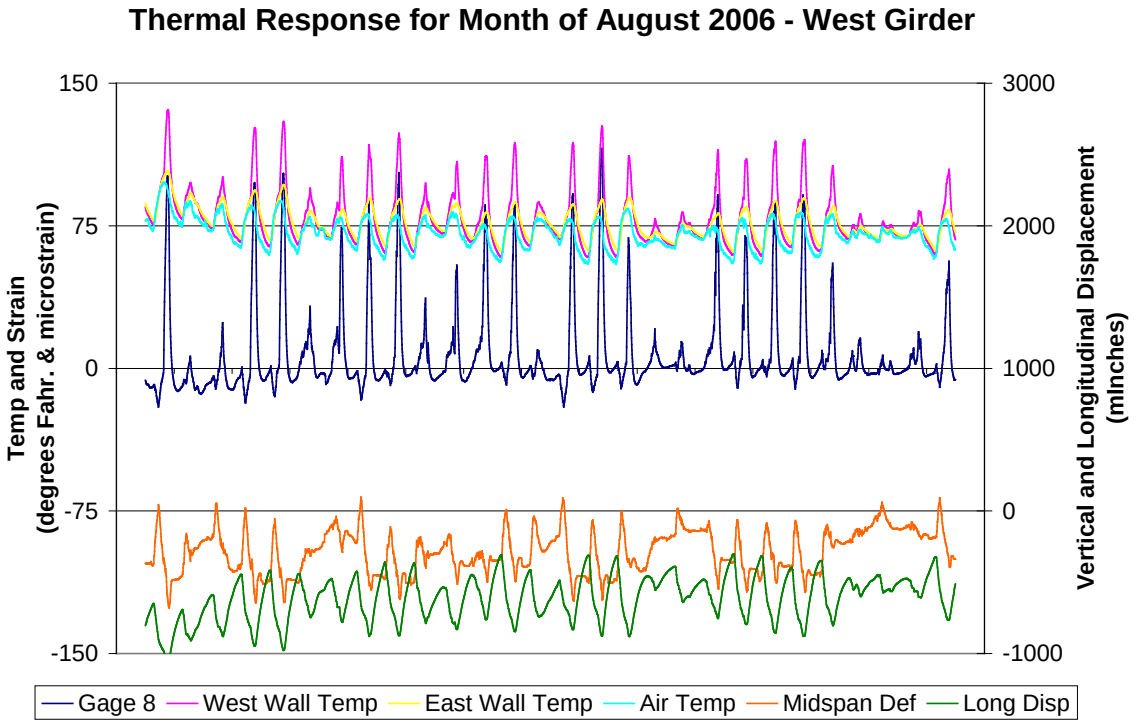
Thermal Response for Month of August 2006 - West Girder
Temp and Strain (degrees Fahr. & microstrain)
Vertical and Longitudinal Displacement (mInches)
150
75
0
-75
-150
3000
2000
1000
0
-1000
Gage 8
West Wall Temp
East Wall Temp
Air Temp
Midspan Def
Long Disp

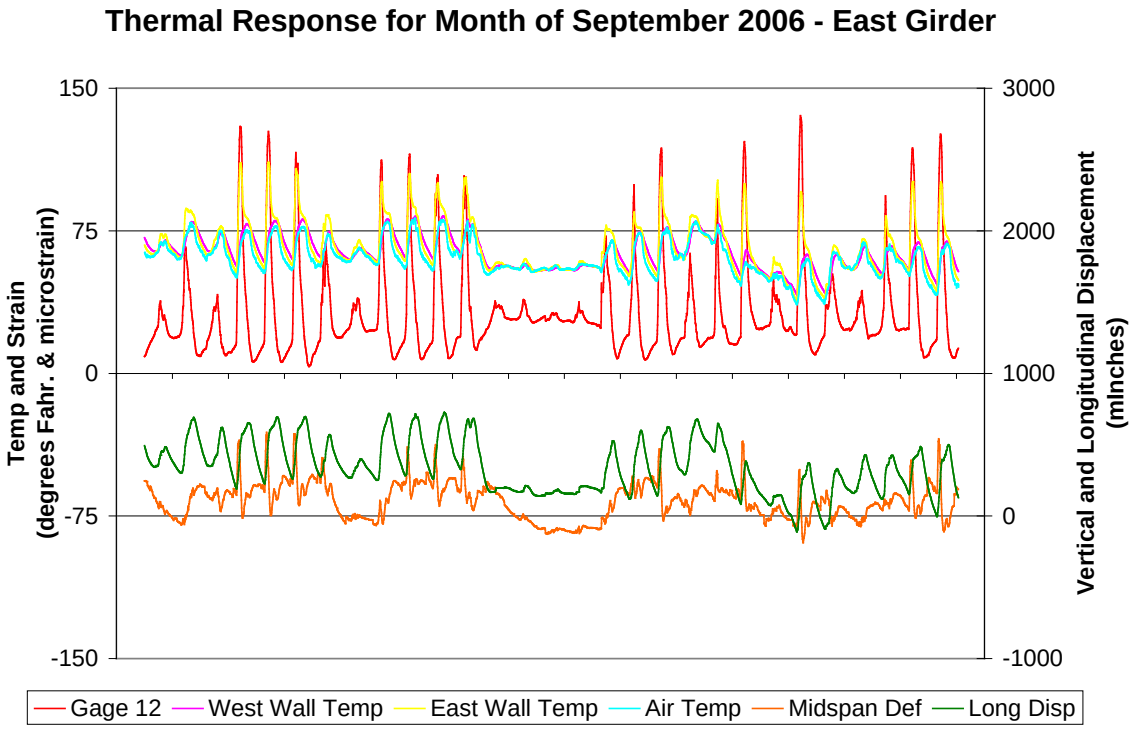
Thermal Response for Month of September 2006 - East Girder
Temp and Strain (degrees Fahr. & microstrain)
Vertical and Longitudinal Displacement (mInches)
150
75
0
-75
-150
3000
2000
1000
0
-1000
Gage 12
West Wall Temp
East Wall Temp
Air Temp
Midspan Def
Long Disp

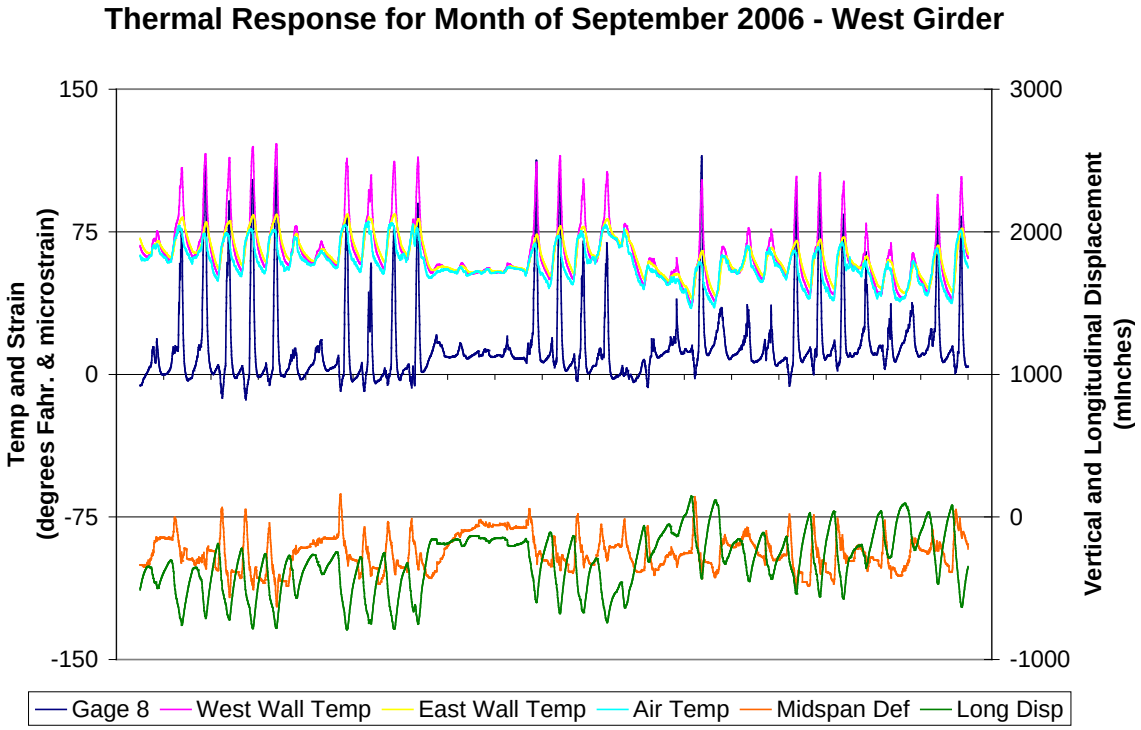
Thermal Response for Month of September 2006 - West Girder
Temp and Strain (degrees Fahr. & microstrain)
Vertical and Longitudinal Displacement (mInches)
150
75
0
-75
-150
3000
2000
1000
0
-1000
Gage 8
West Wall Temp
East Wall Temp
Air Temp
Midspan Def
Long Disp

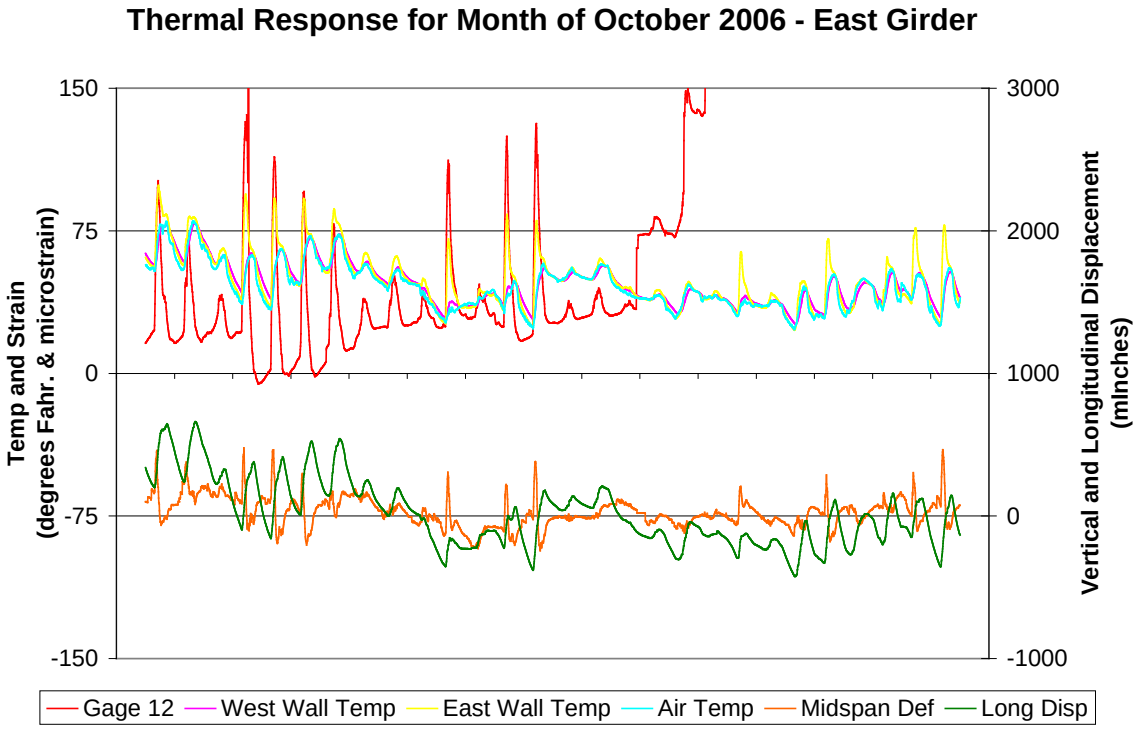
Thermal Response for Month of October 2006 - East Girder
Temp and Strain (degrees Fahr. & microstrain)
Vertical and Longitudinal Displacement (mInches)
150
75
0
-75
-150
3000
2000
1000
0
-1000
Gage 12
West Wall Temp
East Wall Temp
Air Temp
Midspan Def
Long Disp

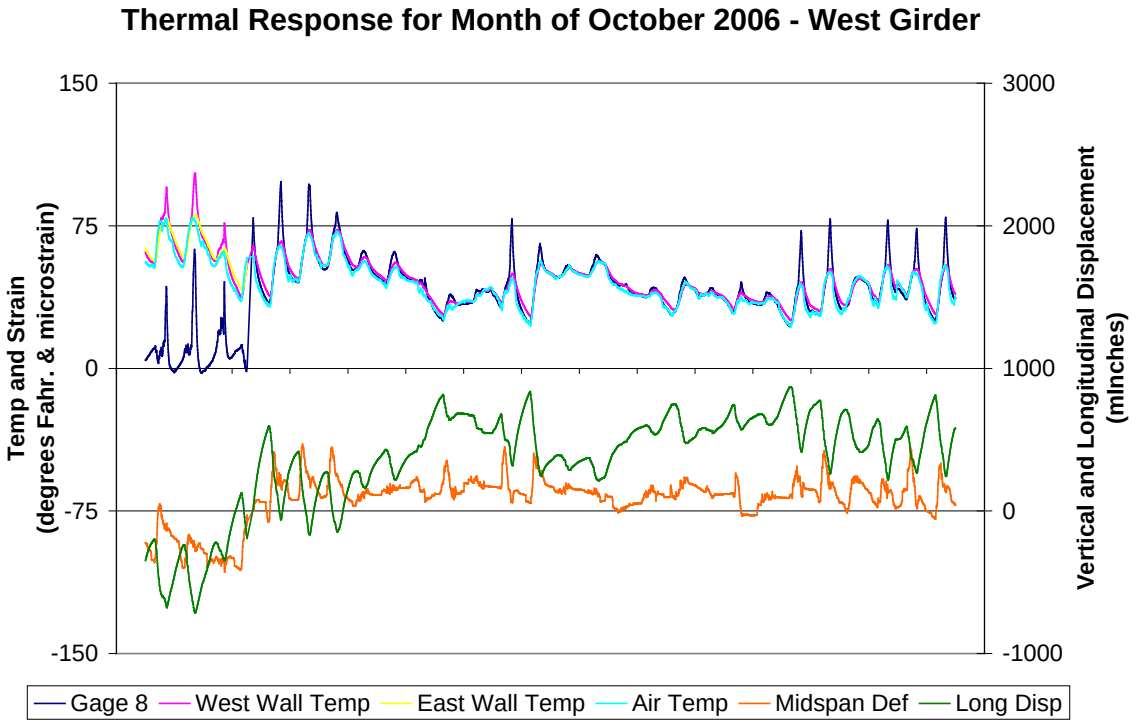
Thermal Response for Month of October 2006 - West Girder
Temp and Strain (degrees Fahr. & microstrain)
Vertical and Longitudinal Displacement (mInches)
150
75
0
-75
-150
3000
2000
1000
0
-1000
Gage 8
West Wall Temp
East Wall Temp
Air Temp
Midspan Def
Long Disp

Thermal Response for Month of November 2006 - East Girder

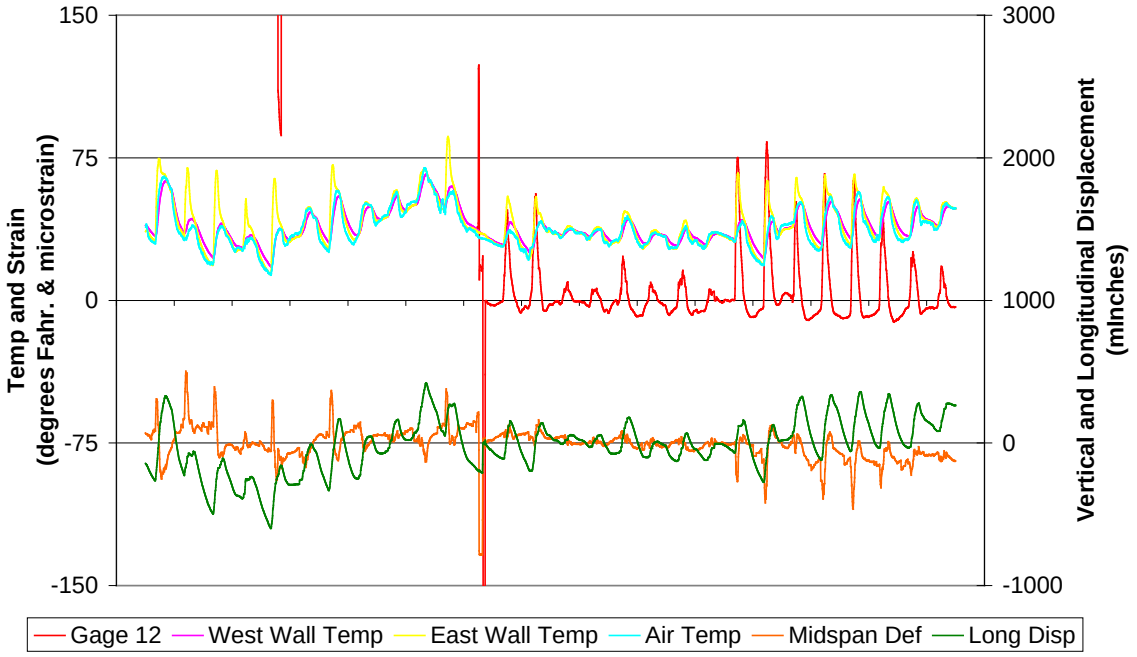

Thermal Response for Month of November 2007 - West Girder

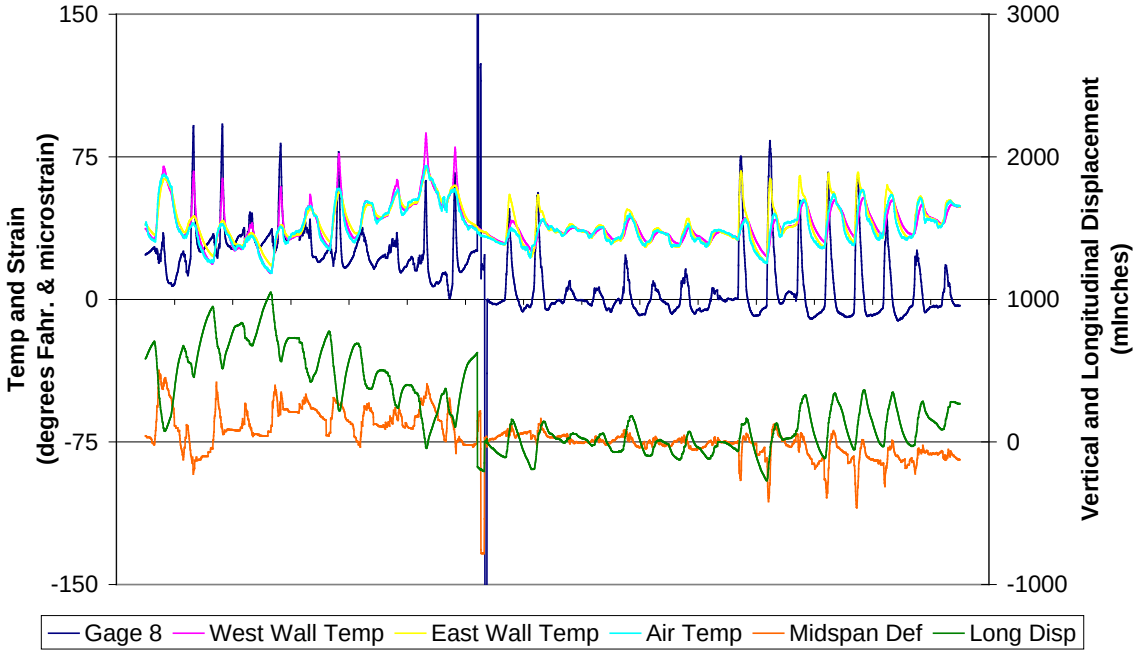

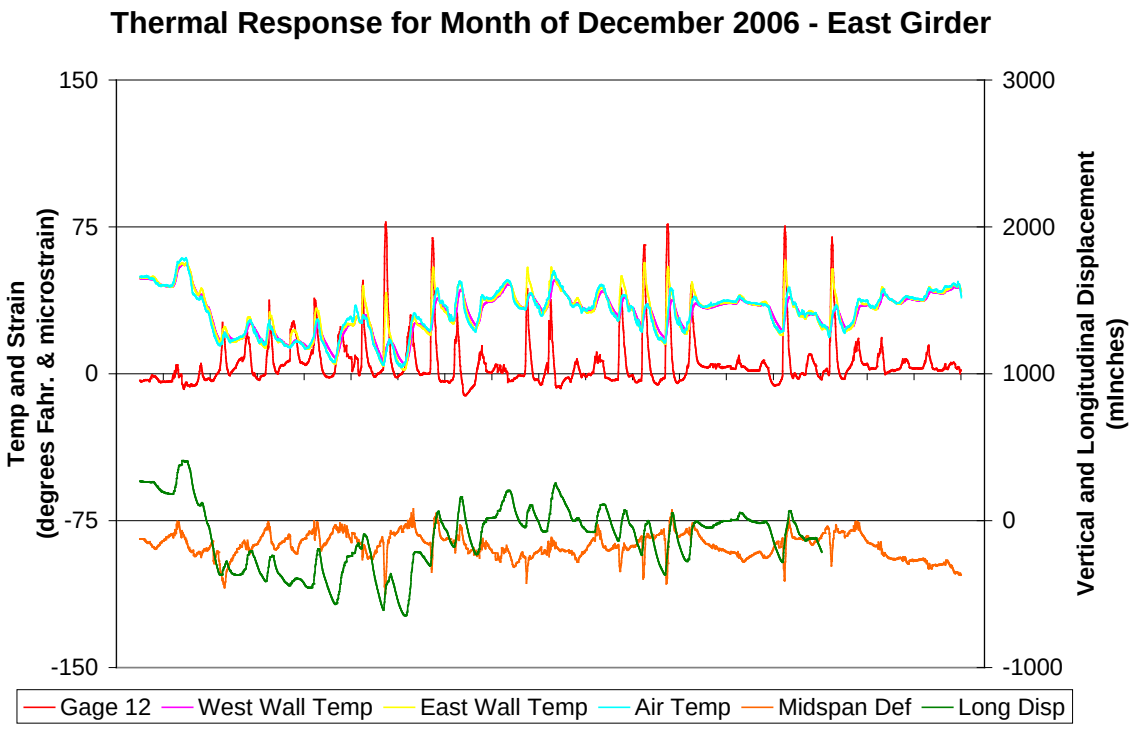
Thermal Response for Month of December 2006 - East Girder
Temp and Strain (degrees Fahr. & microstrain)
Vertical and Longitudinal Displacement (mInches)
150
75
0
-75
-150
3000
2000
1000
0
-1000
Gage 12
West Wall Temp
East Wall Temp
Air Temp
Midspan Def
Long Disp

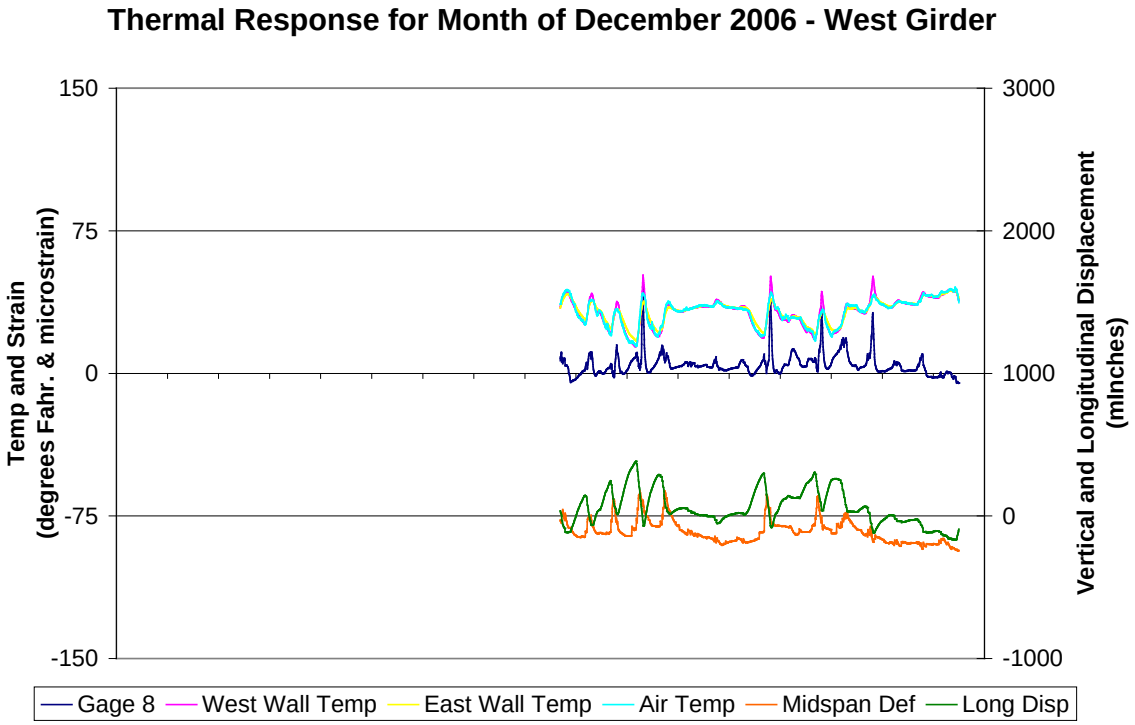
Thermal Response for Month of December 2006 - West Girder
Temp and Strain (degrees Fahr. & microstrain)
Vertical and Longitudinal Displacement (mInches)
150
75
0
-75
-150
3000
2000
1000
0
-1000
Gage 8
West Wall Temp
East Wall Temp
Air Temp
Midspan Def
Long Disp

APPENDIX B

SAMPLE OF MONTHLY TRAFFIC CYCLE GRAPHS

The graphs shown in Appendix B are an example of those prepared for each month of structural monitoring. Graphs from 2006 have been presented as they are representative of the yearly data observed. Data is presented for both the east and the west girders.

As previously mentioned in the body of this report, live load results were very consistent from year to year; no significant change in traffic load pattern was observed. As seen in this data, stress cycle counts were relatively consistent from month to month as well. A majority (approximately 95%)of the 8,000 to 9,000 traffic load cycles recorded per year occurred at the stress range level of 1.3 ksi or lower. The remainder of the traffic load cycles occurred in the 1.6 to 3.9 ksi stress ranges.

Distribution of Traffic Stress Cycles for Month of January 2006 - East Girder

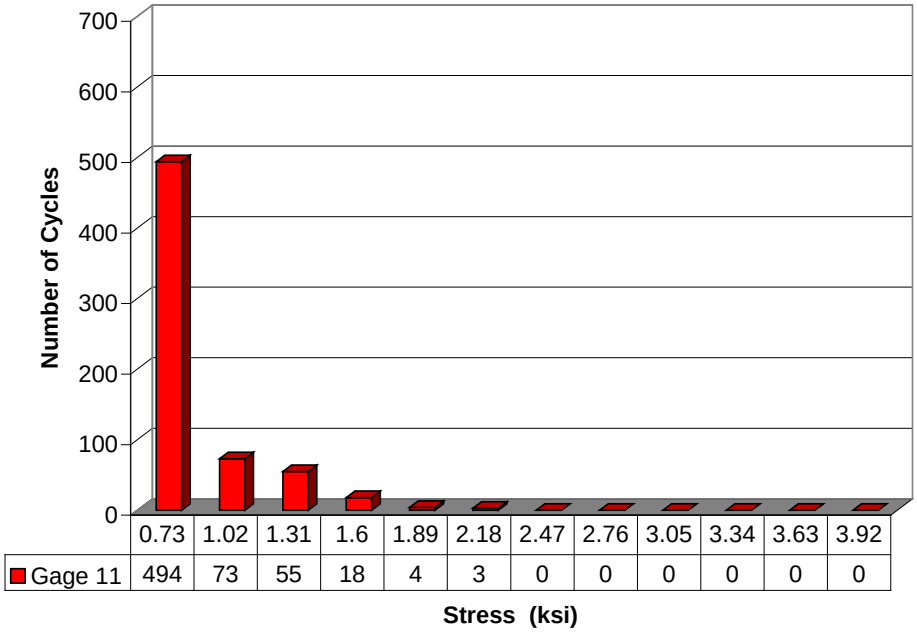

	0.73	1.02	1.31	1.6	1.89	2.18	2.47	2.76	3.05	3.34	3.63	3.92
Gage 11	494	73	55	18	4	3	0	0	0	0	0	0

Stress (ksi)

Distribution of Traffic Stress Cycles for Month of January 2006 - West Girder

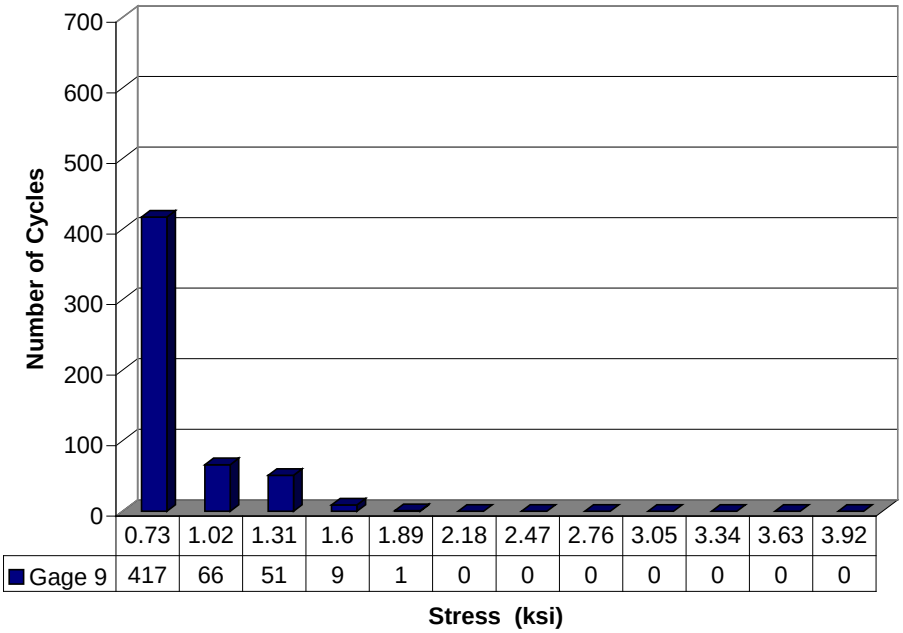

	0.73	1.02	1.31	1.6	1.89	2.18	2.47	2.76	3.05	3.34	3.63	3.92
Gage 9	417	66	51	9	1	0	0	0	0	0	0	0

Stress (ksi)

Distribution of Traffic Stress Cycles for Month of February 2006 - East Girder

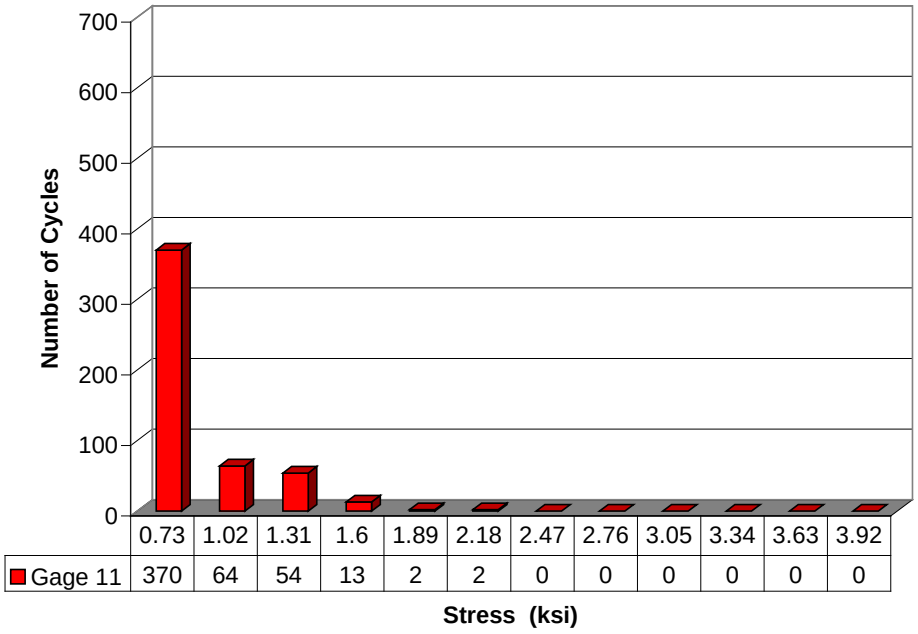

Distribution of Traffic Stress Cycles for Month of February 2006 - West Girder

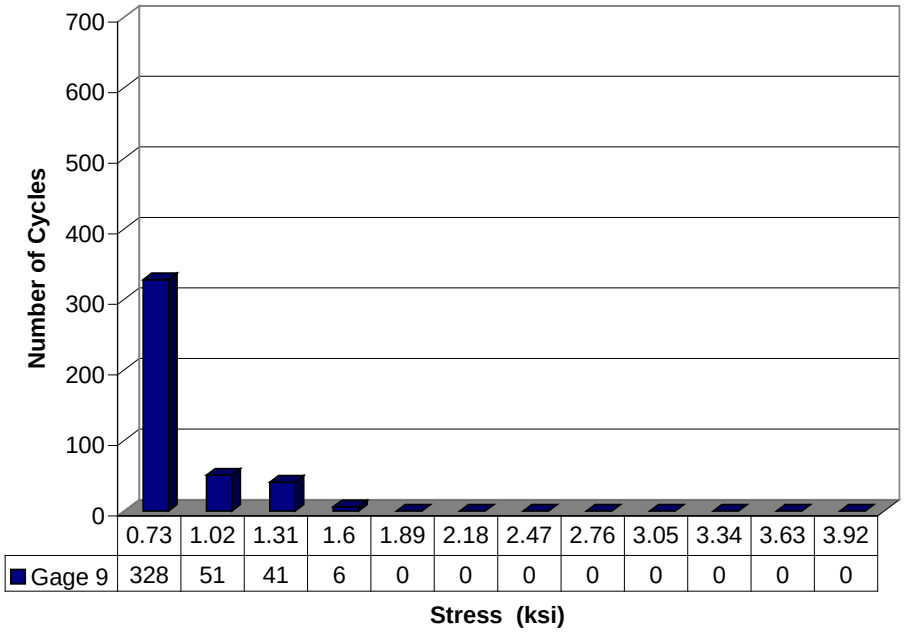

Distribution of Traffic Stress Cycles for Month of March 2006 - East Girder

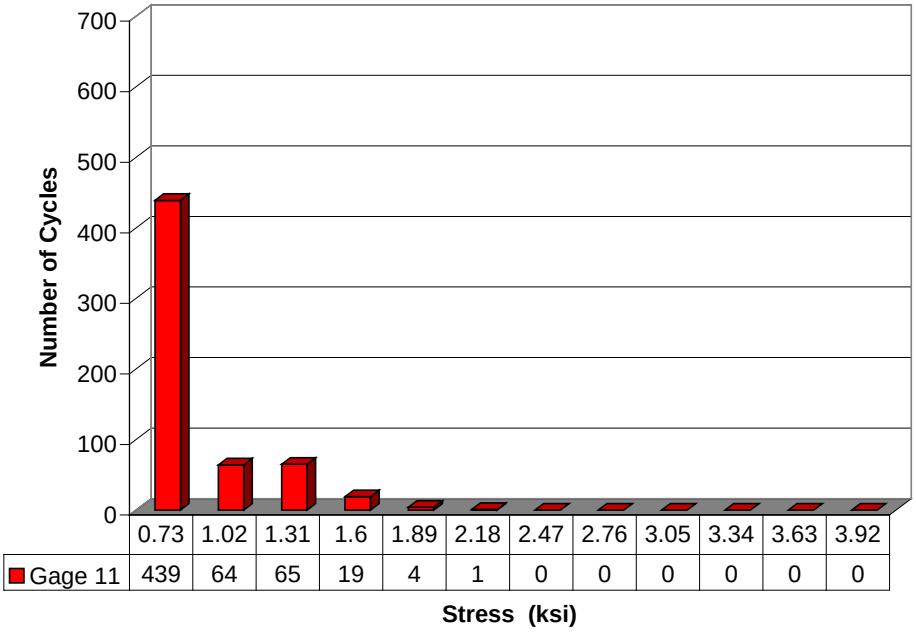

	0.73	1.02	1.31	1.6	1.89	2.18	2.47	2.76	3.05	3.34	3.63	3.92
Gage 11	439	64	65	19	4	1	0	0	0	0	0	0

Stress (ksi)

Distribution of Traffic Stress Cycles for Month of March 2006 - West Girder

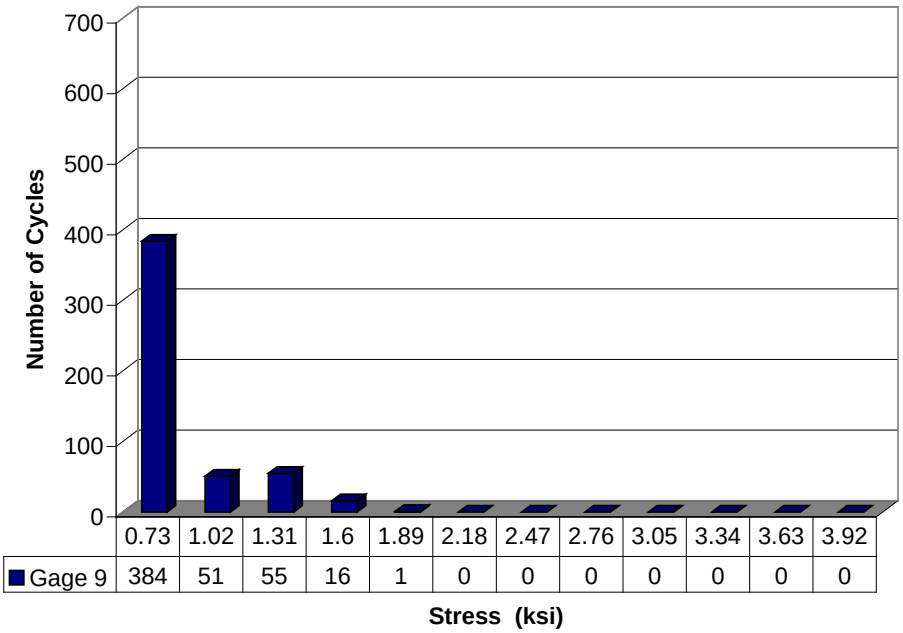

	0.73	1.02	1.31	1.6	1.89	2.18	2.47	2.76	3.05	3.34	3.63	3.92
Gage 9	384	51	55	16	1	0	0	0	0	0	0	0

Stress (ksi)

Distribution of Traffic Stress Cycles for Month of April 2006 - East Girder

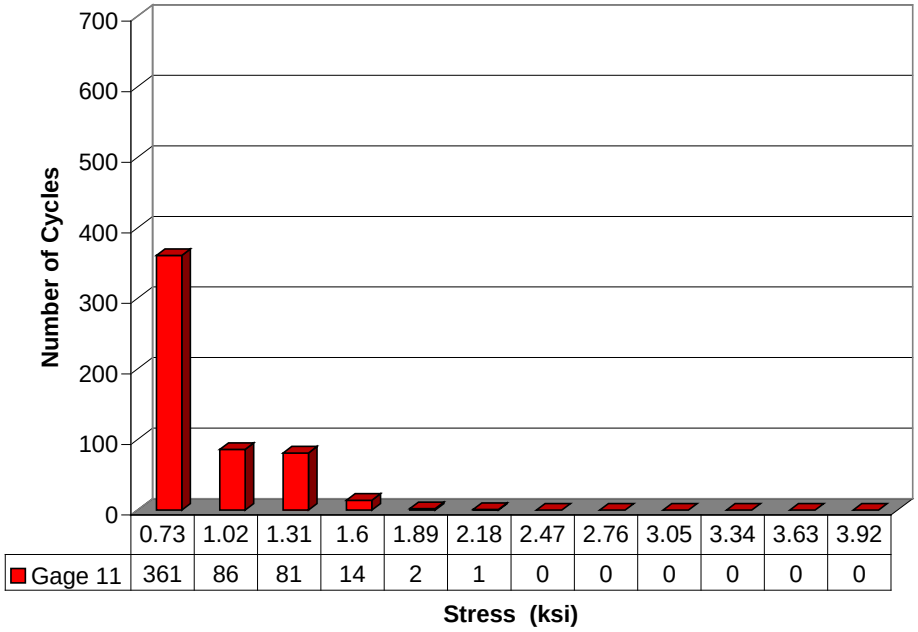

	0.73	1.02	1.31	1.6	1.89	2.18	2.47	2.76	3.05	3.34	3.63	3.92
Gage 11	361	86	81	14	2	1	0	0	0	0	0	0

Stress (ksi)

Distribution of Traffic Stress Cycles for Month of April 2006 - West Girder

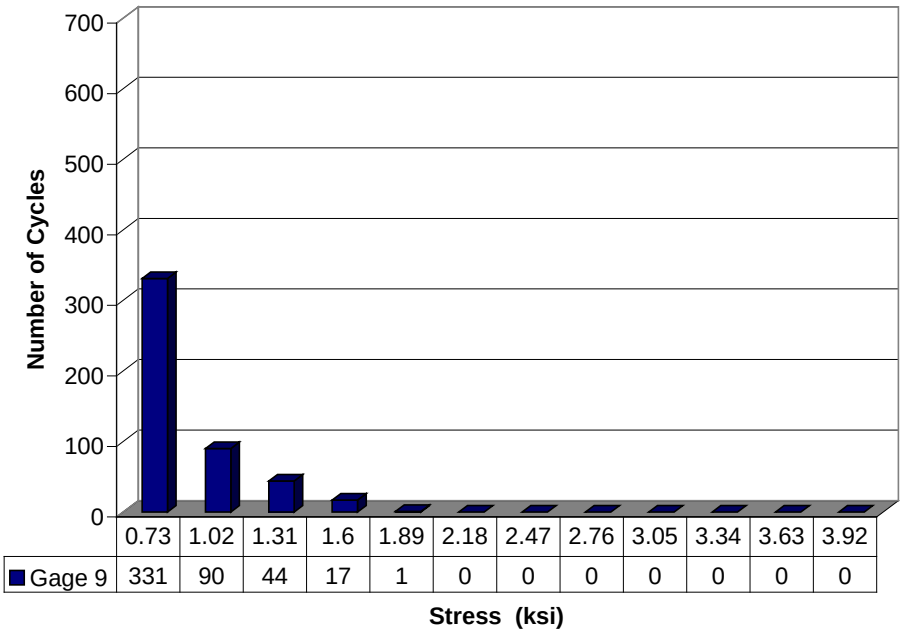

	0.73	1.02	1.31	1.6	1.89	2.18	2.47	2.76	3.05	3.34	3.63	3.92
Gage 9	331	90	44	17	1	0	0	0	0	0	0	0

Stress (ksi)

Distribution of Traffic Stress Cycles for Month of May 2006 - East Girder

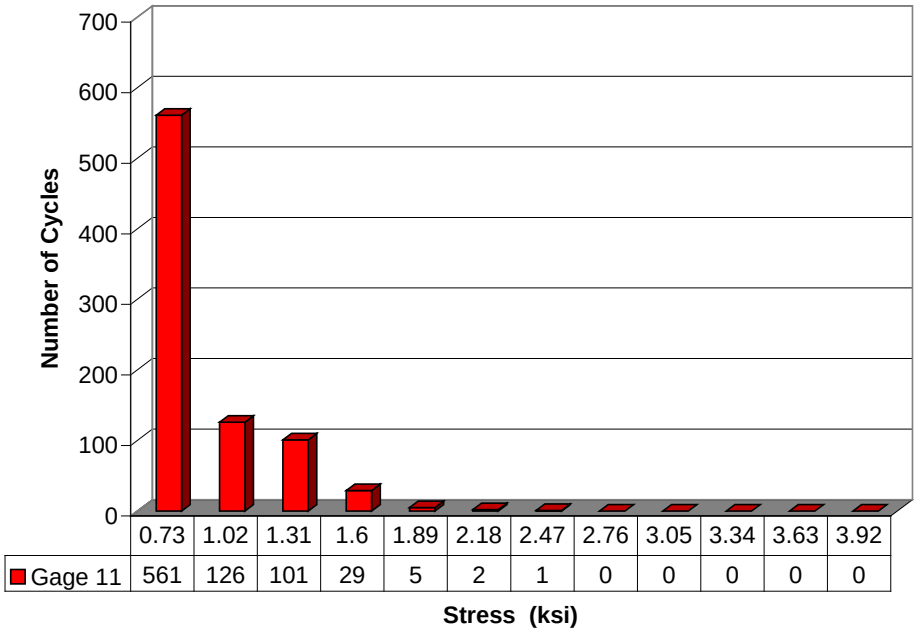

Distribution of Traffic Stress Cycles for Month of May 2006 - West Girder

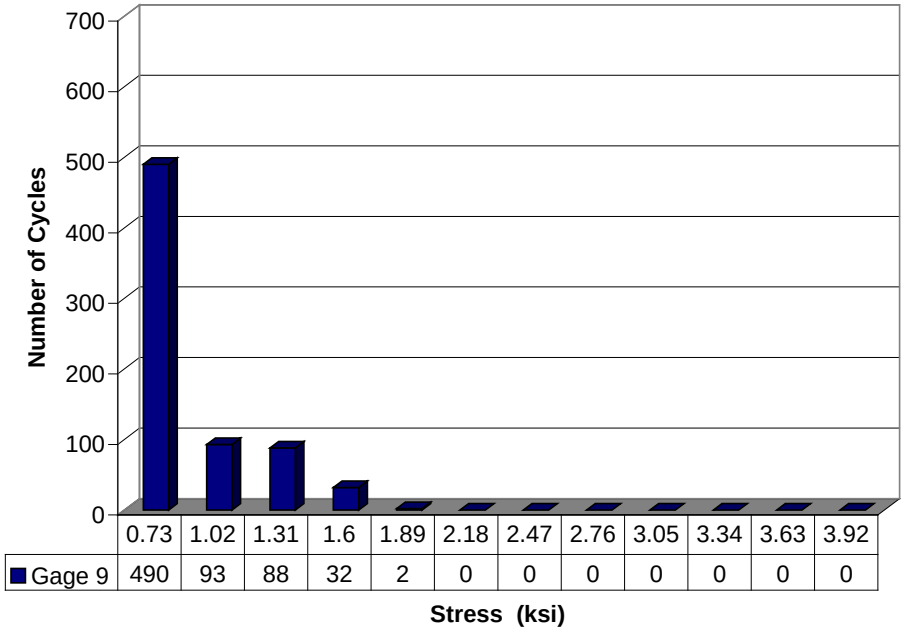

Distribution of Traffic Stress Cycles for Month of June 2006 - East Girder

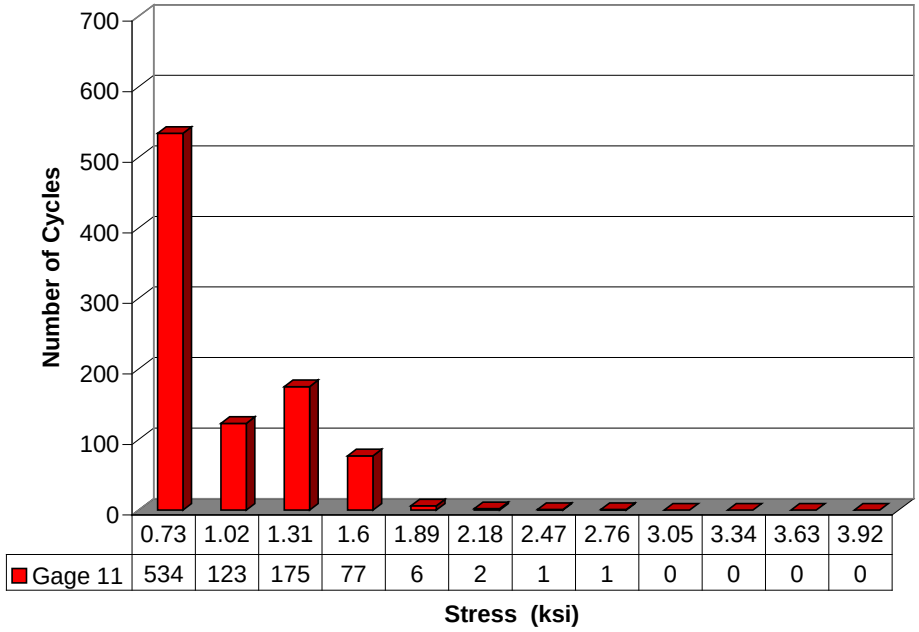

Distribution of Traffic Stress Cycles for Month of June 2006 - West Girder

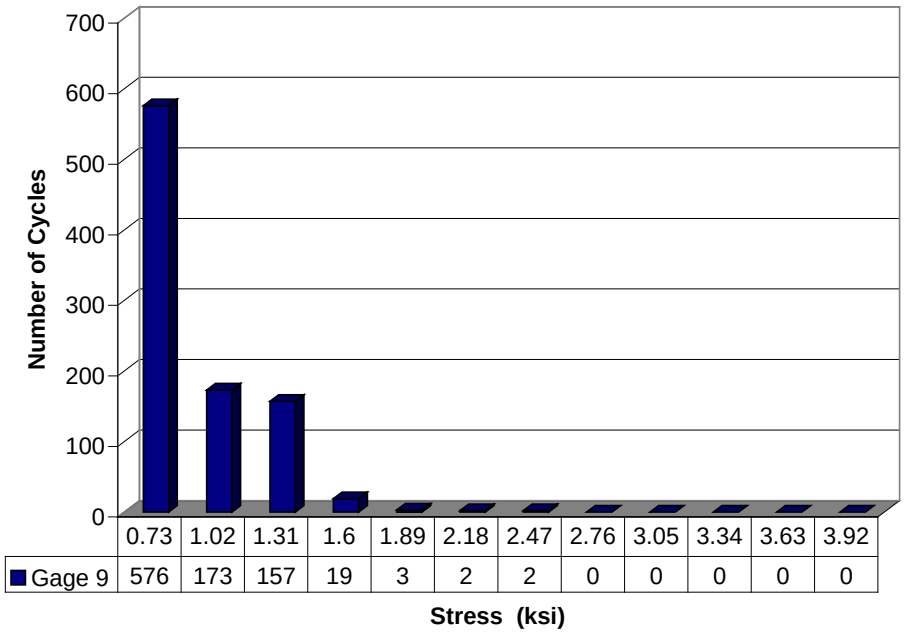

Distribution of Traffic Stress Cycles for Month of July 2006 - East Girder

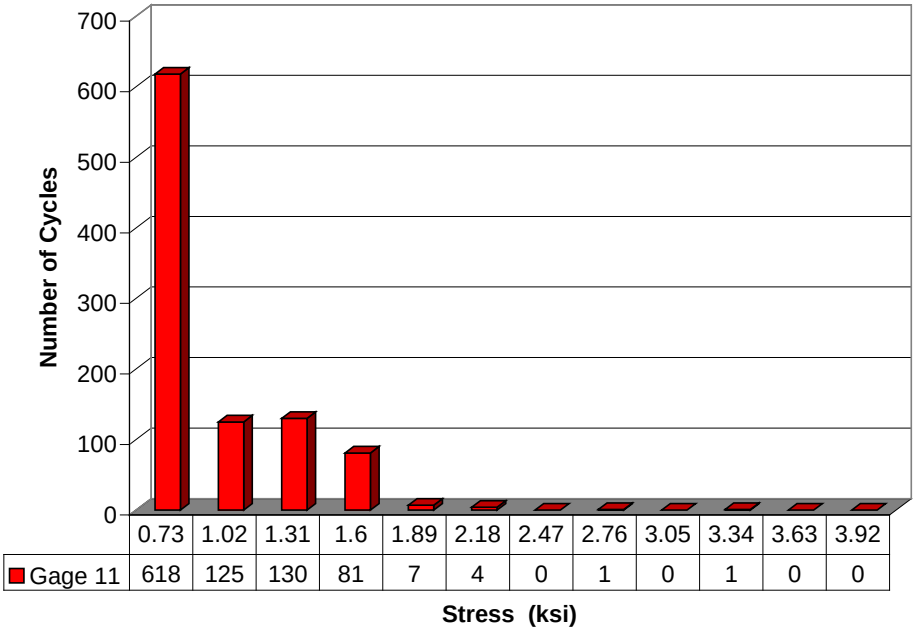

	0.73	1.02	1.31	1.6	1.89	2.18	2.47	2.76	3.05	3.34	3.63	3.92
Gage 11	618	125	130	81	7	4	0	1	0	1	0	0

Stress (ksi)

Distribution of Traffic Stress Cycles for Month of July 2006 - West Girder

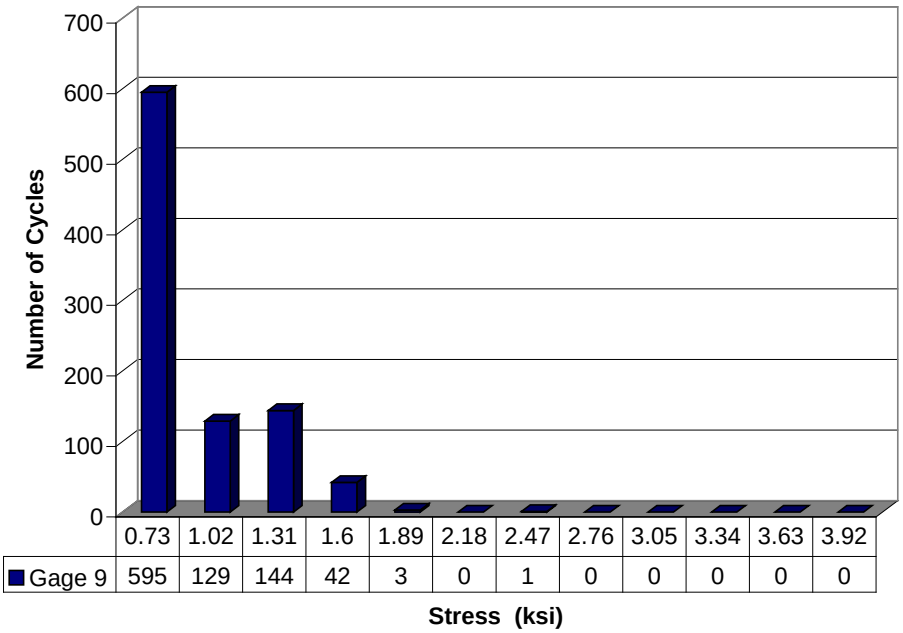

	0.73	1.02	1.31	1.6	1.89	2.18	2.47	2.76	3.05	3.34	3.63	3.92
Gage 9	595	129	144	42	3	0	1	0	0	0	0	0

Stress (ksi)

Distribution of Traffic Stress Cycles for Month of August 2006 - East Girder

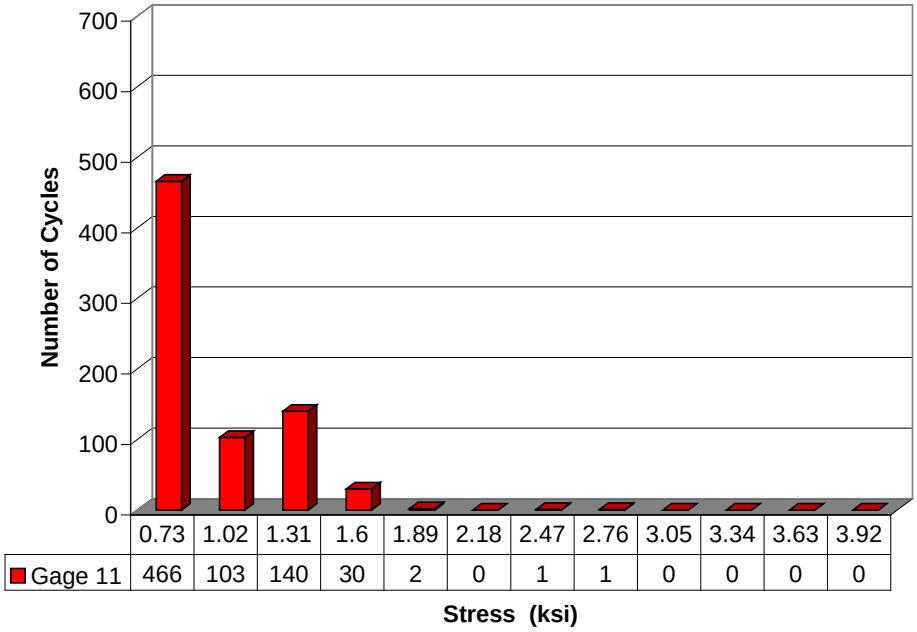

Distribution of Traffic Stress Cycles for Month of August 2006 - West Girder

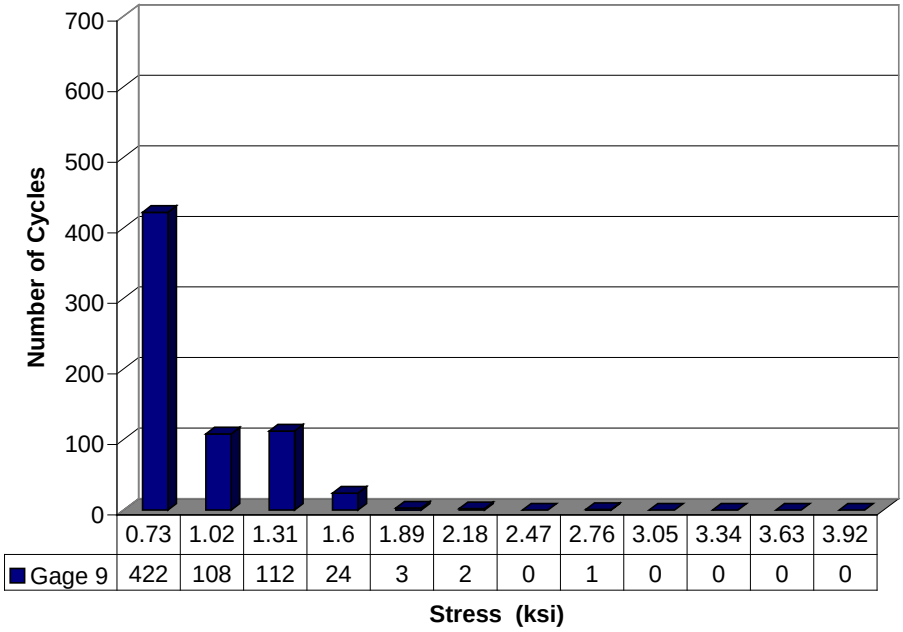

Distribution of Traffic Stress Cycles for Month of September 2006 - East Girder

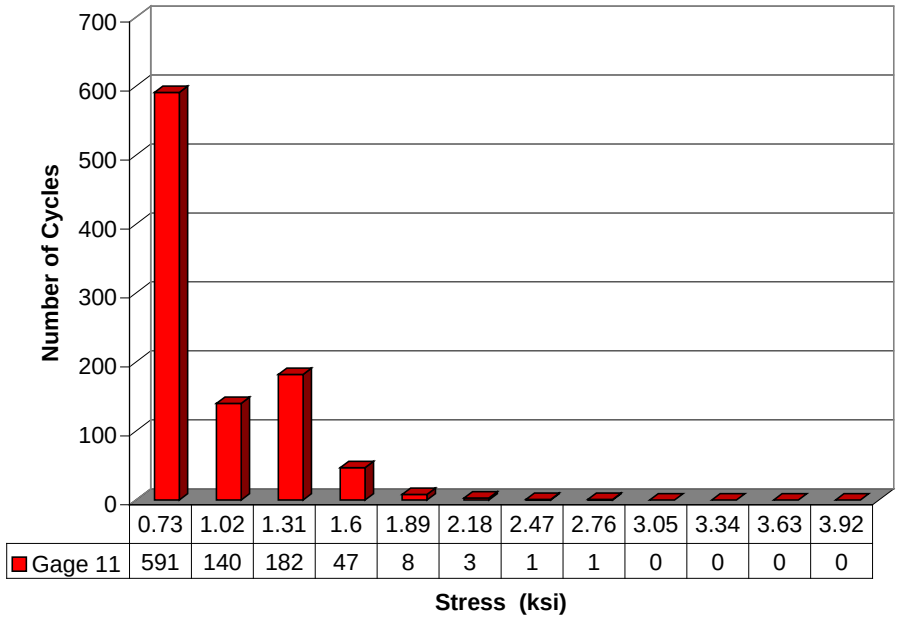

	0.73	1.02	1.31	1.6	1.89	2.18	2.47	2.76	3.05	3.34	3.63	3.92
Gage 11	591	140	182	47	8	3	1	1	0	0	0	0

Stress (ksi)

Distribution of Traffic Stress Cycles for Month of September 2006 - West Girder

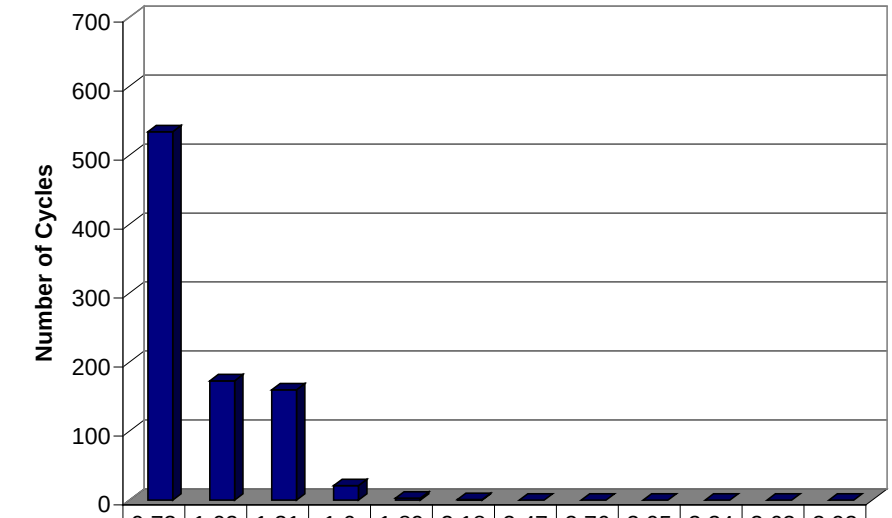

	0.73	1.02	1.31	1.6	1.89	2.18	2.47	2.76	3.05	3.34	3.63	3.92
Gage 9	534	173	160	21	3	1	0	0	0	0	0	0

Stress (ksi)

Distribution of Traffic Stress Cycles for Month of October 2006 - East Girder

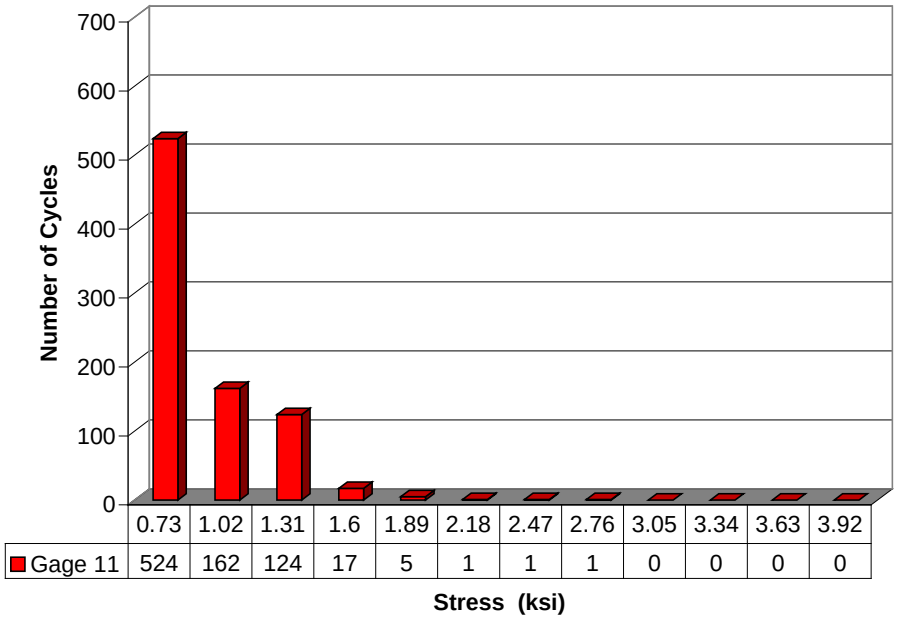

	0.73	1.02	1.31	1.6	1.89	2.18	2.47	2.76	3.05	3.34	3.63	3.92
Gage 11	524	162	124	17	5	1	1	1	0	0	0	0

Stress (ksi)

Distribution of Traffic Stress Cycles for Month of October 2006 - West Girder

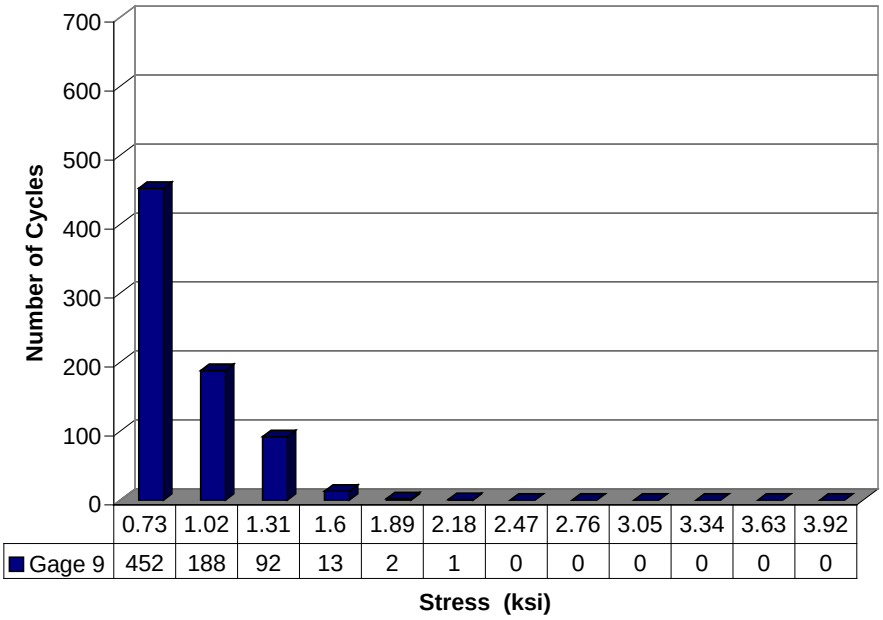

	0.73	1.02	1.31	1.6	1.89	2.18	2.47	2.76	3.05	3.34	3.63	3.92
Gage 9	452	188	92	13	2	1	0	0	0	0	0	0

Stress (ksi)

Distribution of Traffic Stress Cycles for Month of November 2006 - East Girder

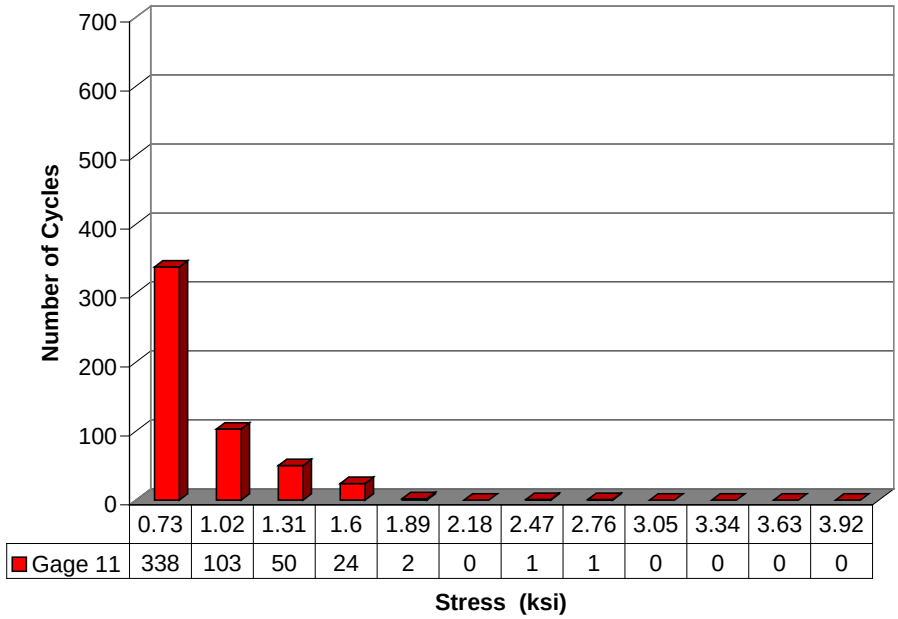

Distribution of Traffic Stress Cycles for Month of November 2007 - West Girder

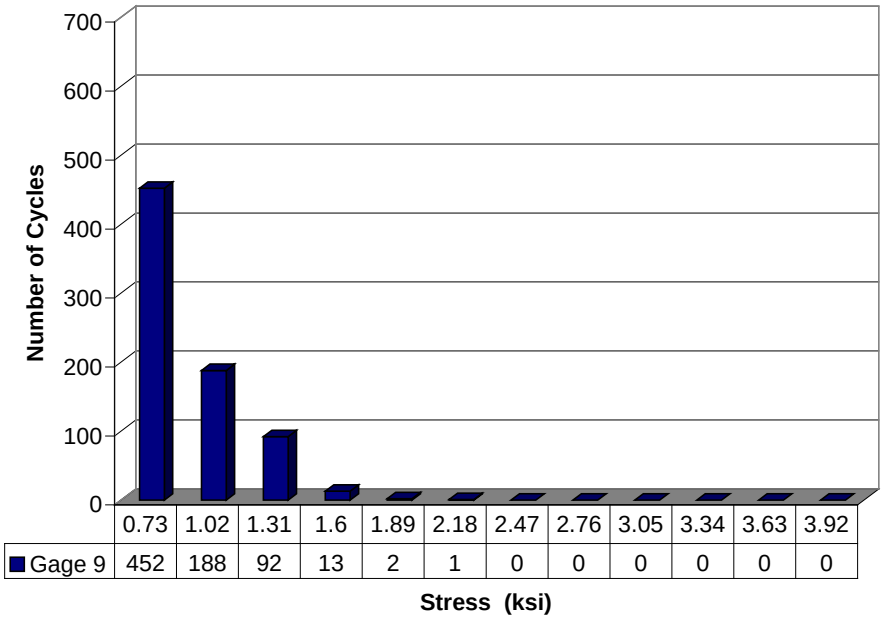

Distribution of Traffic Stress Cycles for Month of December 2006 - East Girder

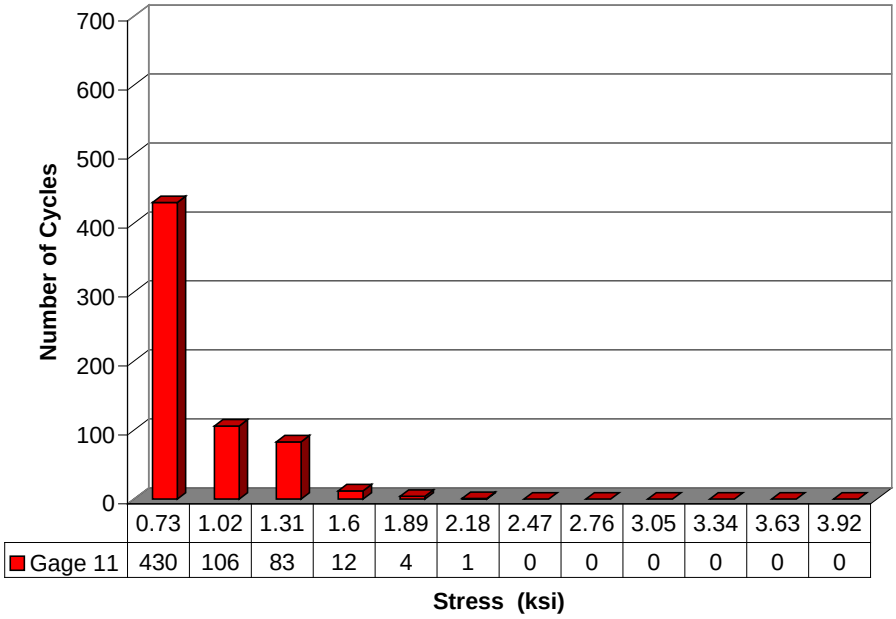

	0.73	1.02	1.31	1.6	1.89	2.18	2.47	2.76	3.05	3.34	3.63	3.92
Gage 11	430	106	83	12	4	1	0	0	0	0	0	0

Stress (ksi)

Distribution of Traffic Stress Cycles for Month of December 2006 - West Girder

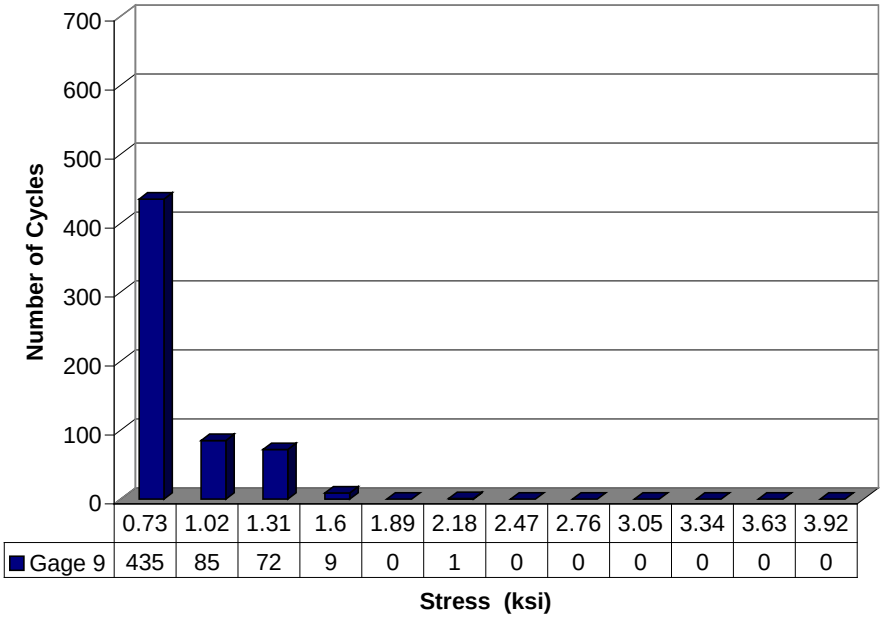

	0.73	1.02	1.31	1.6	1.89	2.18	2.47	2.76	3.05	3.34	3.63	3.92
Gage 9	435	85	72	9	0	1	0	0	0	0	0	0

Stress (ksi)

APPENDIX C

TRUCK LOADING COMBINATIONS

The figures shown in Appendix C are a representation of the different truck loading combinations that were performed for the field testing. Each truck run was performed to the best of the research team's ability to assure that the actual truck spacing represented what is shown in each figure. These truck loading combinations were chosen not only to calculate the live load distribution factors but to also verify that the stresses obtained from the field testing were accurate.

Truck Run #1: Truck 1 at 2’ from east railing (At Crawling Speed)

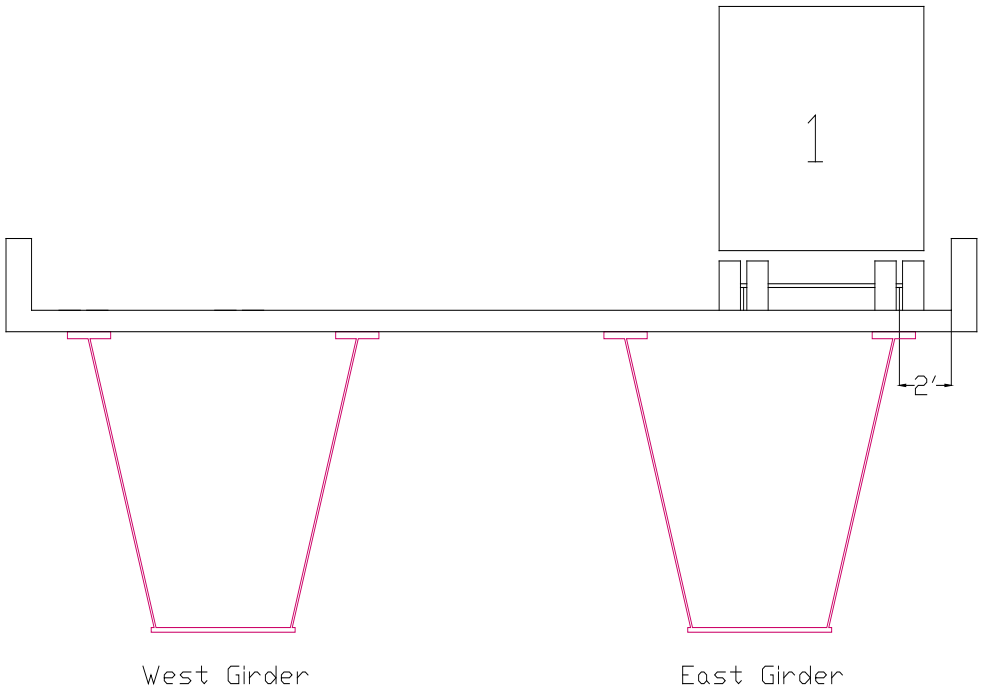

Truck Run #2: Truck 1 at 2’ from west railing (At Crawling Speed)

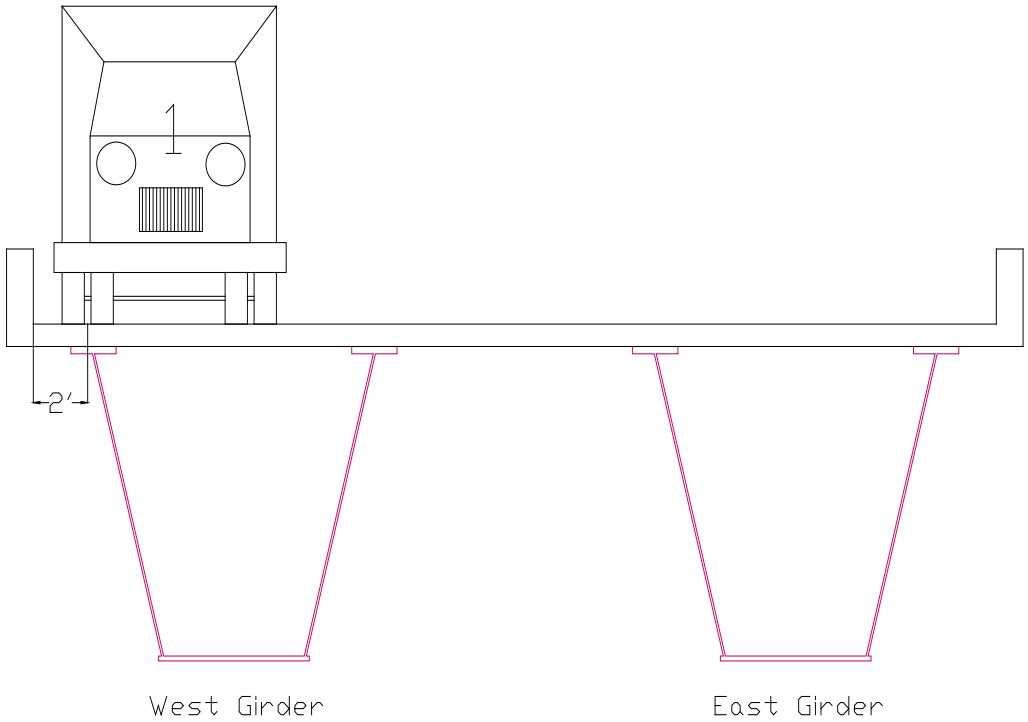

Truck Run #3: Truck 1 at 12.5’ from east railing (At Crawling Speed)

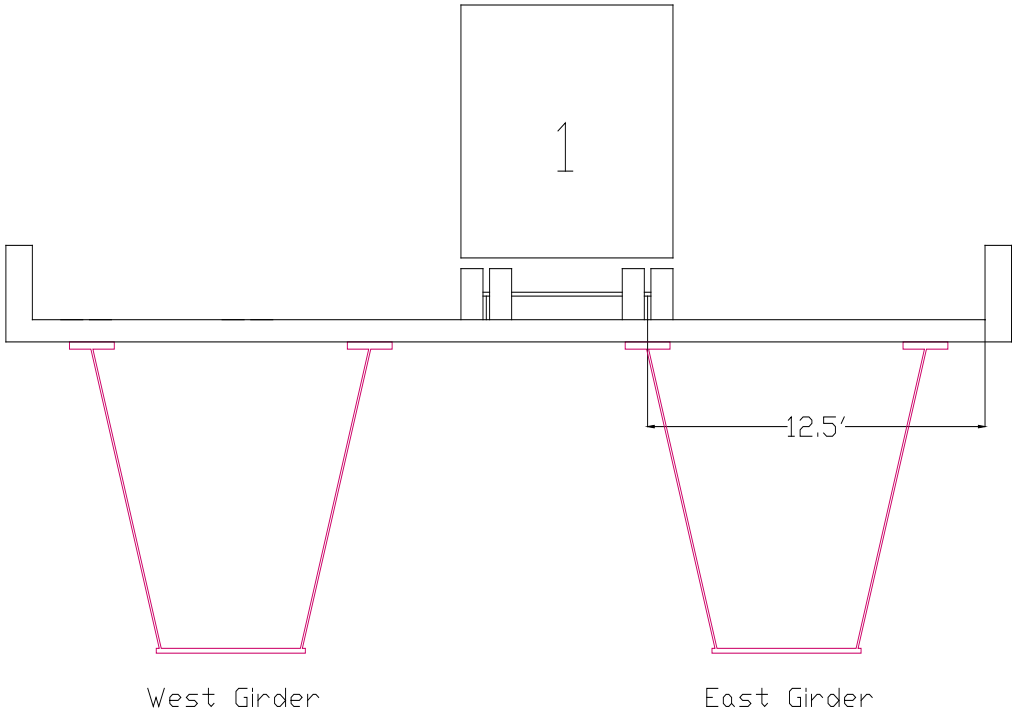

Truck Run #4: Truck 1 at 12.5' from west railing (At Crawling Speed)

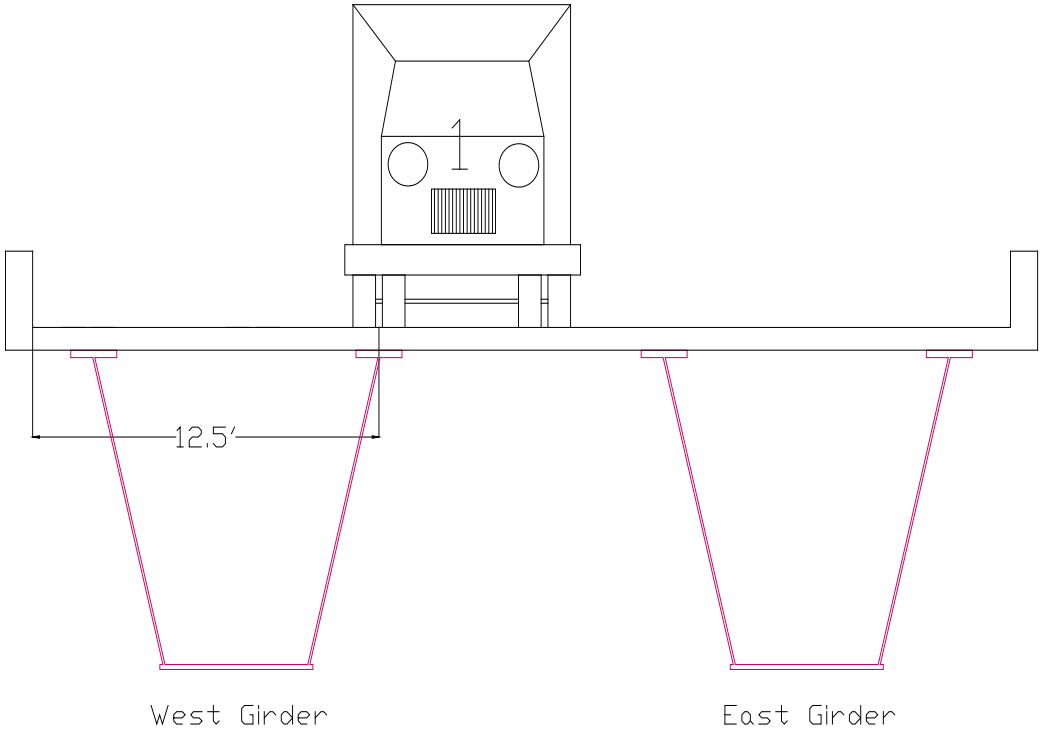

Truck Run #5: Truck 1 in east traffic lane (At Crawling Speed)

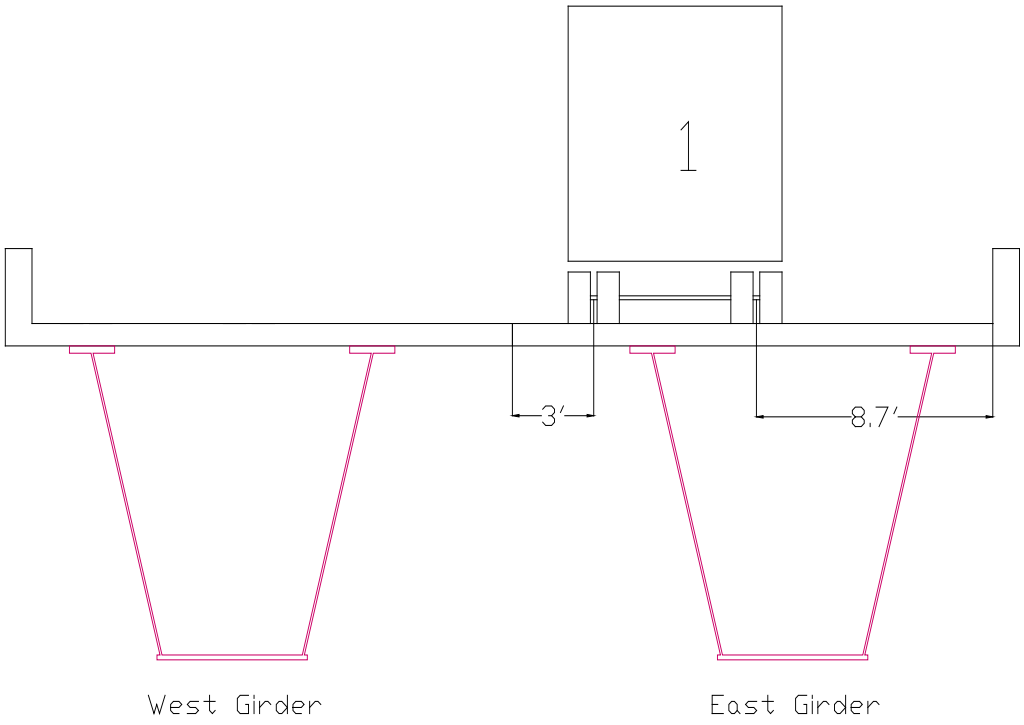

Truck Run #6: Truck 1 in west traffic lane (At Crawling Speed)

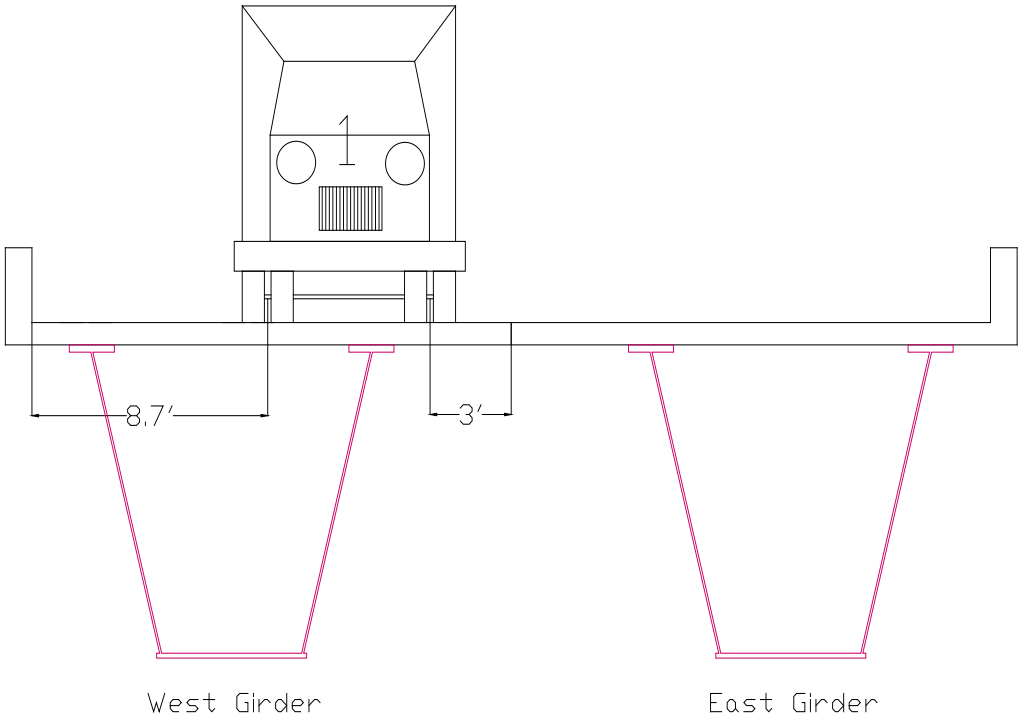

Truck Run #7: Truck 1 in east traffic lane (At Highway Speed)

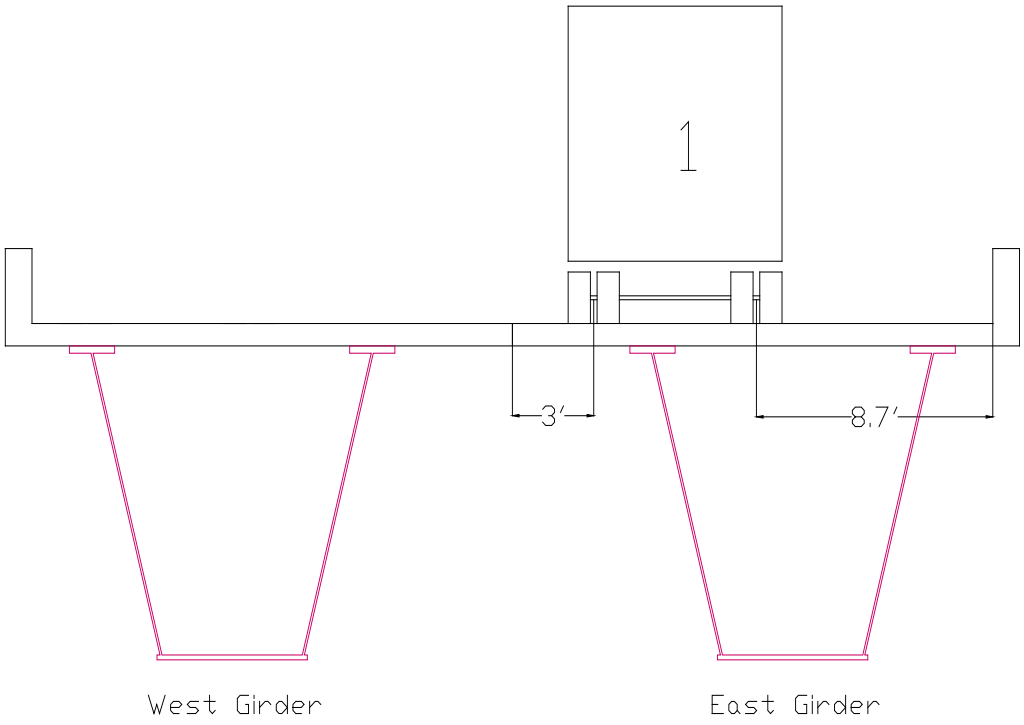

Truck Run #8: Truck 1 in west traffic lane (At Highway Speed)

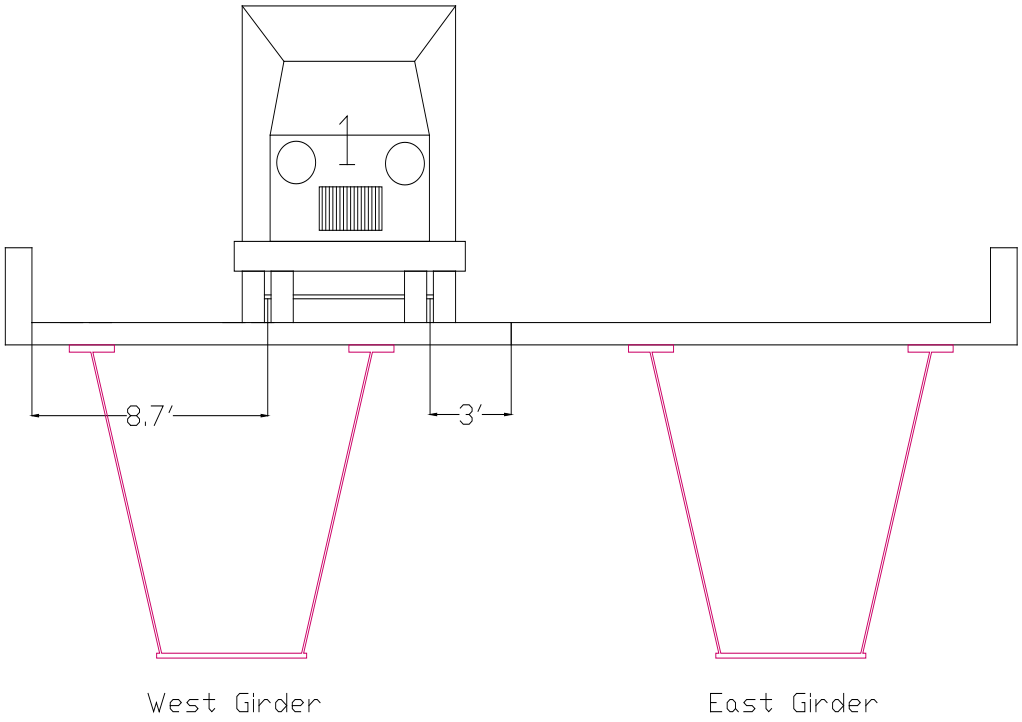

Truck Run #9: Truck 1 at 2’ from east railing and truck 2 at 4 from truck 1 (At Crawling Speed)

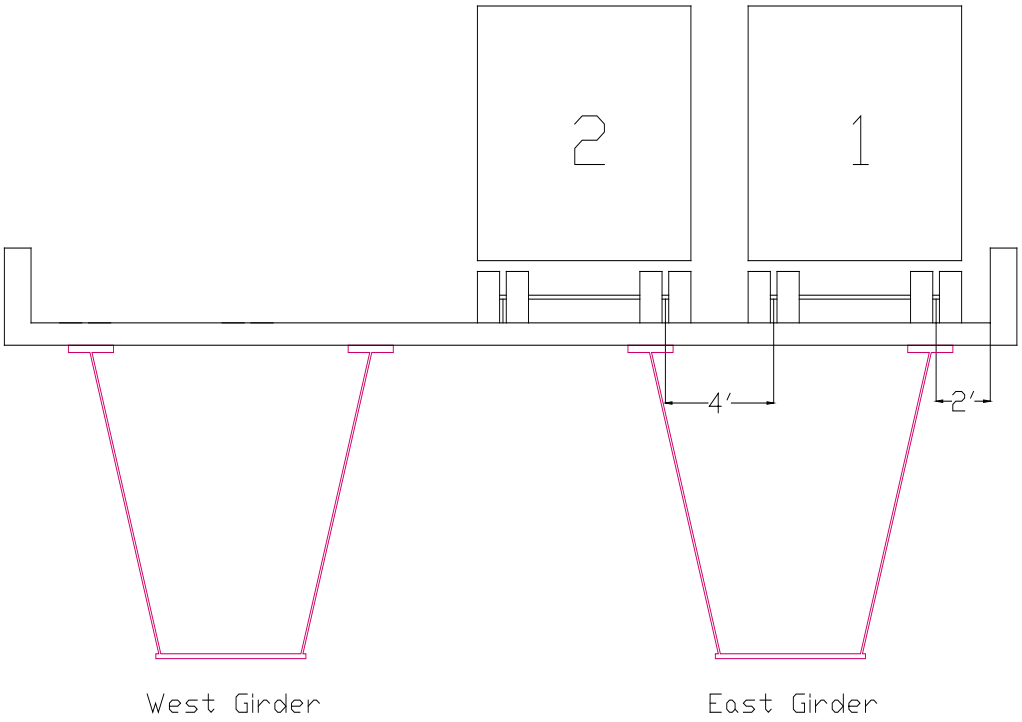

Truck Run #10: Truck 1 at 2’ from west railing and truck 2 at 4 from truck 1 (At Crawling Speed)

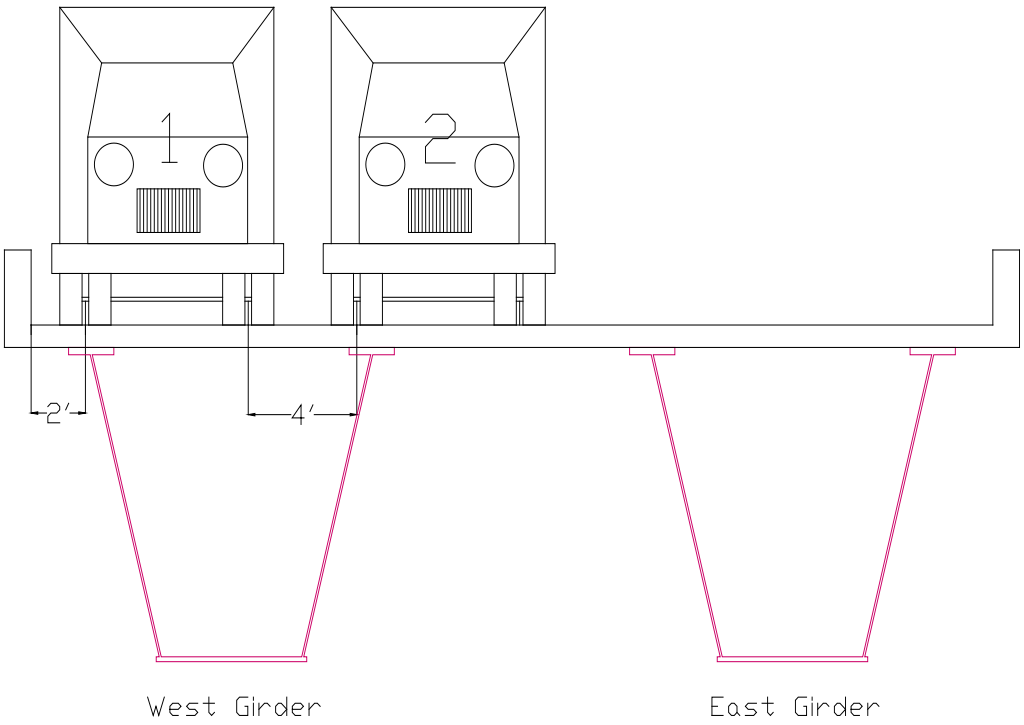

Truck Run #11: Truck 1 in west lane and truck 2 in east lane at the same time (At Crawling Speed)

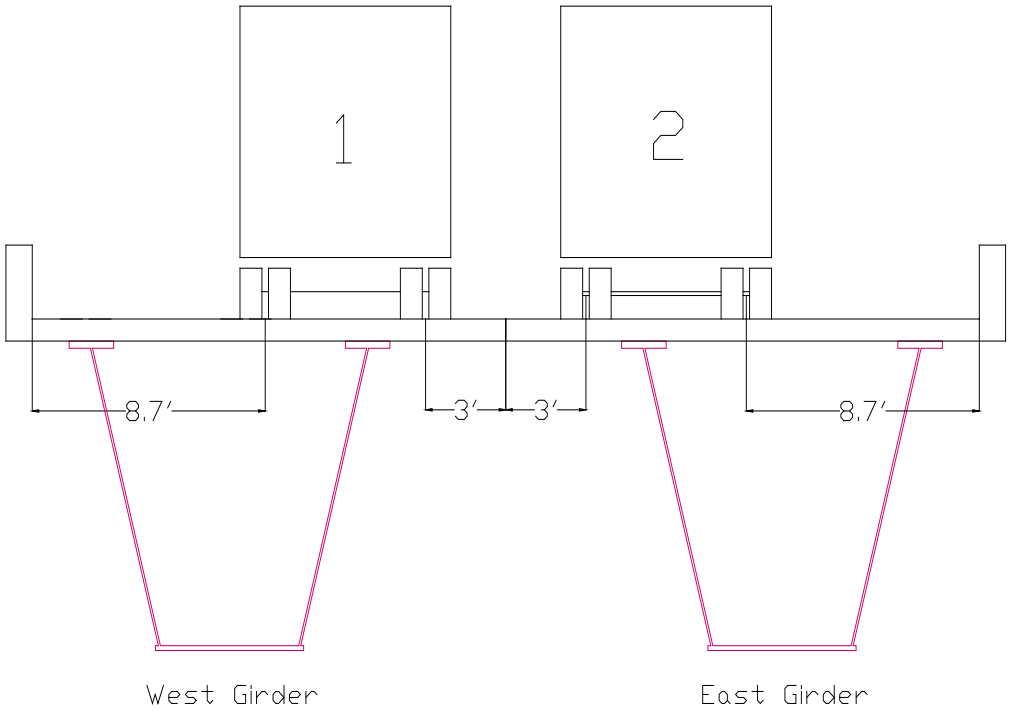

Truck Run #12: Truck 1 in west lane and truck 2 in east lane at the same time (At Highway Speed)

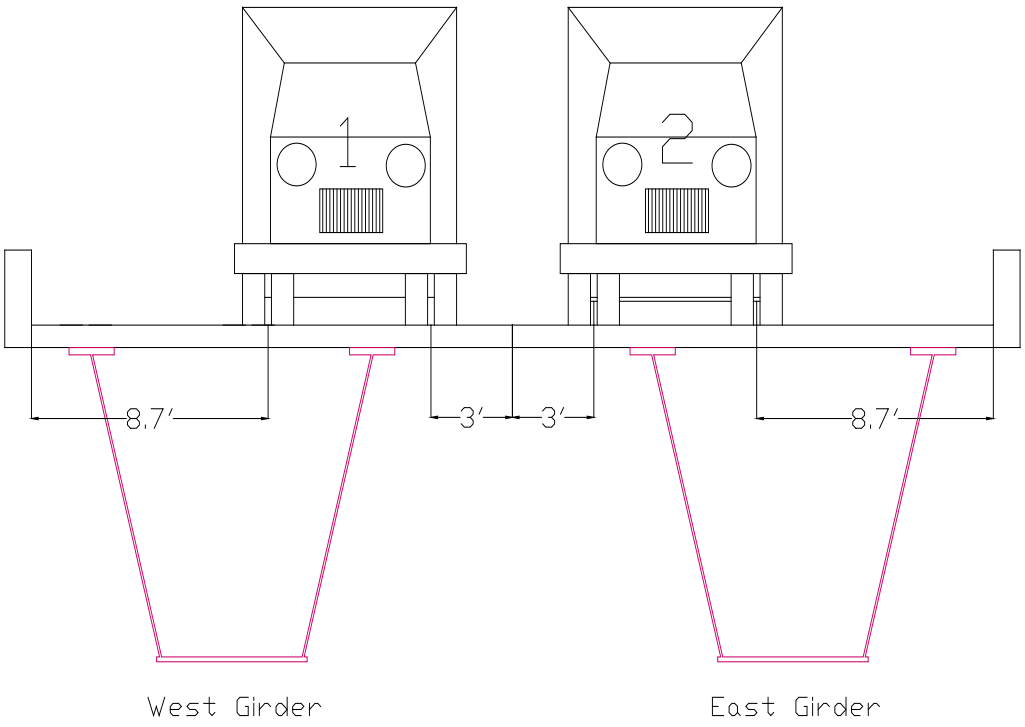

Truck Run #13: Truck 1 in west lane and truck 2 in east lane going toward each other (At Crawling Speed)

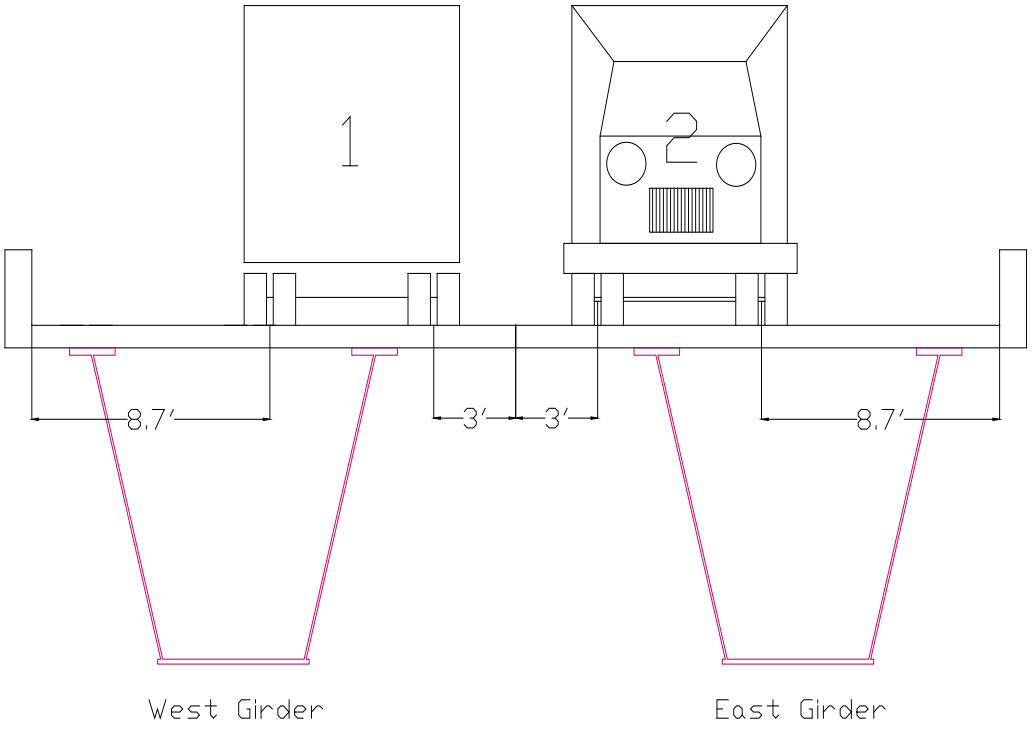

Truck Run #14: Truck 1 in west lane and truck 2 in east lane going toward each other (At Highway Speed)

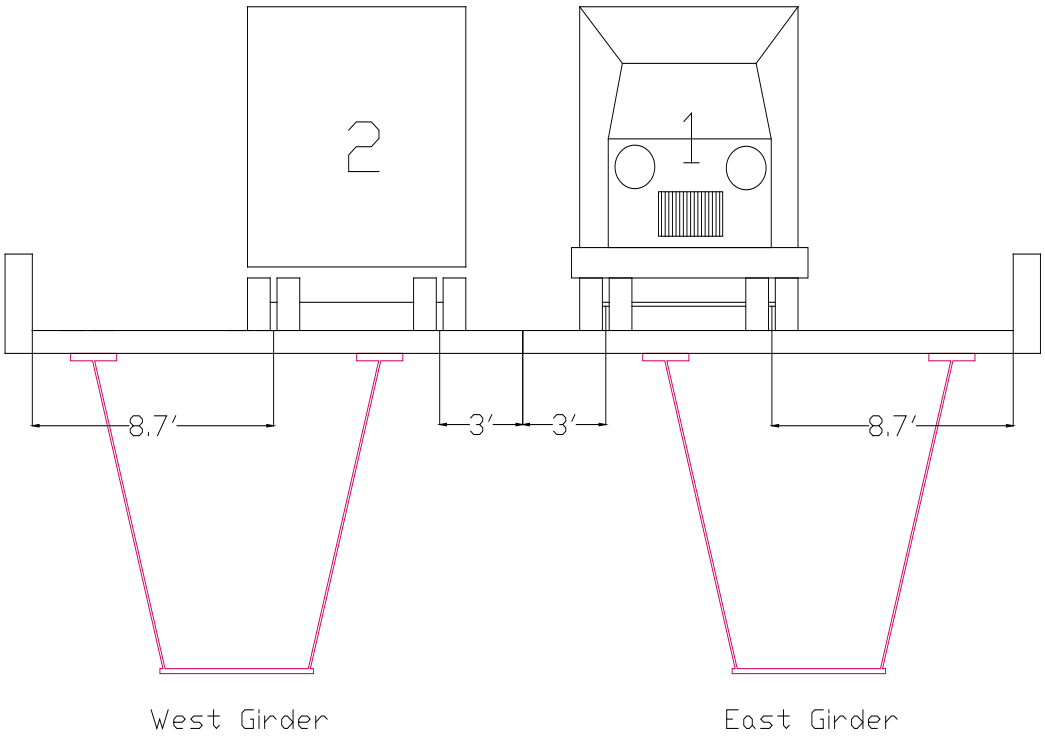

Truck Run #15: Truck 1 in west lane and truck 2 in east lane at the same time stopping at ¼ span, mid span, and ¾ span (At Crawling Speed)

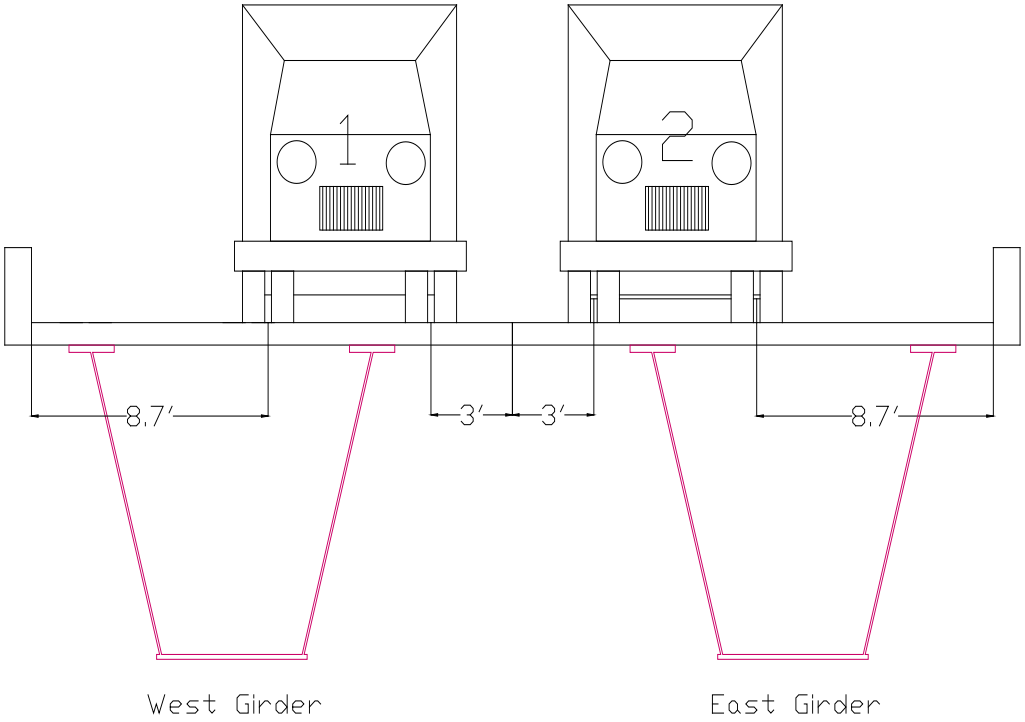

APPENDIX D

SAMPLE OF TRUCK LOADING STRESSES

The graphs shown in Appendix D are an example of the ones that were prepared for each truck loading scenario performed in the field testing. These graphs show the stresses in the girders at mid-span and quarter-span. These stresses were then used to calculate the live load distribution factors for the field test and to verify the numerical analysis to the field testing.

The stresses in the positive regain are in tension and correlate to the bottom flanges. The stresses in the negative regain are in compression and correlate to the top flanges. The order of the y-axis has been reversed in order to better represent the top and bottom flanges.

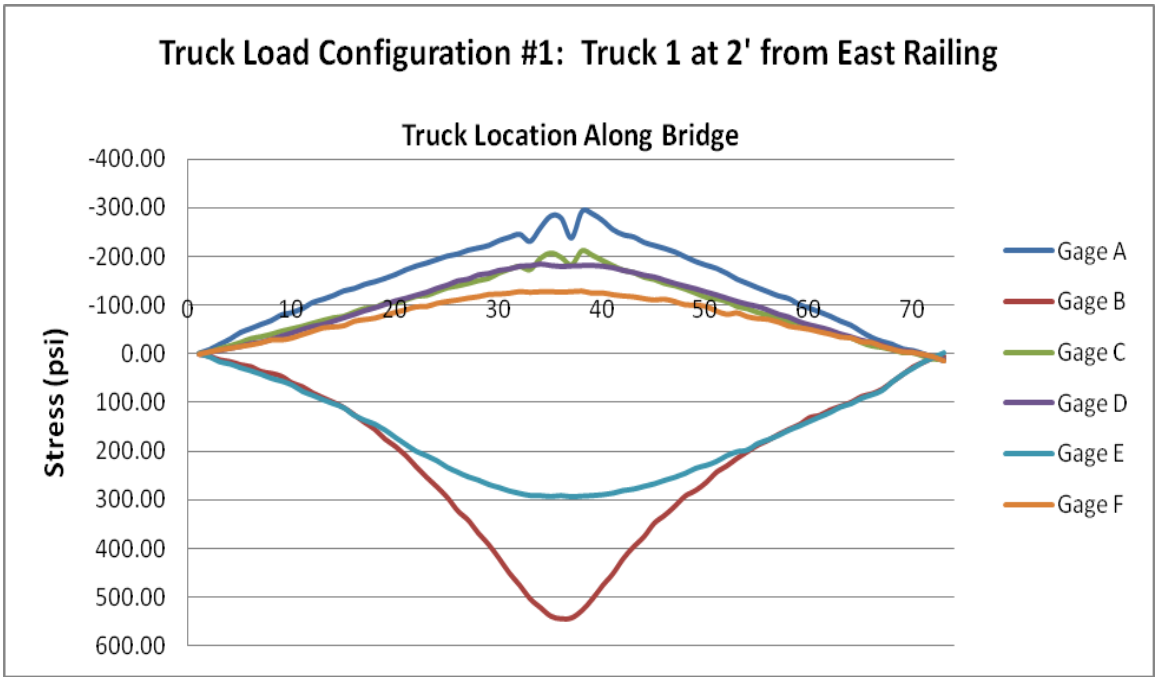

Stresses at Mid-span for Truck Load Configuration #1

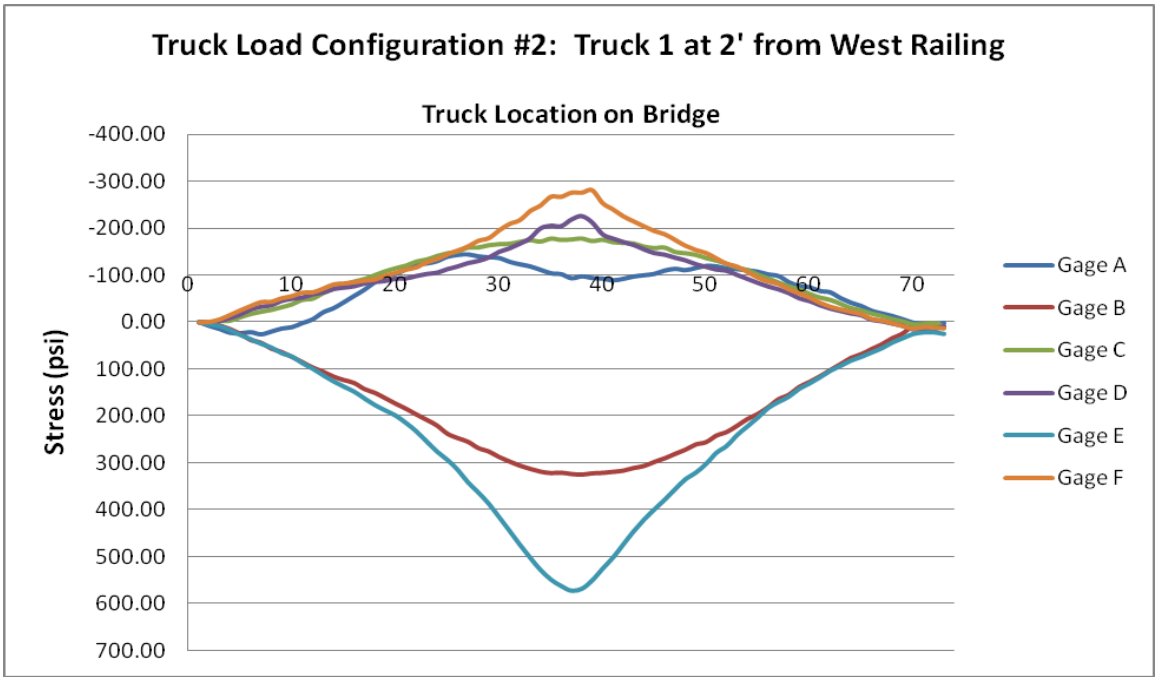

Stresses at Mid-span for Truck Load Configuration #2

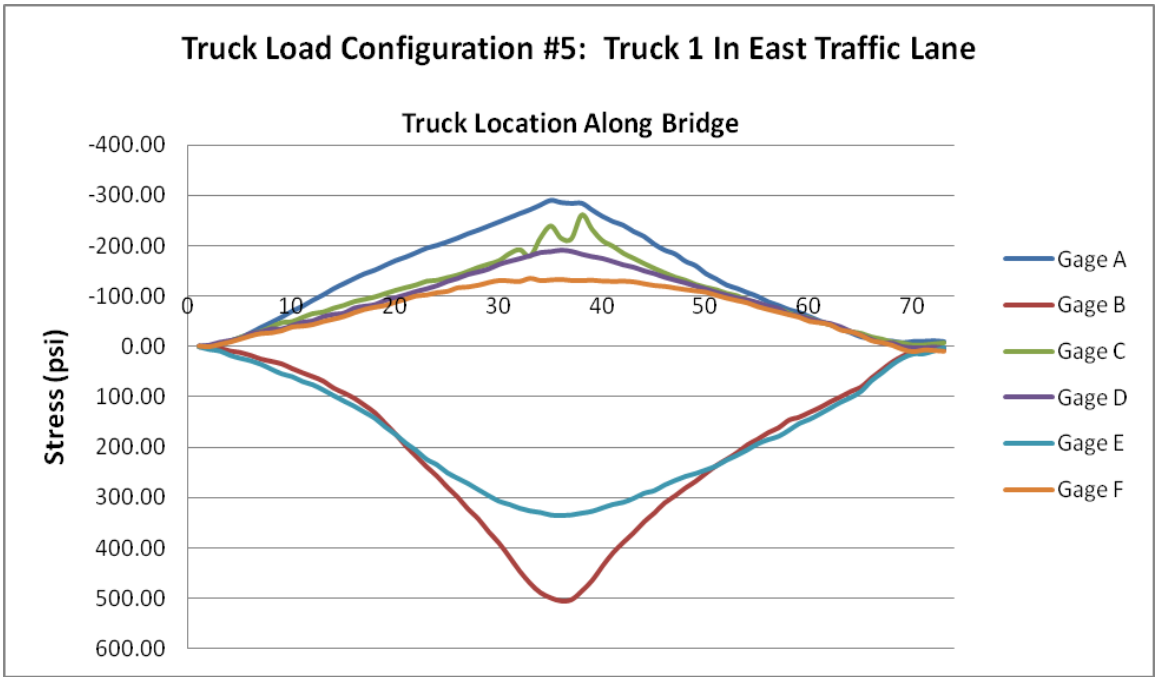

Stresses at Mid-span for Truck Load Configuration #5

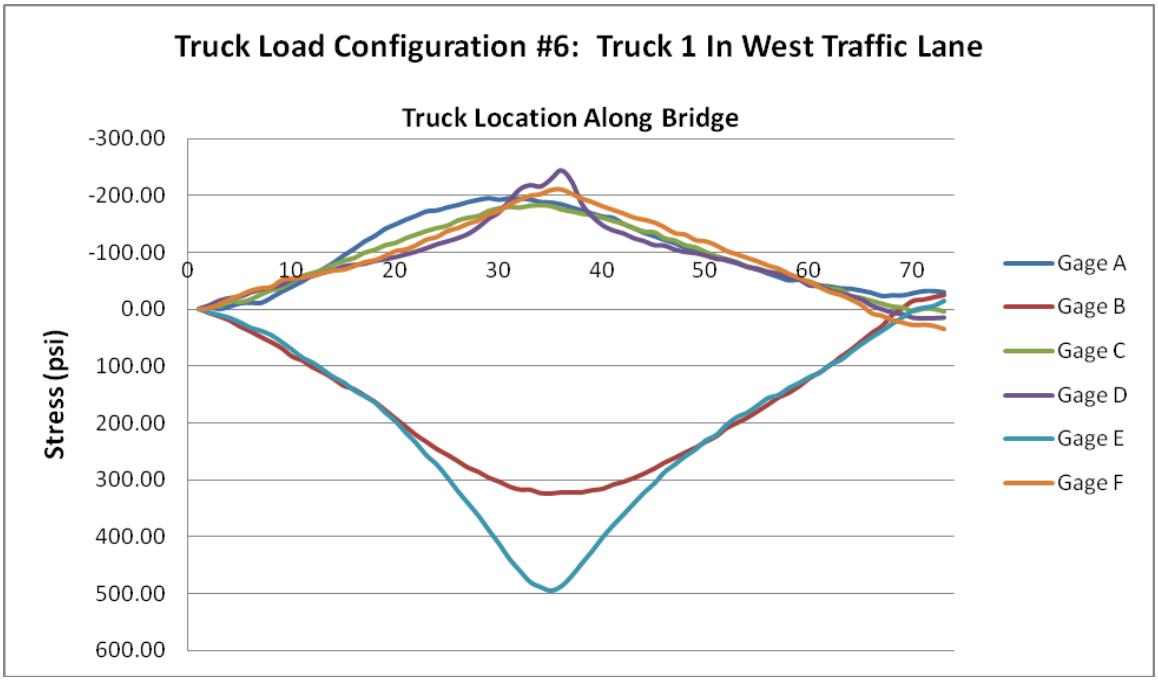

Stresses at Mid-span for Truck Load Configuration #6

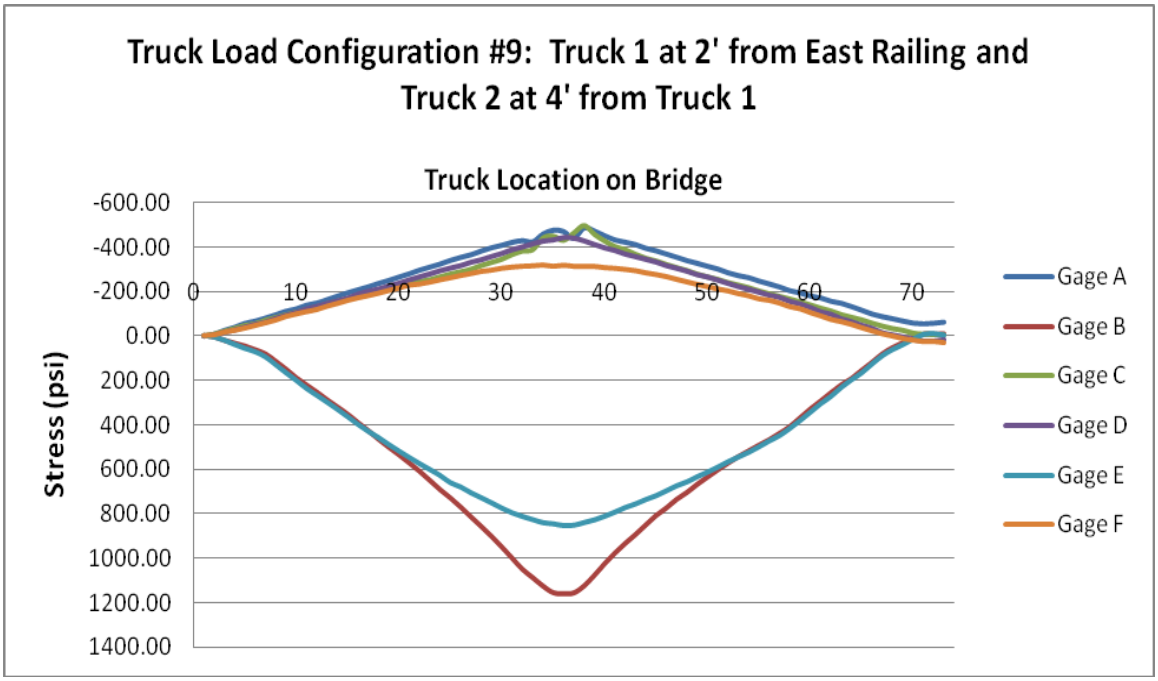

Stresses at Mid-span for Truck Load Configuration #9

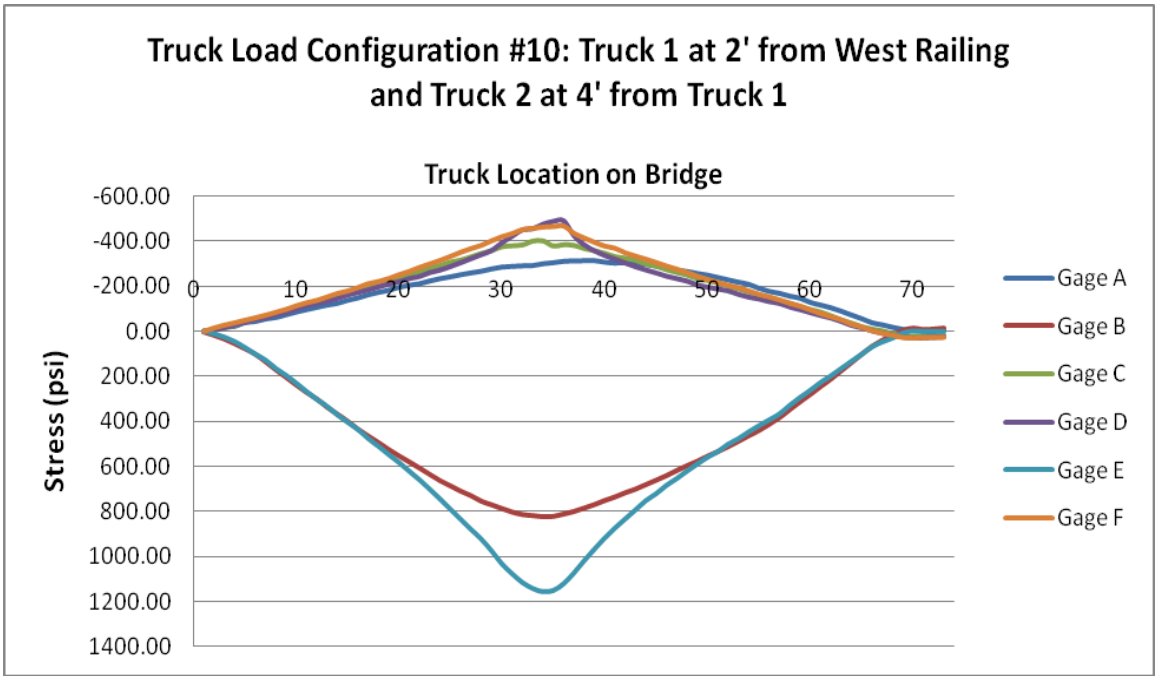

Stresses at Mid-span for Truck Load Configuration #10

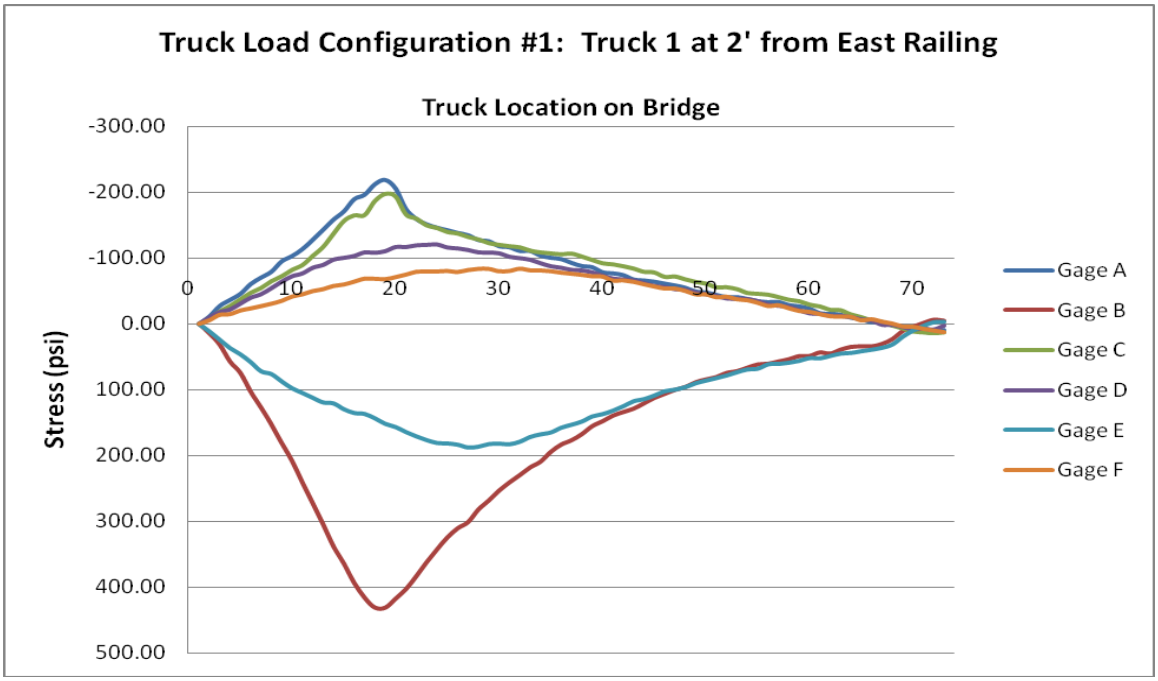

Stresses at Quarter-span for Truck Load Configuration #1

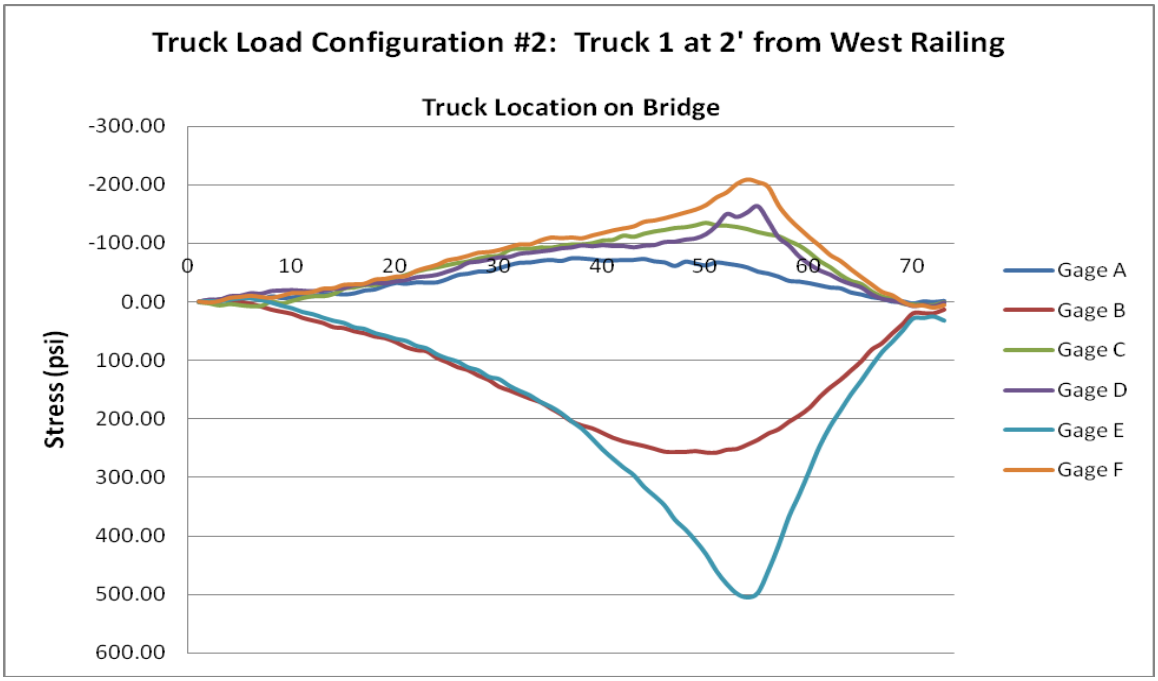

Stresses at Quarter-span for Truck Load Configuration #2

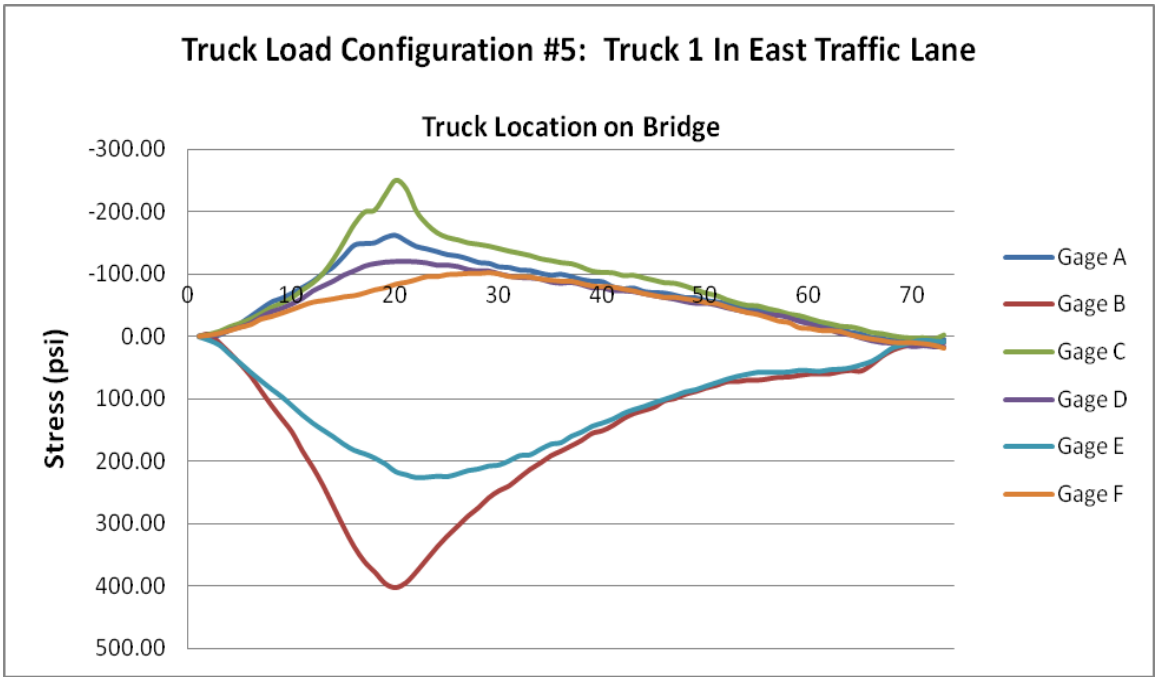

Stresses at Quarter-span for Truck Load Configuration #5

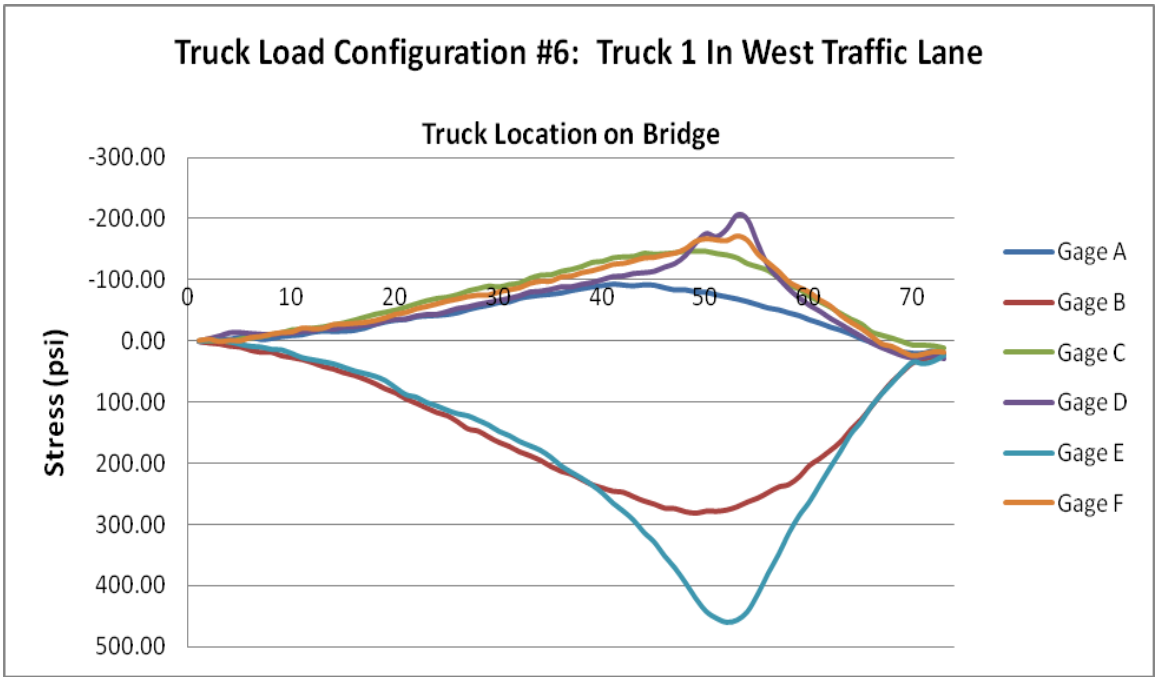

Stresses at Quarter-span for Truck Load Configuration #6

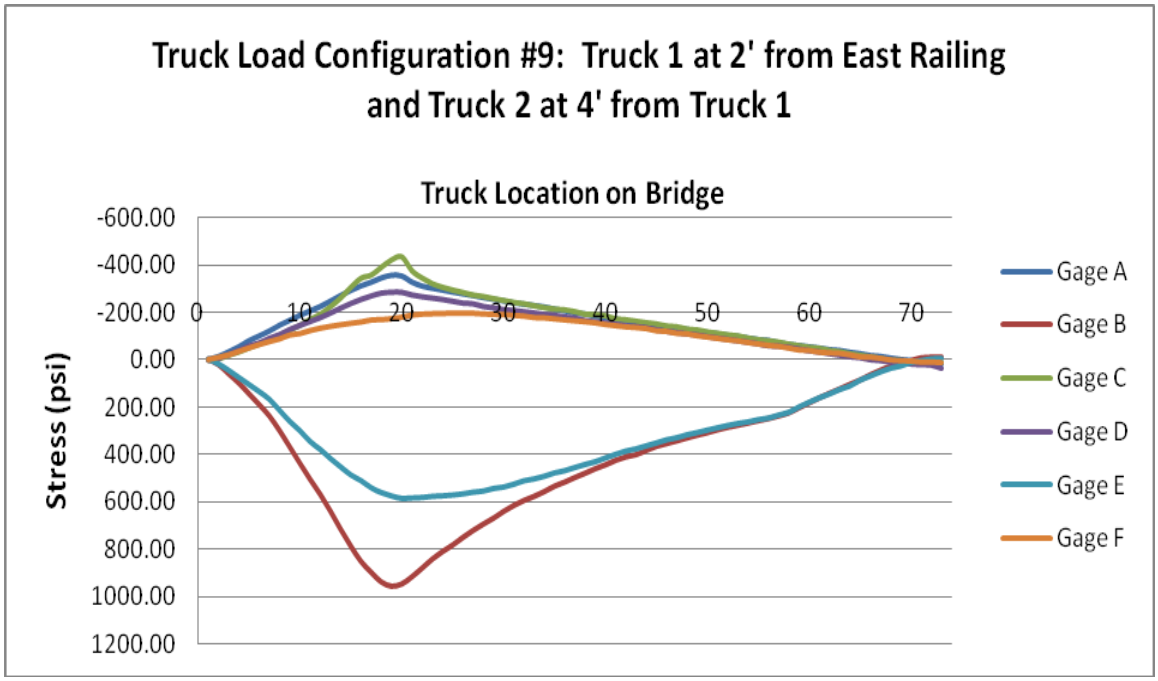

Stresses at Quarter-span for Truck Load Configuration #9

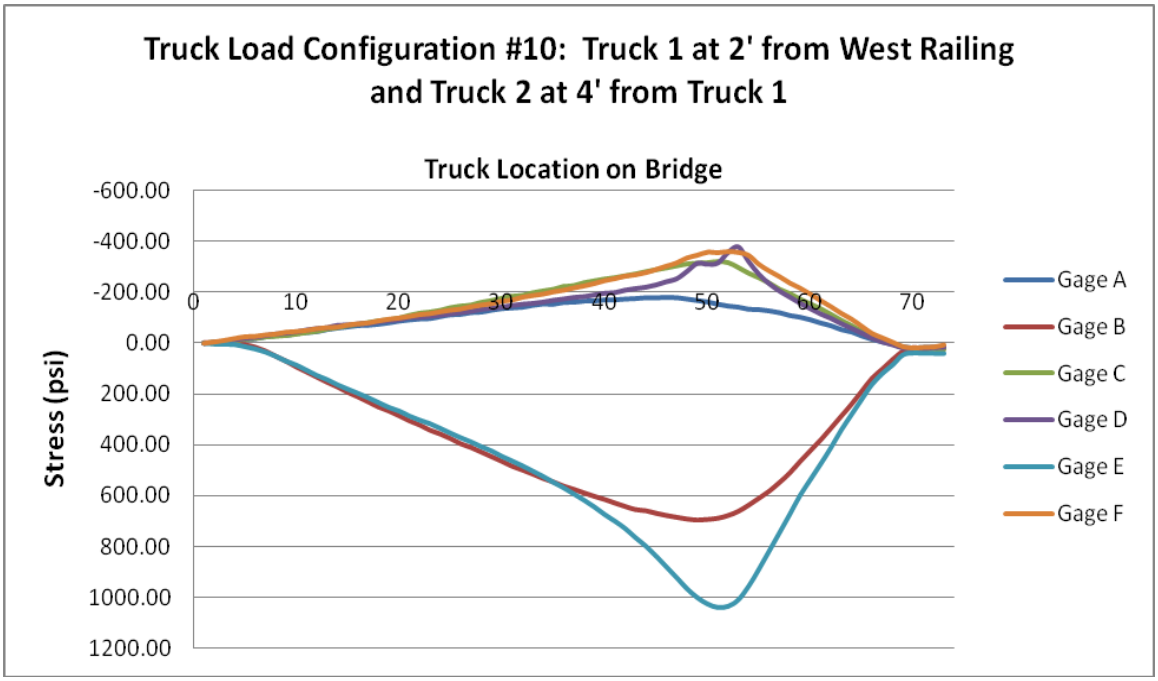

Stresses at Quarter-span for Truck Load Configuration #10

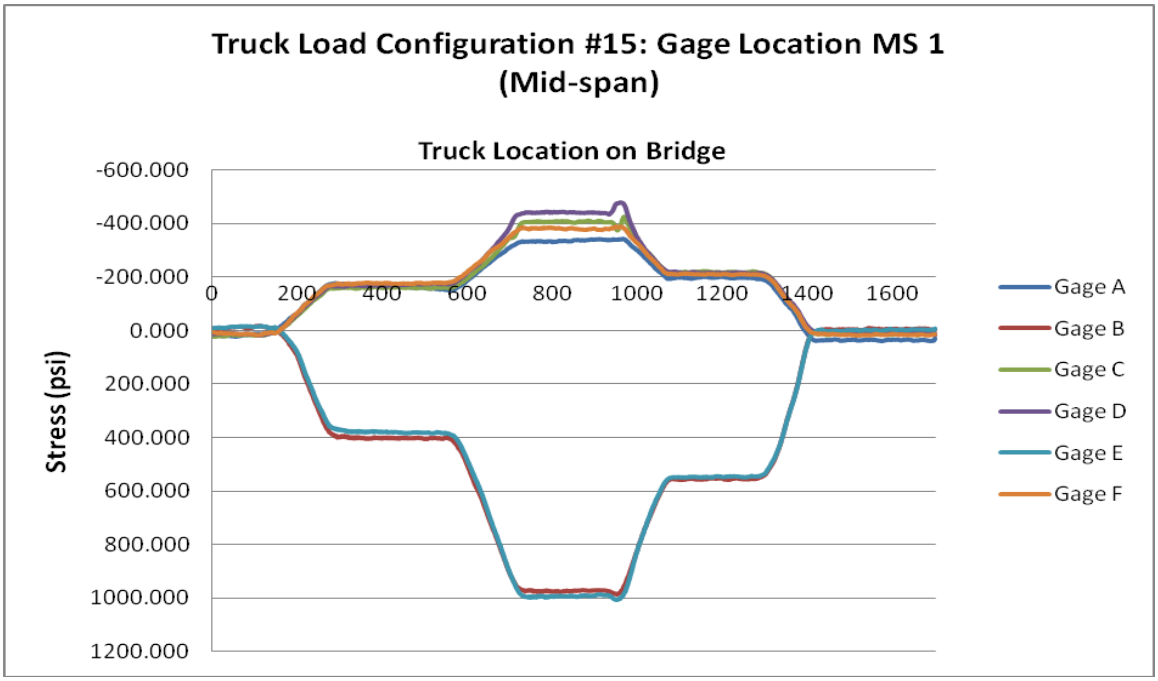

Stresses at MS 1 (Mid-span) for Truck Load Configuration #15

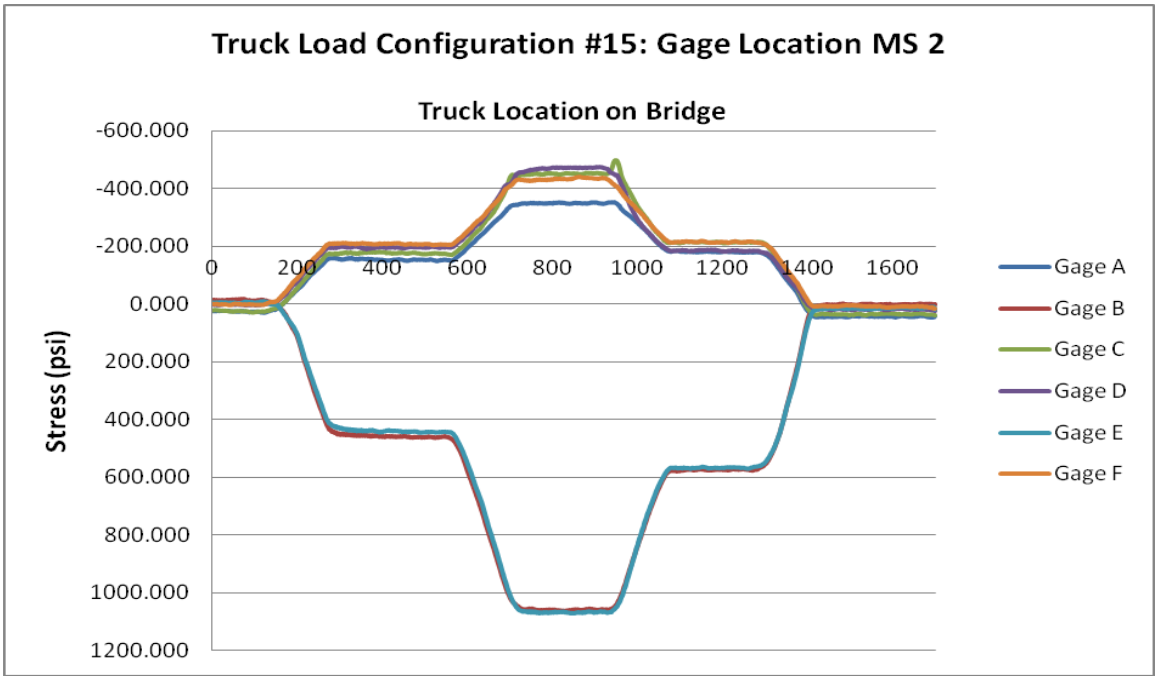

Stresses at MS 2 for Truck Load Configuration #15

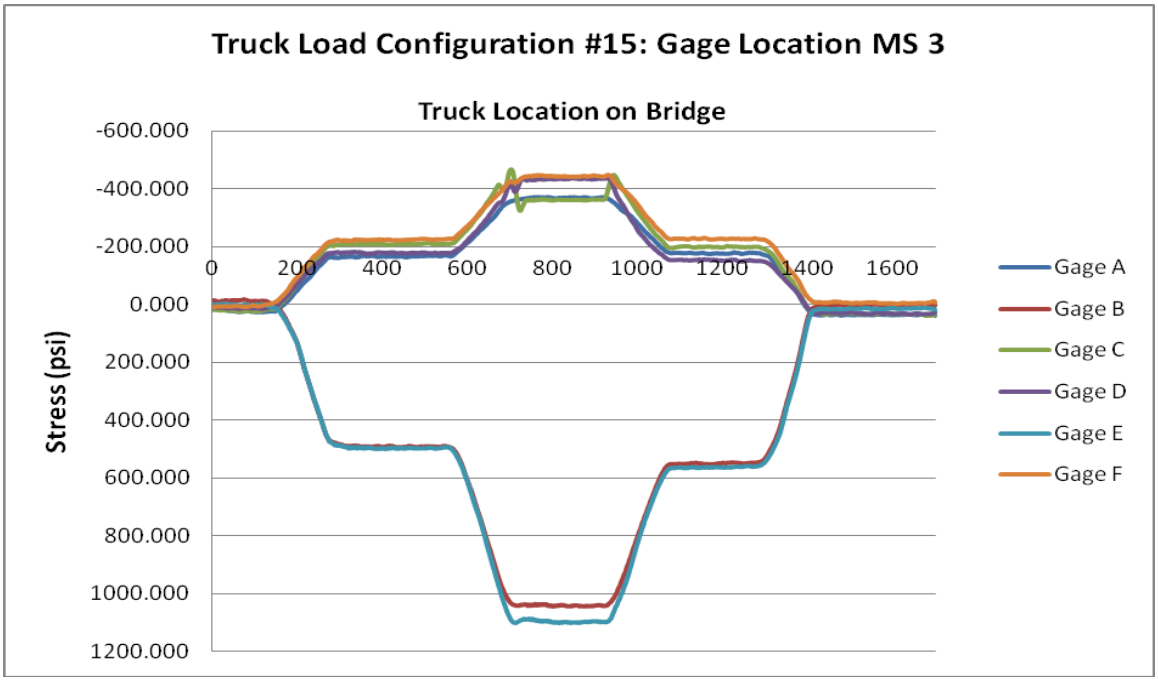

Stresses at MS 3 for Truck Load Configuration #15

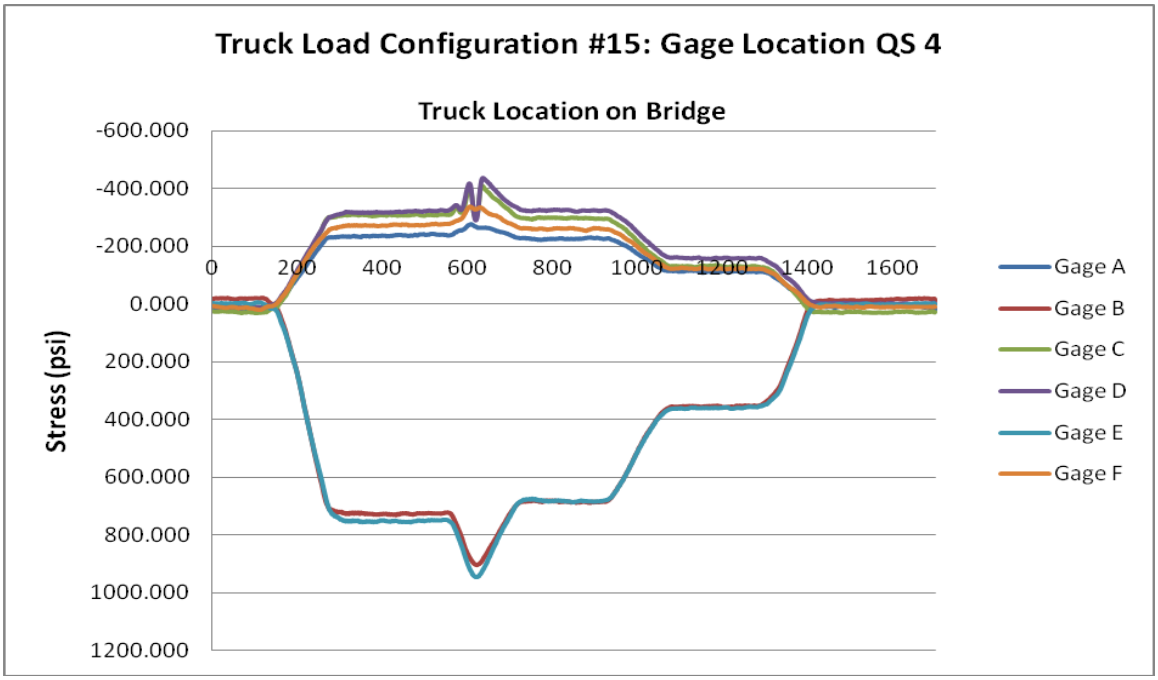

Stresses at Q4 for Truck Load Configuration #15

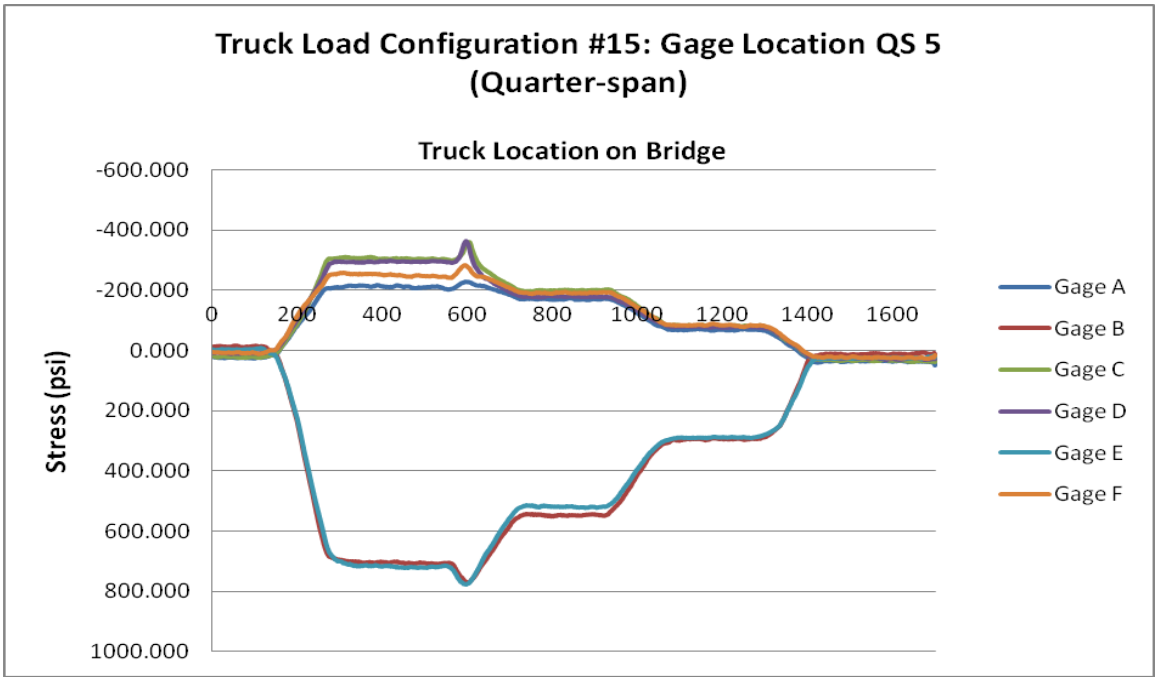

Stresses at Q5 (Quarter-span) for Truck Load Configuration #15

APPENDIX E

VERIFICATION AND LOAD DISTRIBUTION FACTORS

The tables shown in Appendix E are a representation of the stresses in the top and bottom flanges and of the load distribution factors for the field results and numerical analysis. They also show the numerical analysis verification to the field results. The stresses for the field results were taken as if the truck was traveling from south to north so the maximum stress at quarter span is always represented at quarter span.

East Girder from Truck Runs #2 and #9								
Top Flange								
Load at Span Location	Number of Lanes Loaded	Stress Values at Gages					% of Stress	Distribution Factor
		A	C	D	F	Total		
1/8	2	-122	-107	-105	-98	-433	53	1.37
	1	-11	-37	-50	-56	-154	31	
1/4	2	-251	-218	-224	-205	-897	52	1.57
	1	-97	-108	-88	-99	-392	52	
3/8	2	-384	-318	-342	-292	-1335	53	1.55
	1	-139	-159	-131	-173	-602	50	
1/2	2	-441	-465	-439	-314	-1659	55	1.44
	1	-93	-176	-219	-275	-763	35	
5/8	2	-355	-308	-304	-255	-1223	54	1.54
	1	-113	-149	-138	-175	-575	46	
3/4	2	-235	-191	-183	-160	-769	55	1.65
	1	-101	-93	-77	-87	-357	54	
7/8	2	-117	-73	-48	-36	-273	69	2.03
	1	-34	-24	-15	-17	-91	64	
							Average =	1.59
							Max =	2.03
							Min =	1.37
							Standard Deviation =	0.20
Bottom Flange								
Load at Span Location	Number of Lanes Loaded	Stress Values at Gages					% of Stress	Distribution Factor
		B		E		Total		
1/8	2	189		201		390	48	1.47
	1	74		74		148	50	
1/4	2	500		488		988	51	1.47
	1	162		189		351	46	
3/8	2	856		726		1582	54	1.51
	1	268		364		632	42	
1/2	2	1154		849		2003	58	1.51
	1	324		573		897	36	
5/8	2	734		672		1406	52	1.48
	1	281		357		638	44	
3/4	2	467		472		939	50	1.49
	1	181		184		365	50	
7/8	2	155		167		322	48	1.44
	1	68		74		143	48	
							Average =	1.48
							Max =	1.51
							Min =	1.44
							Standard Deviation =	0.02

East Girder Field Distribution Factors at Mid-span for Truck Runs #2 & #9

East Girder from Truck Runs #6 and #9								
Top Flange								
Load at Span Location	Number of Lanes Loaded	Stress Values at Gages					% of Stress	Distribution Factor
		A	C	D	F	Total		
1/8	2	-122	-107	-105	-98	-433	53	1.74
	1	-32	-19	-16	-8	-76	68	
1/4	2	-251	-218	-224	-205	-897	52	1.52
	1	-62	-65	-65	-77	-270	47	
3/8	2	-384	-318	-342	-292	-1335	53	1.55
	1	-116	-121	-104	-134	-475	50	
1/2	2	-441	-465	-439	-314	-1659	55	1.54
	1	-179	-172	-224	-204	-779	45	
5/8	2	-355	-308	-304	-255	-1223	54	1.63
	1	-192	-165	-143	-157	-657	54	
3/4	2	-235	-191	-183	-160	-769	55	1.69
	1	-141	-113	-87	-94	-435	58	
7/8	2	-117	-73	-48	-36	-273	69	1.84
	1	-39	-48	-51	-54	-193	45	
							Average =	1.64
							Max =	1.84
							Min =	1.52
							Standard Deviation =	0.11
Bottom Flange								
Load at Span Location	Number of Lanes Loaded	Stress Values at Gages					% of Stress	Distribution Factor
		B		E		Total		
1/8	2	189		201		390	48	1.45
	1	57		62		120	48	
1/4	2	500		488		988	51	1.53
	1	168		157		325	52	
3/8	2	856		726		1582	54	1.57
	1	262		273		535	49	
1/2	2	1154		849		2003	58	1.56
	1	323		469		791	41	
5/8	2	734		672		1406	52	1.49
	1	287		362		649	44	
3/4	2	467		472		939	50	1.49
	1	178		182		360	49	
7/8	2	155		167		322	48	1.50
	1	84		72		155	54	
							Average =	1.51
							Max =	1.57
							Min =	1.45
							Standard Deviation =	0.04

East Girder Field Distribution Factors at Mid-span for Truck Runs #6 & #9

West Girder from Truck Runs #1 and #10								
Top Flange								
Load at Span Location	Number of Lanes Loaded	Stress Values at Gages					% of Stress	Distribution Factor
		A	C	D	F	Total		
1/8	2	-85	-107	-101	-114	-408	53	1.42
	1	-83	-51	-43	-33	-211	36	
1/4	2	-182	-229	-211	-235	-857	52	1.45
	1	-154	-104	-102	-80	-440	41	
3/8	2	-267	-347	-341	-383	-1339	54	1.51
	1	-216	-151	-162	-118	-647	43	
1/2	2	-313	-383	-425	-437	-1557	55	1.53
	1	-237	-183	-180	-128	-729	42	
5/8	2	-271	-263	-235	-277	-1046	49	1.40
	1	-208	-140	-144	-108	-601	42	
3/4	2	-177	-149	-134	-154	-613	47	1.38
	1	-126	-80	-90	-72	-367	44	
7/8	2	-55	-22	-18	-19	-115	32	1.09
	1	-44	-23	-28	-26	-121	44	
							Average =	1.40
							Max =	1.53
							Min =	1.09
							Standard Deviation =	0.14
Bottom Flange								
Load at Span Location	Number of Lanes Loaded	Stress Values at Gages					% of Stress	Distribution Factor
		B		E		Total		
1/8	2	236		231		467	49	1.51
	1	59		64		124	52	
1/4	2	524		547		1071	51	1.50
	1	175		157		332	47	
3/8	2	755		921		1676	55	1.51
	1	367		260		628	41	
1/2	2	800		1071		1872	57	1.50
	1	541		294		836	35	
5/8	2	618		654		1271	51	1.48
	1	312		254		566	45	
3/4	2	412		394		806	49	1.48
	1	177		177		354	50	
7/8	2	99		103		202	51	1.53
	1	87		92		179	51	
							Average =	1.50
							Max =	1.53
							Min =	1.48
							Standard Deviation =	0.02

West Girder Field Distribution Factors at Mid-span for Truck Runs #1 & #10

West Girder from Truck Runs #5 and #10								
Top Flange								
Load at Span Location	Number of Lanes Loaded	Stress Values at Gages					% of Stress	Distribution Factor
		A	C	D	F	Total		
1/8	2	-85	-107	-101	-114	-408	53	1.45
	1	-70	-50	-41	-38	-199	40	
1/4	2	-182	-229	-211	-235	-857	52	1.43
	1	-161	-106	-91	-81	-440	39	
3/8	2	-267	-347	-341	-383	-1339	54	1.49
	1	-232	-157	-148	-122	-659	41	
1/2	2	-313	-383	-425	-437	-1557	55	1.50
	1	-285	-214	-189	-131	-820	39	
5/8	2	-271	-263	-235	-277	-1046	49	1.41
	1	-184	-138	-132	-116	-570	44	
3/4	2	-177	-149	-134	-154	-613	47	1.42
	1	-88	-78	-80	-73	-319	48	
7/8	2	-55	-22	-18	-19	-115	32	1.13
	1	-18	-27	-21	-21	-87	49	
							Average =	1.41
							Max =	1.50
							Min =	1.13
							Standard Deviation =	0.12
Bottom Flange								
Load at Span Location	Number of Lanes Loaded	Stress Values at Gages					% of Stress	Distribution Factor
		B		E		Total		
1/8	2	236		231		467	49	1.57
	1	43		60		103	58	
1/4	2	524		547		1071	51	1.53
	1	152		160		311	51	
3/8	2	755		921		1676	55	1.55
	1	341		285		626	45	
1/2	2	800		1071		1872	57	1.55
	1	501		335		837	40	
5/8	2	618		654		1271	51	1.50
	1	296		266		562	47	
3/4	2	412		394		806	49	1.50
	1	170		185		355	52	
7/8	2	99		103		202	51	1.55
	1	79		89		168	53	
							Average =	1.54
							Max =	1.57
							Min =	1.50
							Standard Deviation =	0.02

West Girder Field Distribution Factors at Mid-span for Truck Runs #5 & #10

East Girder from Truck Runs #2 and #9								
Top Flange								
Load at Span Location	Number of Lanes Loaded	Stress Values at Gages					% of Stress	Distribution Factor
		A	C	D	F	Total		
1/8	2	-188	-147	-147	-110	-592	57	1.53
	1	-12	-31	-24	-42	-109	40	
1/4	2	-360	-423	-287	-172	-1242	63	1.59
	1	-48	-116	-139	-196	-499	33	
3/8	2	-264	-269	-227	-192	-952	56	1.55
	1	-61	-127	-103	-147	-438	43	
1/2	2	-198	-205	-178	-163	-744	54	1.55
	1	-74	-99	-93	-110	-376	46	
5/8	2	-134	-142	-116	-111	-502	55	1.55
	1	-52	-75	-69	-83	-279	45	
3/4	2	-81	-82	-61	-60	-284	58	1.61
	1	-27	-34	-32	-39	-131	46	
7/8	2	-24	-21	-11	-11	-68	67	1.56
	1	-7	-2	-20	-15	-44	21	
							Average =	1.56
							Max =	1.61
							Min =	1.53
							Standard Deviation =	0.03
Bottom Flange								
Load at Span Location	Number of Lanes Loaded	Stress Values at Gages					% of Stress	Distribution Factor
		B		E		Total		
1/8	2	439		301		740	59	1.62
	1	101		134		235	43	
1/4	2	957		575		1532	62	1.58
	1	224		460		684	33	
3/8	2	695		554		1249	56	1.52
	1	256		372		628	41	
1/2	2	499		455		954	52	1.55
	1	204		204		407	50	
5/8	2	344		330		675	51	1.54
	1	125		117		242	52	
3/4	2	251		247		498	50	1.52
	1	61		58		119	52	
7/8	2	88		89		177	50	1.64
	1	20		11		31	65	
							Average =	1.57
							Max =	1.64
							Min =	1.52
							Standard Deviation =	0.04

East Girder Field Distribution Factors at Quarter-span for Truck Runs #2 & #9

East Girder from Truck Runs #6 and #9								
Top Flange								
Load at Span Location	Number of Lanes Loaded	Stress Values at Gages					% of Stress	Distribution Factor
		A	C	D	F	Total		
1/8	2	-188	-147	-147	-110	-592	57	1.67
	1	-4	-28	-8	-20	-60	54	
1/4	2	-360	-423	-287	-172	-1242	63	1.67
	1	-54	-116	-123	-127	-421	40	
3/8	2	-264	-269	-227	-192	-952	56	1.58
	1	-84	-145	-127	-143	-499	46	
1/2	2	-198	-205	-178	-163	-744	54	1.59
	1	-83	-117	-89	-105	-395	51	
5/8	2	-134	-142	-116	-111	-502	55	1.61
	1	-56	-86	-60	-74	-277	51	
3/4	2	-81	-82	-61	-60	-284	58	1.68
	1	-32	-47	-33	-37	-149	53	
7/8	2	-24	-21	-11	-11	-68	67	1.85
	1	-10	-18	-13	-14	-55	50	
							Average =	1.66
							Max =	1.85
							Min =	1.58
							Standard Deviation =	0.08
Bottom Flange								
Load at Span Location	Number of Lanes Loaded	Stress Values at Gages					% of Stress	Distribution Factor
		B		E		Total		
1/8	2	439		301		740	59	1.68
	1	128		131		259	49	
1/4	2	957		575		1532	62	1.65
	1	249		379		628	40	
3/8	2	695		554		1249	56	1.54
	1	275		370		646	43	
1/2	2	499		455		954	52	1.55
	1	219		214		433	51	
5/8	2	344		330		675	51	1.55
	1	148		129		277	53	
3/4	2	251		247		498	50	1.56
	1	78		64		142	55	
7/8	2	88		89		177	50	1.57
	1	27		20		47	57	
							Average =	1.58
							Max =	1.68
							Min =	1.54
							Standard Deviation =	0.05

East Girder Field Distribution Factors at Quarter-span for Truck Runs #6 & #9

West Girder from Truck Runs #1 and #10								
Top Flange								
Load at Span Location	Number of Lanes Loaded	Stress Values at Gages					% of Stress	Distribution Factor
		A	C	D	F	Total		
1/8	2	-29	-47	-40	-66	-183	58	1.55
	1	-103	-82	-72	-41	-298	38	
1/4	2	-127	-236	-235	-284	-882	59	1.48
	1	-218	-198	-110	-67	-593	30	
3/8	2	-179	-303	-254	-315	-1052	54	1.51
	1	-127	-128	-108	-83	-447	43	
1/2	2	-161	-226	-181	-217	-785	51	1.45
	1	-93	-107	-82	-75	-356	44	
5/8	2	-123	-160	-134	-150	-566	50	1.45
	1	-58	-72	-53	-53	-236	45	
3/4	2	-80	-92	-90	-94	-356	52	1.45
	1	-33	-44	-29	-27	-133	42	
7/8	2	-38	-36	-45	-46	-165	55	1.51
	1	-7	-10	-7	-5	-29	41	
							Average =	1.49
							Max =	1.55
							Min =	1.45
							Standard Deviation =	0.04
Bottom Flange								
Load at Span Location	Number of Lanes Loaded	Stress Values at Gages					% of Stress	Distribution Factor
		B		E		Total		
1/8	2	190		220		409	54	1.39
	1	209		98		307	32	
1/4	2	581		815		1396	58	1.43
	1	432		152		583	26	
3/8	2	683		920		1604	57	1.55
	1	283		187		469	40	
1/2	2	574		592		1166	51	1.48
	1	177		153		330	46	
5/8	2	428		407		835	49	1.47
	1	101		100		200	50	
3/4	2	267		252		519	49	1.47
	1	61		61		122	50	
7/8	2	95		86		181	48	1.50
	1	34		41		76	54	
							Average =	1.47
							Max =	1.55
							Min =	1.39
							Standard Deviation =	0.05

West Girder Field Distribution Factors at Quarter-span for Truck Runs #1 & #10

West Girder from Truck Runs #5 and #10								
Top Flange								
Load at Span Location	Number of Lanes Loaded	Stress Values at Gages					% of Stress	Distribution Factor
		A	C	D	F	Total		
1/8	2	-29	-47	-40	-66	-183	58	1.59
	1	-68	-62	-53	-43	-226	42	
1/4	2	-127	-236	-235	-284	-882	59	1.52
	1	-158	-226	-120	-79	-583	34	
3/8	2	-179	-303	-254	-315	-1052	54	1.52
	1	-118	-147	-106	-101	-472	44	
1/2	2	-161	-226	-181	-217	-785	51	1.47
	1	-95	-116	-87	-89	-387	45	
5/8	2	-123	-160	-134	-150	-566	50	1.45
	1	-65	-85	-60	-63	-273	45	
3/4	2	-80	-92	-90	-94	-356	52	1.47
	1	-39	-44	-35	-30	-148	44	
7/8	2	-38	-36	-45	-46	-165	55	1.30
	1	-3	-11	-2	-1	-18	20	
							Average =	1.47
							Max =	1.59
							Min =	1.30
							Standard Deviation =	0.08
Bottom Flange								
Load at Span Location	Number of Lanes Loaded	Stress Values at Gages					% of Stress	Distribution Factor
		B		E		Total		
1/8	2	190		220		409	54	1.49
	1	154		111		265	42	
1/4	2	581		815		1396	58	1.51
	1	396		205		601	34	
3/8	2	683		920		1604	57	1.58
	1	275		213		487	44	
1/2	2	574		592		1166	51	1.49
	1	175		160		335	48	
5/8	2	428		407		835	49	1.46
	1	99		95		194	49	
3/4	2	267		252		519	49	1.43
	1	68		57		125	46	
7/8	2	95		86		181	48	1.40
	1	55		45		100	45	
							Average =	1.48
							Max =	1.58
							Min =	1.40
							Standard Deviation =	0.06

West Girder Field Distribution Factors at Quarter-span for Truck Runs #5 & #10

East Girder Mid-span								
Top Flange								
Load at Span Location	Number of Lanes Loaded	Stress Values at Gages					% of Stress	Distribution Factor
		A	C	D	F	Total		
1/8	3	-112	-119	-94	-102	-427	54	1.62
1/4	3	-222	-239	-190	-212	-863	53	1.60
3/8	3	-334	-359	-292	-318	-1303	53	1.60
1/2	3	-420	-514	-395	-382	-1711	55	1.64
5/8	3	-332	-359	-290	-315	-1296	53	1.60
3/4	3	-225	-240	-187	-206	-858	54	1.63
7/8	3	-116	-121	-90	-96	-423	56	1.68
							Average =	1.62
							Max =	1.68
							Min =	1.60
							Standard Deviation =	0.03
Bottom Flange								
Load at Span Location	Number of Lanes Loaded	Stress Values at Gages					% of Stress	Distribution Factor
		B		E		Total		
1/8	3	433		433		866	50	1.50
1/4	3	880		872		1752	50	1.51
3/8	3	1352		1300		2652	51	1.53
1/2	3	1775		1626		3401	52	1.57
5/8	3	1345		1295		2640	51	1.53
3/4	3	873		870		1743	50	1.50
7/8	3	426		434		860	50	1.49
							Average =	1.52
							Max =	1.57
							Min =	1.49
							Standard Deviation =	0.02

Stresses and Distribution Factors at the Mid-span for the East Girder – Numerical Analysis

East Girder Quarter-span								
Top Flange								
Load at Span Location	Number of Lanes Loaded	Stress Values at Gages					% of Stress	Distribution Factor
		A	C	D	F	Total		
1/8	3	-169	-178	-148	-149	-644	54	1.62
1/4	3	-323	-392	-320	-276	-1311	55	1.64
3/8	3	-292	-321	-265	-273	-1151	53	1.60
1/2	3	-236	-255	-204	-220	-915	54	1.61
5/8	3	-177	-192	-150	-159	-678	54	1.63
3/4	3	-120	-128	-97	-100	-445	56	1.67
7/8	3	-63	-64	-47	-46	-220	58	1.73
							Average =	1.64
							Max =	1.73
							Min =	1.60
							Standard Deviation =	0.04
Bottom Flange								
Load at Span Location	Number of Lanes Loaded	Stress Values at Gages					% of Stress	Distribution Factor
		B		E		Total		
1/8	3	748		646		1394	54	1.61
1/4	3	1479		1254		2733	54	1.62
3/8	3	1303		1173		2476	53	1.58
1/2	3	1015		942		1957	52	1.56
5/8	3	750		701		1451	52	1.55
3/4	3	493		465		958	51	1.54
7/8	3	242		230		472	51	1.54
							Average =	1.57
							Max =	1.62
							Min =	1.54
							Standard Deviation =	0.03

Stresses and Distribution Factors at the Quarter-span for the East Girder – Numerical Analysis

Truck Run #15: Stress Comparison with Truck at Mid-span										
								Ratio Between Gages		
	Location	Gage A	Gage B	Gage C	Gage D	Gage E	Gage F	A & C	D & F	B & E
Field Results	MS 1 (Mid-span)	-365	979	-422	-454	999	-394	0.864	1.152	0.980
	MS 2	-383	1060	-483	-477	1054	-433	0.794	1.101	1.005
	MS 3	-396	1037	-398	-444	1078	-438	0.996	1.014	0.962
	QS 4	-238	691	-321	-324	673	-268	0.741	1.207	1.026
	QS 5 (Quarter-span)	-197	539	-227	-194	502	-203	0.869	0.954	1.073
Numerical Results	MS 1 (Mid-span)	245	1101	350	282	1098	270	0.700	1.044	1.003
	MS 2	230	945	260	223	933	249	0.885	0.896	1.013
	QS 5 (Quarter-span)	142	620	157	130	598	149	0.904	0.872	1.037

Stress Comparison between Field and Numerical Results

Wisconsin Highway Research Program
University of Wisconsin-Madison
1415 Engineering Drive
Madison, WI 53706
608/262-2013
www.whrp.org